Design and Development of Microneedle Pads for Automated External Defibrillators (AEDs)

by

Dominic Tung

A thesis

presented to the University of Waterloo

in fulfillment of the

thesis requirement for the degree of

Master of Applied Science

in

Mechanical and Mechatronics Engineering

Waterloo, Ontario, Canada, 2024

Author’s Declaration

I hereby declare that I am the sole author of this thesis. This is a true copy of the thesis, including any required final revisions, as accepted by my examiners.

I understand that my thesis may be made electronically available to the public.

Abstract

With the prominent and life-threatening issue of sudden cardiac arrest (SCA), the demands for increased accessibility and effectiveness of AEDs continue to rise. Timely access to automated external defibrillators (AEDs) can vastly increase the chances of survival for someone who suffers an SCA. As we acknowledge the importance of AEDs, there is also a vested interest in improving the portability of defibrillators. Historically, they have been bulky and cumbersome to transport efficiently, particularly in non-traditional settings. The first step towards achieving this goal is reducing the patient's transthoracic impedance (TI), which serves as a barrier preventing the optimal delivery of shock energy. One promising avenue involves advancing microneedle (MN) electrodes to tackle the electrode-skin barrier, a key element of TI that can be externally mitigated. The purpose of this study was to assess the feasibility and effectiveness of MN based AED electrodes through a functional proof of concept.

An iterative design and experimentation approach was used to evaluate various electrode prototypes. A circuit for measuring interelectrode resistance was created to mimic the functionality of an operational AED, providing quantitative assessment of the resistance at the electrode-skin interface. Test specimens comprised of a multitude of animal skin samples, with a gradual transition to human cadaver mediums. The final pad iteration consisted of 8 arrays of microneedles, fabricated using bulk micromachining, and affixed to a flexible 3D-printed TPU base. Each cluster was made of gold-coated silicon, featuring 25 needles per cluster and a needle height of 0.7mm, resulting in a total conductive area of 13.52 cm^2. Due to resource constraints, it was not feasible to manufacture an MN pad of equivalent size, which would have been eight times larger. Therefore, an extrapolated experimental approach was employed, where the performance of the 8 microneedle clusters was evaluated, and the behavior of the cluster numbers equivalent to the AED pad was inferred. In a direct pad comparison, the results indicated an average 20% reduction in human transthoracic skin resistance for a single MN pad. With increased efficiency, it was conjectured that the performance of an AED could be proportionally downscaled by 35%, resulting in the reduction in size and weight of all major components. Preliminary biocompatibility and safety evaluations concluded that the MN electrodes are safe and have the potential to improve safety compared to conventional methods. In the end, the advancement of AED microneedle electrodes makes a substantial impact in the field by further optimizing the effectiveness of AED defibrillation, improving portability, and consequently enhancing patient outcomes by raising the survival rate of sudden cardiac arrest.

Acknowledgements

I would like to express my deepest gratitude to my supervisors, Dr. Naveen Chandrashekar and Dr. Manoj Sachdev, for their unwavering support, invaluable guidance, and great insights throughout the course of my master's thesis. Their expertise and encouragement have been instrumental in shaping the direction of my research and furthering my growth as an engineer. I would also like to thank Tom Gawel, Dr. Sanjit Jolly, and Sheida Gohardehi for their encouragement, aid in procuring equipment, and constructive feedback. Furthermore, I wish to express my sincere appreciation to Dr. James Tung and Dr. Duane Cronin for dedicating their time and offering invaluable contributions as members of my thesis reading committee.

Additionally, I am grateful to Dr. Bo Cui and his PhD student Zihao Wang from the Waterloo Institute for Nanotechnology, for their collaboration and assistance in manufacturing the microneedle arrays utilized in the final prototype. I would also like to express my appreciation to Tamara Maciel from the School of Anatomy for her assistance in procuring suitable test specimens and coordinating human cadaver experiments.

I am also indebted to my lab mates Raj Indira, Dhanush Indira, Mercy Ombogo, Pratishtha Gupta, Howard Kao, Anandita Gautam, and my undergraduate research assistant Vanessa Chen for their collaboration, support, exchange of ideas, and their assistance in running experiments.

Lastly, I am grateful to my parents, family, Daisy Chak, and other close friends for their unwavering love, patience, and encouragement during this endeavor. This journey would not have been possible without the support of each and every one of you.

Table of Contents

List of Figures

List of Tables

Chapter 1

1. Introduction

1.1. Project Motivation

In emergency medical care, defibrillators play a pivotal role in restoring the heart to a regular, healthy rhythm during critical cardiac events stemming from heart conditions such as arrythmia and other heart abnormalities. Despite advancements in technology, the effectiveness and accessibility of these life-saving devices can be significantly compromised by their limited portability. The traditional bulky design of Automated External Defibrillators (AEDs), coupled with the cumbersome nature of large electrode pads, presents substantial challenges in swiftly deploying these devices in critical situations, particularly in non-traditional settings such as homes, public spaces, and remote areas without access to direct medical care. On average, an AED weights between 2.5 – 7 pounds and ranges from 92 – 570 cubic inches in volume [1]. As a comparison, this would be equivalent to carrying a 17-inch laptop which can be demanding for most. In terms of retail cost, an AED can range between $1,200 to upwards of $3,000 [2].

A sudden cardiac arrest (SCA) is one of the most prominent and life-threatening forms of cardiac events, which typically requires immediate defibrillation and cardiopulmonary resuscitation (CPR). According to the SCA foundation, SCA causes 356,000 deaths in the US annually making it the third leading cause of death [3]. SCA occurs when the heart suddenly stops beating, leading to the stoppage of blood flow within the body [4]. As this occurs, the person will lose consciousness and can die within minutes if blood and oxygen are not restored to the brain, among other major organs. As the vast majority (69.8%) of SCA's occur at home, with timely access to an AED, this can significantly improve their chances of survival [3]. Recognizing the critical importance of rapid defibrillation in improving patient outcomes, there is a growing imperative to enhance the portability of defibrillators through innovative advancements. In this context, one promising avenue lies in the development of improved electrode pads that not only facilitate easier deployment but also optimize the efficacy of defibrillation interventions. The primary challenge in reducing overall weight, the majority being the battery and electronics, is the transthoracic impedance of the human body. Despite a high degree of shock energy delivered from the AED, only a small part of that energy is delivered to the heart muscles, with the bulk of it scattered across the skin [5].

This thesis aims to explore the need for enhancing the portability of AEDs by integrating advanced microneedle-based electrode pads. Studies on electrode microneedle technology in other applications have indicated positive relevancy for AEDs, with the goal of improving the electrode-body interface. By tackling

this aspect, it facilitates a reduction in size and specifications of critical components such as the battery, capacitors, transformer, and housing, thereby enhancing portability. Moreover, this thesis seeks to contribute to the ongoing discourse regarding the optimization of defibrillator technology, including enhanced control and optimal delivery of energy, to facilitate broader and more effective use across various cardiac emergency situations.

1.2. Objectives

The primary objective of this study was to assess the viability and investigate the application of a microneedle-based electrode pad design for AEDs. Specifically, the objectives were as follows:

1. Design and develop a proof-of-concept microneedle pad design that is compact, user-friendly, and is compatible with AED devices, towards ease of integration if put into production.
2. Investigate the effects of this pad through experimental testing pertaining to advantages or disadvantages over a conventional AED pad. The experiment should emulate the behavior of an operational AED, with data presented regarding the effectiveness of microneedle electrodes in reducing the transthoracic skin impedance barrier.
3. Estimate and put into perspective through quantitative and qualitative means, what degree of potential benefit or drawback a microneedle AED pad would provide.

1.3. Thesis Overview

This thesis is organized into five chapters. Chapter 1 (Introduction) describes the motivation and relevant issue upon which this research is conducted and provides an overview of the objectives of this study. Chapter 2 (Literature review) covers the background of AEDs, current and state of art in terms of AED pad technology, microneedle technology, and previous studies based on microneedle pad development. Chapter 3 (Iterative Design of Microneedle Pads) presents the main experimental methodology and the five main iterative microneedle pad designs developed for this study. Under each design, the design process, variation of the experimental methodology, its quantitative and qualitative results, as well as justification on consequent pad design choices will be explored. Chapter 4 (Discussion) investigates the results of the current research, providing comparative context to a conventional AED pad. Additionally, this study will be compared with previous literature, identifying novel findings, and discussing potential contributions. Lastly, Chapter 5 (Conclusion) will present a brief conclusion for this study, its key limitations and gaps, and recommendations for future work.

Chapter 2

2. Literature Review

2.1. AED Background

Automated External Defibrillators (AEDs) have revolutionized the management of sudden cardiac arrests (SCA) by enabling timely intervention in non-medical, public settings. The current survival rate of patients who suffer from SCA is very low, approximately 25% in a hospital setting and 10 – 12% out of hospital [6]. The survival rate drops by about 10% every minute treatment is not delivered, with SCA being fatal if it lasts longer than 8 minutes [7]. Multiple studies have demonstrated the effectiveness of AEDs in improving survival rates from SCA [8], [9], [10]. The American Heart Association (AHA) reports that when bystanders use AEDs to deliver shocks within the first few minutes of SCA onset, the chance of survival can double (50%) or even triple (75%) [8]. For the purpose of increasing awareness and facilitating training, AED training equipment has been developed to simulate various usage scenarios, as depicted in Figure 1 below. By providing individuals with the necessary knowledge and skills to respond effectively to SCA emergencies and instilling confidence, this facilitates faster response times and heightens awareness of the importance of early intervention. Furthermore, AED deployment in public locations such as airports, schools, sports facilities, and workplaces have been associated with higher survival rates compared to reliance solely on emergency medical services [8].

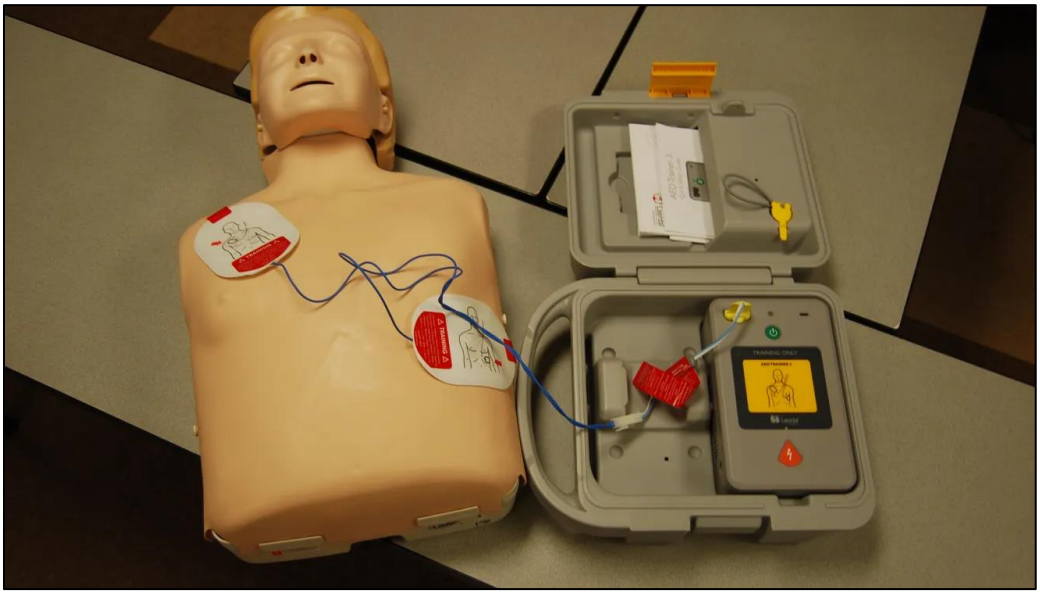

Figure 1 – AED training equipment [11]

The AED is a medical device that first analyzes a patient's electrocardiogram (ECG), the measure of electrical activity in the heart in order to establish whether the patient is suffering from SCA. Following SCA confirmation and properly identifying a shockable ECG rhythm, the AED will deliver an electrical shock through the chest in an attempt to restart the heart. Among the different types of abnormal heart rhythm, there are two types of shockable rhythm being ventricular tachycardia (VT) and ventricular fibrillation (VF) [12], [13]. Non-shockable rhythms include supraventricular tachycardia (SVT), atrial fibrillation (AF), premature ventricular contraction (PVC), sinus rhythm (SR), and so on [12], [13]. VT is marked by a rapid and consistent heartbeat, prompting the heart's ventricles to contract faster than usual, typically without significant interruptions in blood flow [13]. If VT is stable, meaning the patient has a pulse and is fully conscious, treatment may consist of medications to slow the heart rate or allow the rhythm to self-correct [14]. Alternatively, if VT leads to no discernible pulse and the patient loses consciousness, immediate defibrillation will be required to restore a normal heart rhythm. Pulseless VT can also escalate to more severe conditions like VF if treatment is not quickly administered within the first few minutes [14]. VF is characterized by a rapid, irregular heartbeat which also originates in the ventricles [13]. In contrast, this condition results in an immediate loss of pulse, loss of consciousness, and cardiac arrest, necessitating immediate defibrillation [15].

Most modern AEDs utilize direct current (DC) in the form of a biphasic waveform, where the direction of the current flow reverses during each phase of the shock to deliver the shock energy [16]. The energy delivered typically ranges from 120 to 200 joules for biphasic waveforms with an upper limit of 400 J and currents ranging from 20 to 40 amperes with a limit of 50 A, depending on the AED and the patient's condition [17], [18]. A typical AED will deliver a shock for 3 (0.003s) to 9 (0.009s) milliseconds with an average resuscitation requiring 2 – 3 shocks [19]. The number of shocks required for resuscitation can vary depending on several factors, including the underlying rhythm causing arrest such as ventricular fibrillation (type of arrhythmia), response to initial shocks, the distinct AED algorithm tailored by each AED manufacturer, and other medical protocols [20]. Although the voltage stored for defibrillation in an AED ranges from 2000 to 5000 volts via the capacitor, the actual voltage delivered to the heart is between 200 to 1000 volts based on the energy level selected by the AED [21]. The relationship between these electrical characteristics is expressed as follows:

$$\boxed{Energy\ (Joules) = Potential\ (Volts)\ \times\ Current\ (Amperes)\ \times Time\ (seconds)}$$

Despite their effectiveness, transthoracic impedance (TI), which refers to the resistance encountered by an electric current as it passes through the chest wall and skin to the heart, can drastically hinder their efficiency [5]. According to a study by Charbonier, the TI of a human ranged between 35 – 125 ohms, at a defibrillator discharge energy of (200 – 360 J) using typical electrodes, for the 95% of the 300 evaluated patients in the study [17]. Contemporary AEDs estimate a patient's TI impedance prior to shocking, but often 75 ohms is chosen as the median value for shock energy estimation [5]. With higher transthoracic impedance, this can result in a large portion of the electrical energy being dissipated as heat, requiring higher shock energy levels and a multitude of shocks for a successful defibrillation. As a consequence, localized mild to severe skin burns are a common occurrence as a result of defibrillation [22].

External factors influencing the transthoracic impedance (TI) include skin thickness, moisture content, presence of hair, and the skin contact quality of the defibrillation electrodes [23]. Internally, TI may be comprised of elements including chest wall thickness, presence of fluids, and other tissues between the electrode pads and the heart [23]. Optimizing TI is crucial for effective defibrillation. Although existing techniques such as ensuring proper pad placement, adequate skin preparation such as shaving or cleaning the skin and using conductive gel (if required) can help reduce TI, further optimization is possible. Skin impedance (SI), the measure of the skin's ability to conduct electricity, is one of many critical components affecting the efficacy of defibrillation. Although the aforementioned techniques aim to limit moisture content and surface contamination to improve skin impedance, other factors such as skin thickness, temperature, and condition, are not factors which can normally be controlled.

While the contributions of SI to TI varies from person-to-person, with no definitive estimate as a whole, literature has demonstrated that it is the major contributor for transthoracic impedance and a factor which can be further optimized, unlike all other internal aspects [24]. In a study performed to evaluate the contribution of skin impedance to TI during external defibrillation in correlation with external paddle force and lung volume changes, there was an observed reduction in TI where 84% of that reduction was a result of improved electrode-skin contact and 16% was the change in lung volume [25]. Based on the project motivation, the goal is to break the skin impedance barrier to bypass this critical contributor of TI. Through the use of an innovative advancement in defibrillator pad technology, the intent would be to further increase the efficacy of the electrode-skin contact and bypass a large percentage of the skin impedance, lowering the transthoracic impedance.

2.2. Human Skin Characteristics

To understand the skin impedance and to evaluate a criterion of the project, the composition of the skin must first be explored. The skin is the largest organ in the body and is comprised of three main layers, the epidermis, dermis, and hypodermis, as shown below in Figure 2 [26]. The epidermis is the outermost layer of the skin, primarily composed of cells called keratinocytes and acts as a protective shell to the tissues below. As these cells are tightly packed, they have a relatively high resistance to electrical current flow [27]. The stratum corneum, the outermost and majority layer of the epidermis, consists of dead keratinocytes also known as callused skin, which further contributes to its electrical resistive properties along with the lack of moisture in the epidermis [28]. The dermis is connected to the epidermis at the next level of the membrane, which provides skin with its strength and elasticity [26]. This layer is comprised of various structures such as blood vessels, nerves, hair follicles, and sweat glands intertwined in a matrix of connective tissue [28]. While the dermis provides structural support to the skin, it has a lower resistance to the electrical current compared to the epidermis, due to its higher water content and presence of electrolytes in the interstitial fluid, the fluid found between blood vessels and cells [27]. Particularly, conductive structures such as blood vessels and sweat glands contribute to the conductivity of the dermis. Lastly the deepest layer of the skin, the hypodermis is mostly comprised of fat meant for body insulation, energy storage, and shock absorption [26]. Similar to the dermis, this layer has a relatively low electrical resistance compared to the dermis and epidermis due to its high water and electrolyte content. While the electrical resistance of the skin varies across its layers, the epidermis remains the most resistive of the three.

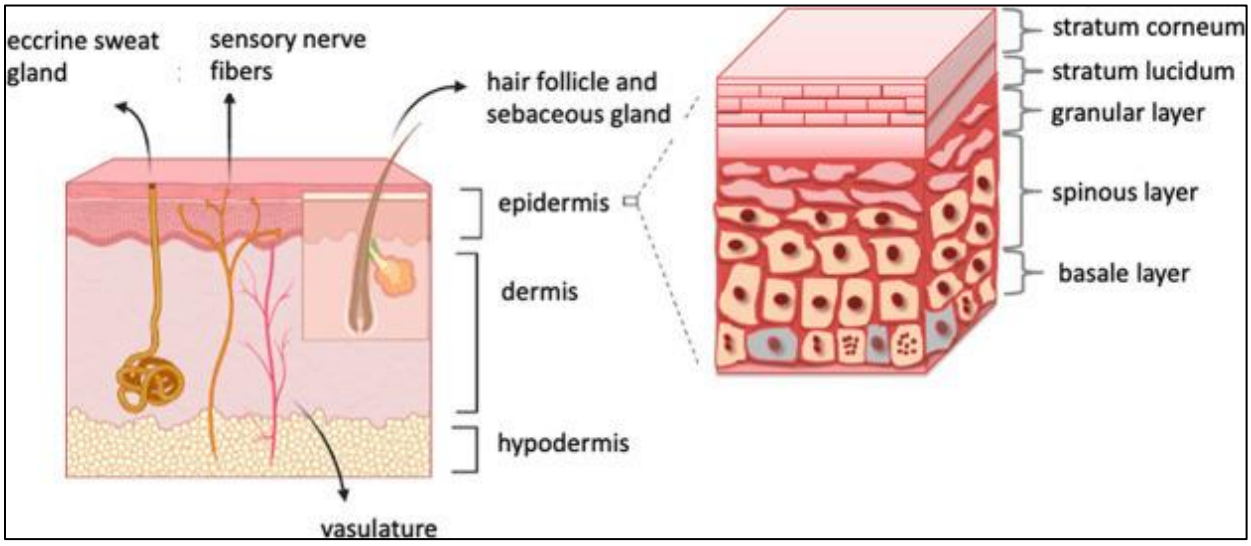

Figure 2 – Skin anatomy [29]

Regarding the skin resistance, sex and gender implications have shown variance between each cohort. Apart from the clear anatomical differences between genders concerning the areas of defibrillator pad deployment, studies have shown that the skin impedance was directly proportional to the body mass index (BMI) as per the skin breakdown above in Figure 2. Notably, there was a higher proportion of females in the upper-impedance group than males [30]. Although there is no inherent gender bias in the effectiveness of defibrillation, a study on gender-based inequalities in access and application of AEDs have illustrated that women were less likely to benefit from access to an AED [31]. Apart from the BMI index, other factors such as the underlying cause of SCA, timing of treatment due to the presentation or lack of symptoms, bystander response to initiate CPR and treatment delivery, and anatomical differences in effectiveness of pad placement, are all influential factors beyond gender alone.

As a design constraint, the thickness of the skin is important to consider, particularly the stratum corneum of the epidermis layer where most of the skin impedance is present. Of course, the thickness of each layer varies depending on the region of the human body, age, gender, skin type, and other dermatologic characteristics. The thickness of the epidermis can vary from the eyelid with the thinnest epidermis, to the genitalia, to the thickest parts of the palms and soles where they are callused and are highly dependent on lifestyle. On average the epidermal thickness ranges from 0.05mm to 0.15mm (50µm – 150µm) [26], [32]. Likewise, the stratum corneum layer ranges from 0.01mm to 0.03mm (10µm – 30µm) [33]. Specifically for the chest area, the epidermis layer tends to fall within this range. Likewise, the dermis layer of the skin also varies but on average, ranges between 1mm to 4mm [34].

2.3. Current Electrode Technology for AEDs

Since the late 1960's, when Prof. Frank Pantridge and Dr. John Geddes first introduced the concept of a portable battery-powered DC defibrillator to the 1990's, when the first commercially successful AED (the 'Heartstream ForeRunner') was introduced by Phillips, AED technology has continued to advance [19]. Today, electrodes used for defibrillation appear in a variety of materials, sizes, and shapes, to satisfy the requirements of a range of applications depending on the manufacturer [18]. However, they all share a common feature which is to serve as the transfer medium for externally generated currents. These electrodes are designed to operate in a resistive coupling, where the electrodes are directly applied to the patient's skin, as opposed to capacitive coupling, where an insulating medium such as an additional conductive gel or pad is placed between the electrodes and the patient. While capacitive coupling may be more consistent in the uniform distribution of electrical energy, particularly in patients with high skin impedance, and can

help reduce the electrode-skin barrier, it is not as straightforward for the user nor practical for remote settings [35]. Alternatively, resistive coupling is a simple and straightforward method that effectively ensures the proper transmission of electrical energy for patients with normal skin impedance, but its performance is more susceptible to factors such as electrode placement and skin condition, as discussed prior [18]. In conjunction with the resistive electrode coupling, low-frequency currents are used, as they are better suited to penetrate through the skin and the underlying tissues. As low-frequency currents have longer wavelengths compared to their high-frequency counterpart, this characteristic allows them to penetrate the skin more effectively [36]. Additionally, low-frequency currents have shown to conduct more through muscle and fatty body tissues, overall increasing the delivery of electrical energy [18].

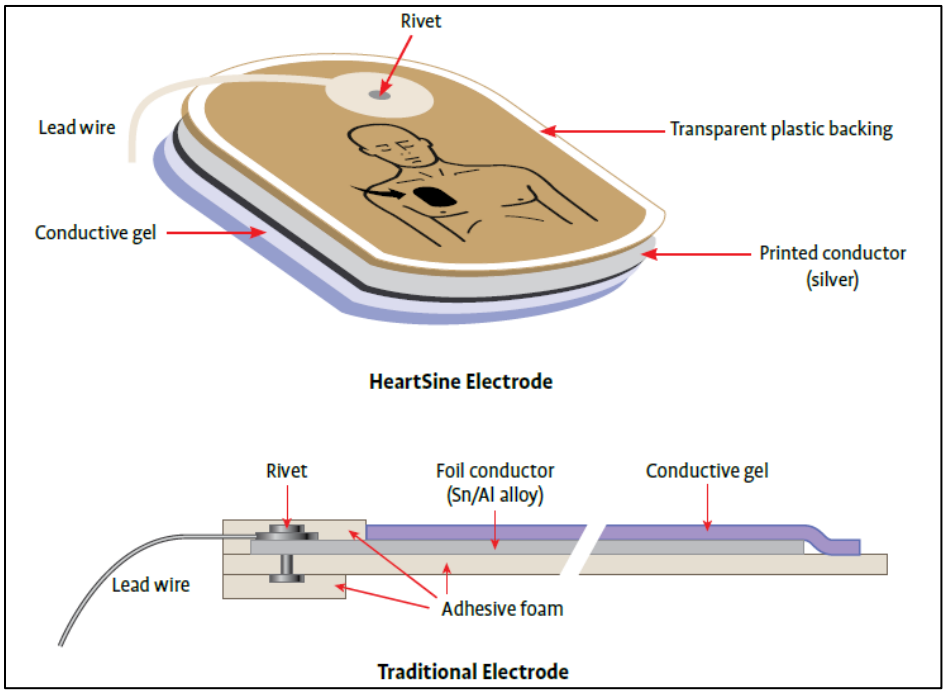

Figure 3 – HeartSine AED electrode composition (Resistive Coupling) [37]

Although there are different kinds of electrodes such as hand-held paddles, internal paddles, or self-adhesive, AED electrodes are generally disposable electrodes. These electrodes have a large paddle size which improves the electrode-surface contact and allows a more uniform distribution of electrical energy across the skin surface [19]. Typical manufacturers offer adults paddles between 8 – 13cm in diameter, and equivalent pediatric paddles, which are naturally smaller to account for chest size [19]. These electrodes are pre-gelled with a combination of ingredients that may include water as the base, glycerin to prevent evaporation, a thickening agent to create a desired viscosity, some form of electrolyte such as sodium

chloride or silver chloride to increase conduction, and preservatives to ensure sterility [38], [39]. Depending on the manufacturer, the electrode's conductive metal film may be comprised of combination of conductive materials or alloys such as stainless steel, tin, aluminum, or silver [19]. To connect to the AED, a cable is soldered or cinched onto the metal plate and fitted with an appropriate adapter. Lastly, these components are secured on a foam backing with a skin-adhesive border, to generate mechanical stability and provide a degree of electrical isolation. An example of the composition of a HeartSine electrode, acquired from its AED electrode documentation, is shown above in Figure 3.

2.4. Microneedle Technology Overview

Microneedle (MN) technology has emerged as a promising approach for various biomedical applications including electrode applications for biosensing, drug delivery, diagnostic purposes, and even cosmetics. Particularly, this brief review will focus on the microneedle types, materials, and fabrication processes specifically tailored for electrode applications. Key design considerations, performance metrics, and recent advancements in the field will be highlighted.

Microneedles are typically characterized by their micron-scale structures, typically measuring 0.1 – 1mm in length for transdermal interaction, bypassing the epidermis layer of the skin [40]. Among the diverse applications of microneedles, literature is most prominently represented by drug delivery and biosensing, where their role as electrodes holds particular promise. The significance of microneedle-based electrodes stems from their unique capabilities to interface with the human body at a microscale level. Unlike conventional electrodes, which are large and bulky, microneedle electrodes offer a minimally invasive approach that enhances patient comfort, reduces tissue damage via a reduction in the necessary energy delivered via an AED or an avoidance of the blood vessels, and enables better control over sensing and stimulation in the case of biosensing or neuromuscular treatment applications [40]. Microneedles do not typically penetrate deeper into the dermis as it contains pain receptor nerves and blood vessels which the MN could puncture. As the needles are long enough to bypass the epidermal barrier but short enough to prevent damage to the dermis or reach nerve endings, the microneedle arrays are designed to be painless. As such, the MN arrays are fabricated to bypass the high impedance layer of the stratum corneum in the epidermis, establishing direct contact between the more conductive layer of the skin, without essential skin preparation [41]. Similar to the high degree of skin impedance by the epidermis, the stratum corneum also prevents the permeation of drugs through the skin [40]. In the case of transdermal drug delivery, various methods and their penetration level are shown below in Figure 4, as a comparison to an MN patch.

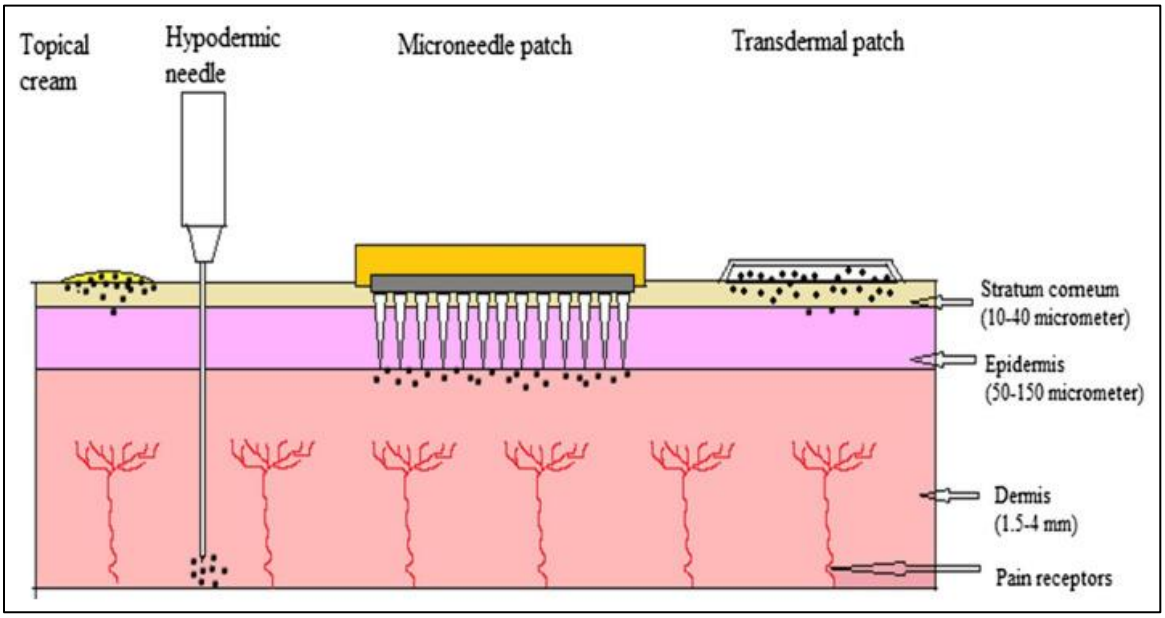

Figure 4 – Transdermal drug delivery systems [40]

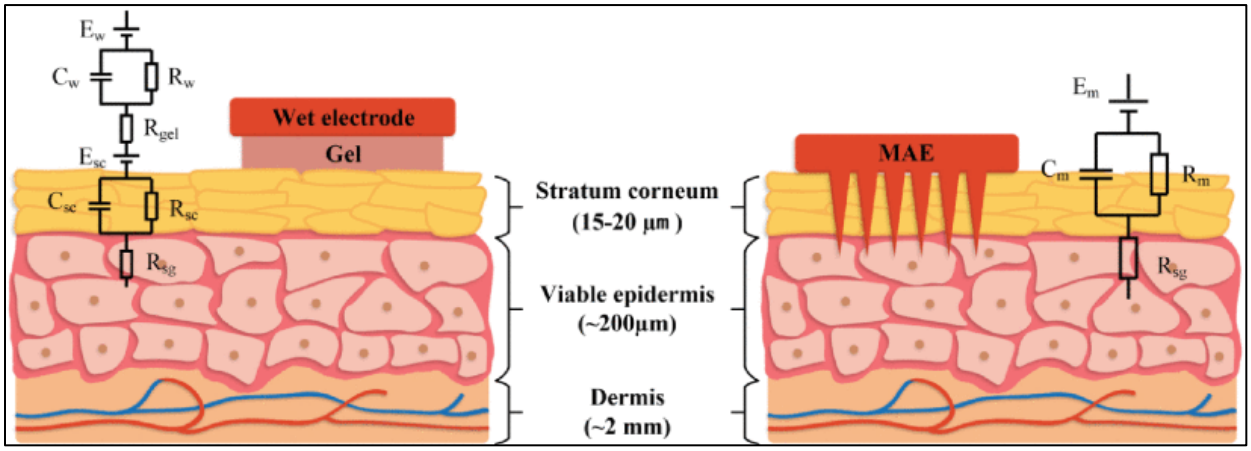

Figure 5 – Equivalent electrical circuit models of (a) typical wet electrode, and (b) MN array [41]

Critical to the success of microneedle-based electrodes are their performance characteristics and biocompatibility. The performance of an electrode directly impacts its ability to accurately sense bioelectrical signals for human biopotential monitoring, deliver therapeutic stimuli such as electrical current for AEDs or electrical stimulation, or facilitate molecular transport in drug delivery across biological barriers. Furthermore, ensuring the biocompatibility of these electrodes is paramount to minimize tissue reactions, inflammation, and immune responses [40]. Specifically for electrodes, factors such as skin impedance, electrode impedance, and signal-to-noise ratio, determine the efficacy and reliability of a MN

based system [40]. In a review for MN electrode technology in biopotential monitoring, the authors illustrated a simplified circuit model in Figure 5, which appropriately represents the performance constraints of an MN needle array to a typical wet electrode, the same as an AED electrode paddle.

First, in the case of a typical wet electrode setup, the impedance of the electrode-skin interface is modelled as a combination of capacitance (C_{sc}), resistance (R_{sc}), and half-cell potential (E_{sc}), which is the electrical potential difference between the two mediums due to differences in electrochemical properties. For the wet electrode, it is simplified in the form of a basic parallel RC circuit, which is a circuit element consisting of a resistor (R_w) and a capacitor (C_w), connected together in series with a resistive gel (R_{gel}). The untreated stratum corneum layer possesses both a resistive and capacitive component, where the viable epidermis (R_{sg}) has been determined to be purely resistive, according to literature [41]. Likewise, an equivalent circuit setup can be made for the MN array. As an immediate observation, the high impedance of the stratum corneum and electrolyte gel are removed as the MN array makes direct contact with the viable layer of the epidermis. With this component removed, in principle, the impedance of the MN array becomes lower than an interface with a wet electrode [41]. The keynote regarding this comparison is that by lowering the skin impedance in a subdermal manner, in coherence with previously limited surface-only skin-preparation techniques, the transthoracic impedance will be further lowered, thus improving AED performance.

In addition to their electrical performance, microneedle electrodes must also possess strong mechanical properties to endure the applied forces during insertion. Factors to be considered include fracture performance, both axial and traverse forces applied to the MN, as well as penetration performance [40], [41]. For fracture performance, it is crucial that the microneedles do not break under load during insertion or removal and determining the failure point for each type of load is important. Research has demonstrated that the fracture performance was correlated with the geometrical dimensions of the MN. The fracture force of MN will increase as the wall thickness and base diameter increase, decreasing as it approaches the tip of the needle [41]. Likewise for penetration and removal performance, the MN tip radius, insertion depth, array density, and microneedle geometry all dictate performance [41].

Different microneedle types are fabricated with a variety of materials, depending on the range of applications. Four main types of microneedles exist: solid, hollow, coated, and dissolving. The brief characteristics of each needle are summarized below in Table 1. Furthermore, a functional demonstration of drug delivery via these various microneedles is presented following this table in Figure 6.

Table 1 – Microneedle Types [40], [42]

MN Type	Characteristics	Common Materials
Solid	Creates solid microscopic channels in the skin for enhanced drug delivery, biosensing, or tissue sampling	Silicon, metal, polymers
Coated	Solid microneedles that are coated with a dissolvable coating to release an encapsulated drug or therapeutic agent	Silicon
Dissolving	Dissolving microneedles that rapidly degrade or dissolve releasing an encapsulated drug or therapeutic agent	Polymers
Hollow	Hollow microneedles feature a channel along their length allowing for direct delivery of drugs, fluids, or biomolecules into the dermis and/or for systemic circulation	Silicon

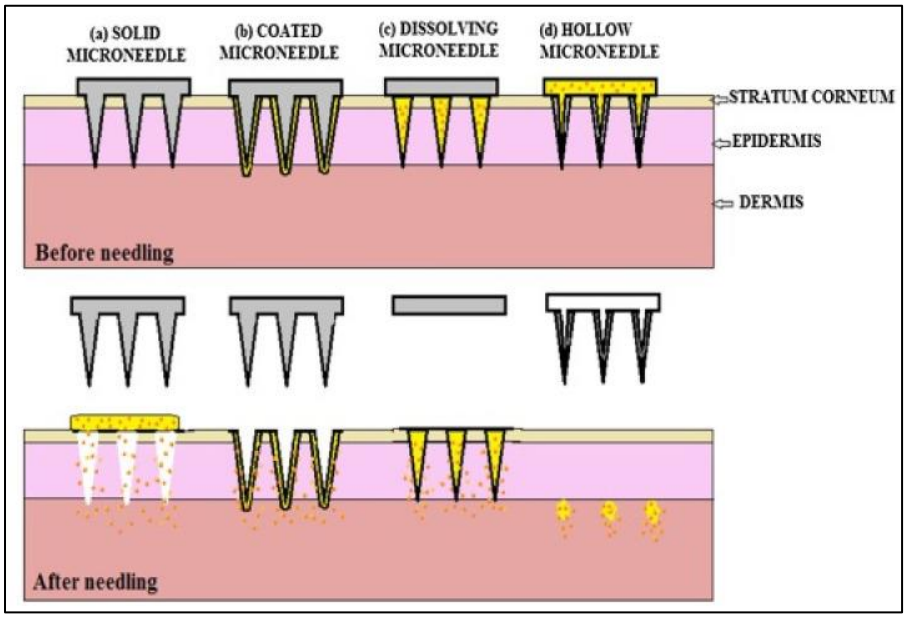

Figure 6 – Comparison of MN types for drug delivery applications [40]

Based on the required needs of biopotential electrodes, a solid microneedle type is typically used due to its simplicity and typically better mechanical strength, versus its counterparts [40], [41]. In addition to performance and biocompatibility, fabrication techniques also play a pivotal role in shaping the design,

functionality, and scalability of MN electrodes. The most common methods for solid MN manufacturing include 1) fabrication without a mold: surface/bulk micromachining, laser engraving, micro-milling, and 3D printing, and 2) fabrication with a mold: injection molding [40], [42]. Each of these fabrication techniques enable the precise fabrication of micron-scale structures with tailored geometries, surface properties, and material compositions. Of course, the advantages, disadvantages, cost, and ease of production vary between each process, in addition to its scalability for commercialization. Lastly, the typical diameter of a microneedle can vary according to method of fabrication, needle type, and purpose. However, for solid microneedles specifically in drug delivery, the normal base width ranges from 50μm to 250μm (0.05mm – 0.25mm) and from 1μm to 25μm (0.001mm – 0.025mm) at the tip [43].

2.5. Experimental Studies and Prototypes

For literature on experimental studies that focus on microneedle architecture, a variety of approaches were used to address the relevant issue, specific to its application area. For this study, the literature focused on electrode development for ECG biopotential signal monitoring and biofeedback stimuli comparisons. Due to the novelty of MN architecture for AED use in particular, the experimental literature in this area was rather limited. However, by evaluating the objectives, experimental design, and biometric results for a broader range of electrode applications, a parallel can be established concerning important factors such as electrode-skin impedance, electrical conductivity, usability, and magnitude of biosignal improvement.

2.5.1. Biopotential Signal Monitoring Applications

Bio-signal monitoring mainly consists of one of three measurements, ECG, EMG, and EEG. The experimental studies on bio-signal monitoring are comprised of performance comparisons between MN and a dry or wet electrode counterpart. ECG is the process of monitoring the electrical activity of the heart via electrodes. The electrodes are responsible for detecting the small electrical changes on the skin that arise from the heart's electrophysiological pattern with each cycle of the heartbeat [41]. Specifically, the heart's rhythm, rate, electrical conduction pathways, spatial positioning of the heart chambers, damage to heart muscles, and function of implanted pacemakers, can be obtained using the ECG signal, the same signal an AED algorithm uses to assess patient state as discussed prior [41], [44]. On the other hand, EMG is a diagnostic technique used to assess the electrical activity produced by muscles and the nerves controlling them [45]. The electrodes are responsible for recording the response of muscles, at rest and in their contracted states. This technique is often used to diagnose neuromuscular conditions or in rehabilitation applications, to act as a control signal for prosthetic devices. Likewise, EEG is a diagnostic test pertaining

to the measurement of electrical activity in the brain. The EEG waveforms provides information regarding brain activity including abnormalities, electrical rhythms, and patterns of neural firing [46]. EEG is used to diagnose or monitor various neurological conditions such as epilepsy, sleep disorders, tumors, and injuries to the brain.

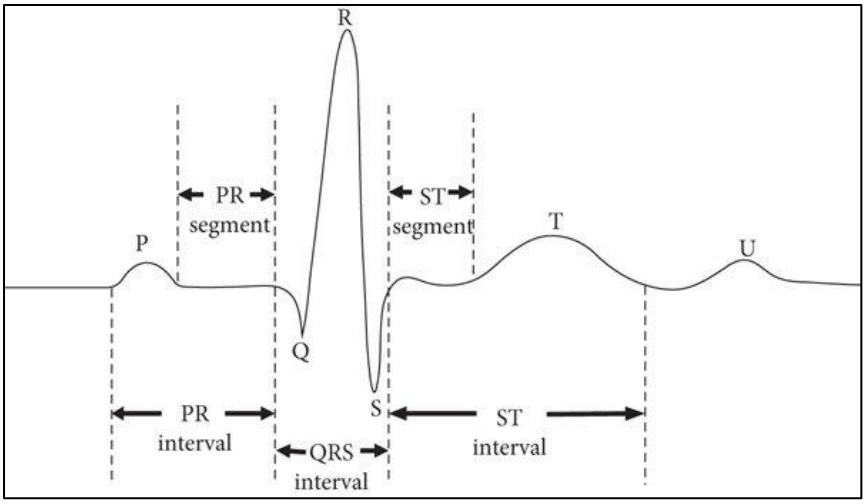

Figure 7 – Complete heartbeat cycle, ECG waveform [47]

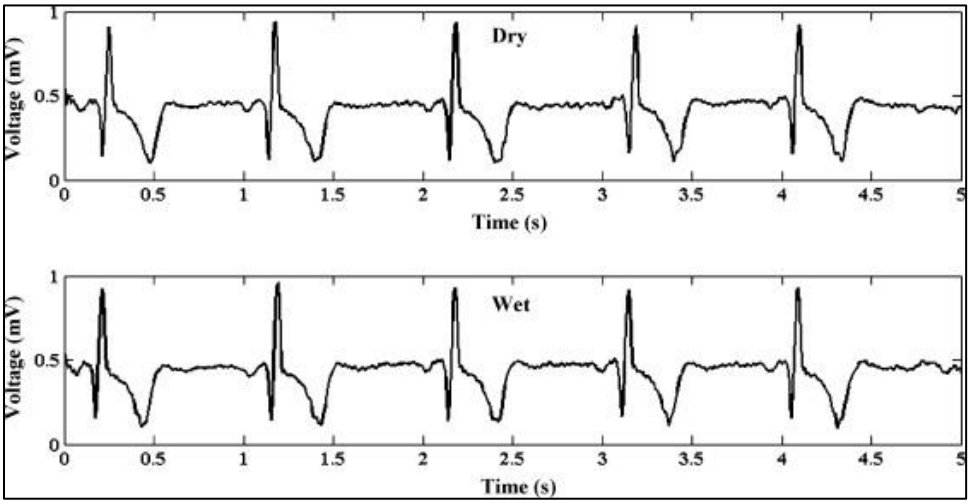

Figure 8 – Typical ECG waveform [48]

Literature pertaining to the measurement of static ECG signals was investigated. Specifically in these studies, the signal performance was compared between conventional dry or traditional wet (Ag/AgCl) electrodes and a MN electrode prototype. To identify a high-fidelity signal, specific characteristics of the ECG signal particularly the P node, QRS interval, and S node waveform must be repeatable and identifiable,

as shown above in Figure 7. An example of this comparison performed by Salvo et al., demonstrates the repeatable behavior with each cycle repetition, as shown above in Figure 8 [48]. Likewise, in Forvi et al. [49], Yu et al. [50], O'Mahony et al. [51], Hsu et al. [52], Matteucci et al.[53], or the aforementioned Salvo et al. [48] studies on microneedle dry electrodes, the authors demonstrated and concluded that the MN electrodes were comparable in performance to the conventional electrode variant. Additionally, as observed by several authors, the ECG signals recorded by their microneedle pad variants had higher amplitudes, as opposed to those recorded by a dry or wet electrode alternative. Sun et al. designed and fabricated a composite microneedle array electrode (CMAE) for detection of body temperature and the three aforementioned bio-signals [54]. In this study, the temperature measurement performance of the MN electrode was similar to that of a clinical thermometer. For the ECG signal in particular, the amplitude of the MN pad was visibly higher than that of the Ag/AgCl electrode, despite identical waveforms, as shown below in Figure 9. Likewise, O'Mahony et al. [51], Chen et al. [55], Dong et al. [56], Ren et al. [57], [58] also observed this behavior in their experiments. Specifically, Ren et al. and Dong et al. provided a good explanation of this phenomenon. By penetrating the stratum corneum layer of the epidermis where the bulk of the electrically isolating skin barrier is present, signal attenuation, which is the loss of signal strength, is hereby reduced.

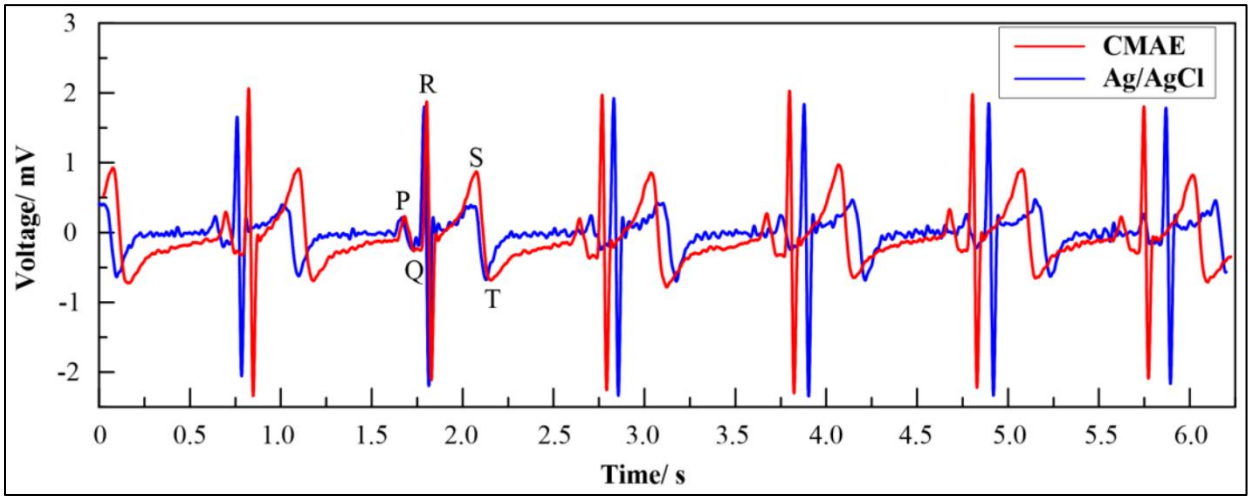

Figure 9 – ECG signals by MN and Ag/AgCl electrodes [54]

Apart from a distinguishable amplitude difference, noise and signal fluctuation were also observed from the dry or wet electrode alternatives in several studies. Specifically, in Srivastava et al. where they evaluated the fidelity of microneedles for long term biopotential monitoring in vivo, the conventional wet electrodes showed a baseline drift and signal disruption within 2 hours after application [59]. In comparison,

the dry MN variant demonstrated equivalent signal amplitude and characteristics without any variance in the same time frame, as illustrated below in Figure 10. Likewise, Yu et al. [50] and Ren et al. [57], [58] as discussed prior, also observed this occurrence. Dong et al. once again commented that this behavior was a result of the increased contact with the inner skin, reducing the electrode-skin barrier [56]. With time, the impedance of the skin causes a distortion or interference with the ECG signal in the gel electrodes, while this effect was minimized in the dry MN electrodes. Additionally, the signal-to-noise ratio (SNR) becomes enhanced, improving clarity and accuracy of the ECG waveform. Over time, although not immediate, gel electrodes can begin to be affected by factors such as evaporation or drying, skin oil and sweat, or physical wear and tear in a dynamic scenario, all which will impact signal strength, stability, and increase the electrode-skin interface impedance [60], [61].

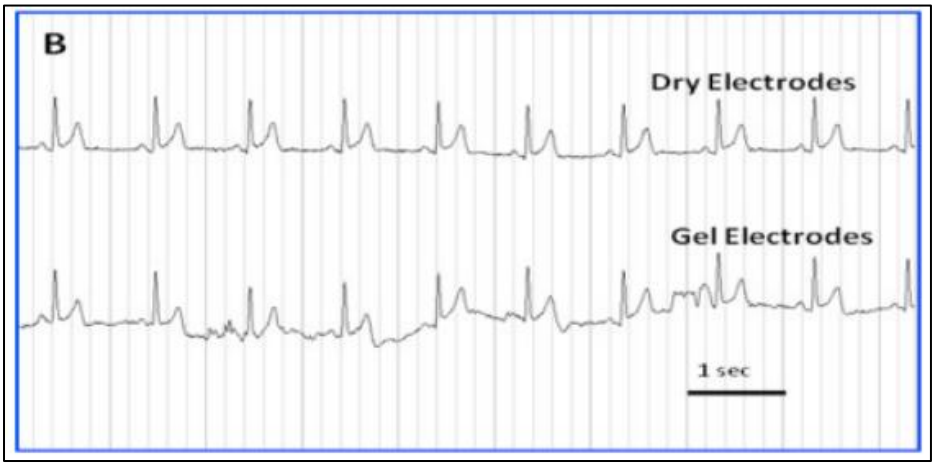

Figure 10 – Dry MN electrode vs gel electrode ECG signal [59]

2.5.2. Electrode Feedback Applications

Apart from being utilized as a biosensing component, MN electrodes have also been used in a more active role. In this role, electrodes have a performance responsibility to provide a transfer of current or voltage into the skin, such as for electrical feedback [41]. Kitamura et al. and Tezuka et al. utilized MN electrodes to develop a thin wearable electrotactile display [62], [63]. The purpose of this device was to allow someone with a sight or hearing disability, to compensate for information using tactile sensation, as a wearable module. Using low voltage, the device would invoke a tactile sensation in the user by stimulating the tactile nerves. The threshold voltage, which was the minimum voltage at which the test subject felt a tactile sensation, was experimentally compared at different points on their arm. The results demonstrated that the

MN device drastically decreased the threshold voltage required to stimulate the tactile receptors, roughly between 70% – 85%, as shown below in Figure 11.

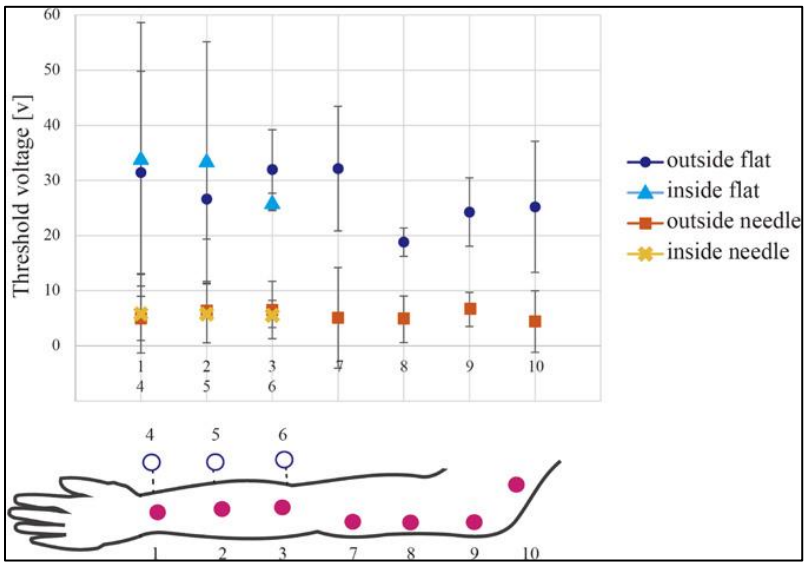

Figure 11 – Distribution of threshold voltage on arm [63]

In Tang et al., they utilized MN electrodes for a bidirectional physiological signal acquisition and transcutaneous electrical nerve stimulation (TENS) sensory feedback [64]. In the TENS experimentation, the MN unit functioned properly and presented a similar performance to regular wet electrodes. Specifically, in their measurement of the electrode-skin interface impedance using an RC parallel circuit model for four test subjects, this circuit briefly covered in section 2.4 – microneedle technology overview, the MN (MAE) demonstrated lower resistance (R) and total impedance (Z) than the wet electrode (FAE) samples at low frequencies. At high frequencies, the R, C, and Z values were very similar. The average values at 20 and 2000 Hz across the four subjects are presented below in Table 2.

Table 2 – Average values of R, C, and Z across four subjects [64]

	FAE		**MAE**	
Frequency (Hz):	**20**	**2000**	**20**	**2000**
R (kΩ)	2560 ± 1246	141 ± 24	298 ± 106	103 ± 60
C (nF)	5.8 ± 2.4	2.5 ± 0.9	23.3 ± 11.2	0.6 ± 0.7
Z (kΩ)	1275 ± 462	34 ± 10	240 ± 93	94 ± 56

2.5.3. AED Electrode Applications

Specific to AED or defibrillator electrode applications, an experimental study was conducted based on the comparison between a needle-based electrode add-on and a conventional AED electrode, by evaluating the electrode-surface interface impedance. No other existing study has evaluated the actual functional aspects of an MN AED electrode beyond ECG evaluation of normal MN prototypes, as discussed before.

A team of bioengineering students at Rice University developed a 3D printed needle add-on prototype, for use with conventional defibrillator pads to reduce the skin impedance barrier [65], [66]. The goal of this device was to allow the existing architecture of an AED to function as normal, where the AED would still be able to measure an appropriate ECG signal for defibrillation. The construction of this device was comprised of 3 layers: a 180 stainless-steel sequin pin (roughly 0.6mm diameter) array mounted on a 3D printed needle base, insulating foam layer, and a plastic casing for needle deployment purposes. Their prototype and device deployment method are illustrated below in Figures 12 and 13.

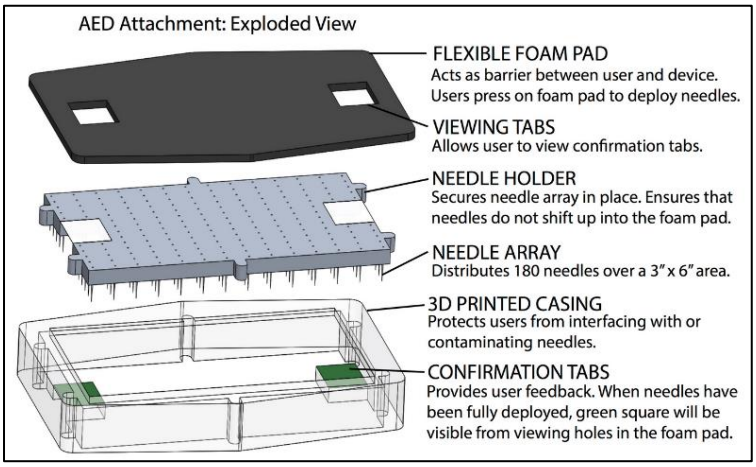

Figure 12 – AED add-on device construction [66]

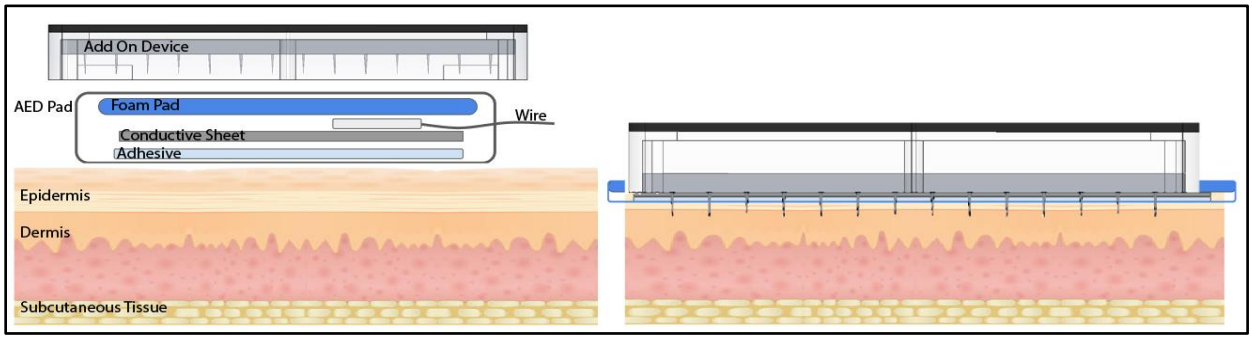

Figure 13 – AED add-on device deployment [66]

To evaluate the prototype, the authors performed a skin impedance test on a post-mortem ovine and pork tissue animal sample. For their experimental model, they utilized an AC (signal generator) powered circuit model, with an assumed to be, equivalent parallel RC circuit to measure the inter-electrode impedance. With the ovine animal sample, the combined needle-AED pad showed an average 70% reduction versus the conventional alone, with a slightly higher improvement in the lower frequency range. However, with the pork animal sample the average reduction was less definitive, with an average of 5% reduction in impedance. We can speculate that the variation in outcomes arises from notable differences in either skin resistance or inter-electrode resistance, as the authors have not provided any details regarding the test mediums or the experimental procedures. These results are illustrated below in Figures 14 and 15.

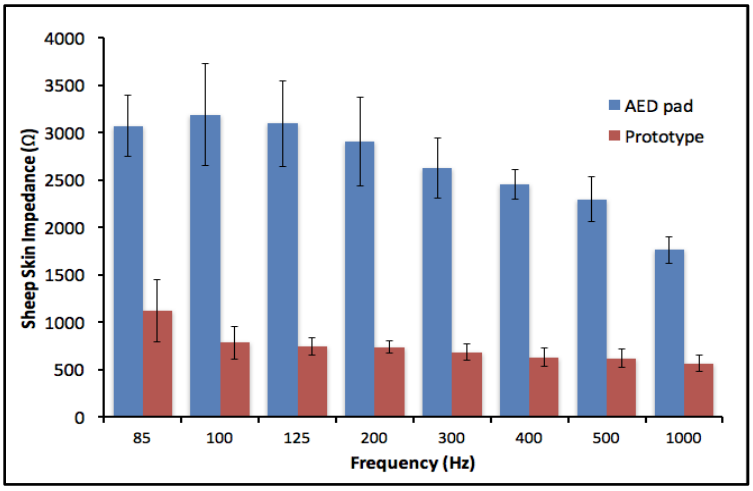

Figure 14 – AED add-on impedance results on ovine model [66]

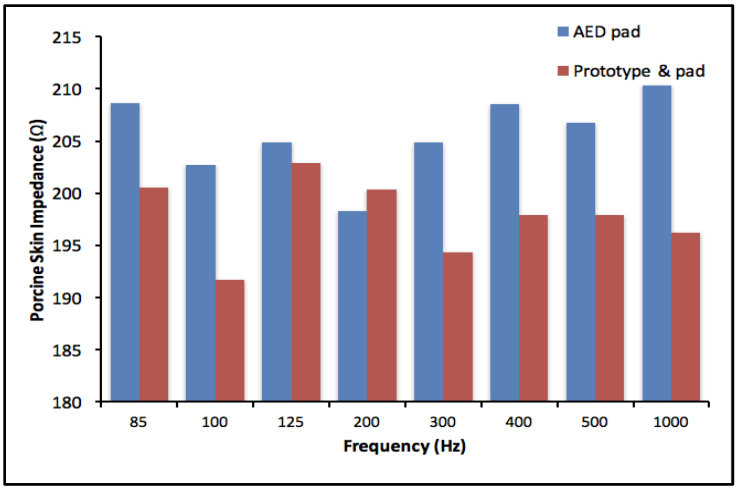

Figure 15 – AED add-on impedance results on pork tissue model [66]

2.6. Summary

This chapter provided an overview of the many parts required to develop a microneedle-based AED electrode. First, the functions of an AED were discussed, from the ECG algorithm to the impact of the transthoracic impedance on defibrillation. Second, the human skin characteristics both physically and electrically were discussed, specifically, the electrode-skin barrier concerning the stratum corneum of the epidermis. Third, we proceeded to dissect the current technology in both the AED defibrillator electrodes and microneedle technology used for electrode development. Lastly, experimental studies concerning microneedle electrode development for biopotential monitoring, electrode feedback, and AED electrode applications, were discussed. For biopotential monitoring, studies demonstrated that MN based electrodes had adequate or equivalent fidelity for ECG signal detection. For longer term monitoring, the MN electrodes exhibited higher performance with less noise and more accuracy compared to a conventional Ag/AgCl wet electrode. For bidirectional usage in electrode feedback applications, positive outcomes were recorded as the MN electrodes produced equivalent levels of feedback stimuli with a lower required input threshold. Additionally, the electrode-skin impedance was observably lower than its counterpart. Lastly, for the sole AED specific study, results showed a good percentage reduction in electrode-surface impedance for various animal test mediums, using a needle-based add-on prototype for a conventional AED electrode.

2.7. Hypothesis

The current study addresses the limitations of the current technology and the gaps from previous research, as presented. For this study, a microneedle-based AED electrode pad prototype was developed and experimentally tested for basic electrical function and effectiveness in reducing the resistance in the electrode-body interface. Based on this approach, it was hypothesized that:

1. The design of the microneedle pad prototype functions as a standalone electrode, with no issues in connectivity between the main lead and the microneedle arrays. This should be confirmed via a connectivity and resistivity test to evaluate the baseline resistance of the pad.
2. The experimentation on human or animal equivalent test mediums (whichever was accessible), exhibits a meaningful reduction in the electrode-skin interface resistance compared to a conventional AED electrode.

Chapter 3

3. Iterative Design of Microneedle Pads

The iterative design segment is separated into six main sections, each addressing the objectives as outlined in Chapter 1. Section 3.1 presents the primary experimental model for which all microneedle pad iterations were quantitatively measured by. Section 3.2 to 3.6 present the design and development of each pad iteration, their correlated experimental approach, and the justification of why a consequent design was developed, based on the quantitative results or unique performance characteristics observed.

3.1. Experimental Model

To develop a proof of concept that establishes that microneedles are providing a favorable effect, by bypassing the resistance inherently presented by the epidermis layer of the skin, this must be evaluated by some quantitative means. To validate each concept iteration, an interelectrode resistance measurement circuit was developed, based on literature which simulates the behavioral aspects of an AED charge and discharge cycle. Kugelberg utilized this process to determine the electrical resistance over a living human myocardium in youth and adults during defibrillation, without using an actual AED, internally and externally [67]. This procedure consisted of delivering a square electrical pulse, with a desired amplitude through a capacitor and controlled via a transistor to manage the pulse duration and interval, simulating the functions of a normal AED. In the first state of the circuit, the capacitor would be charged via a power source to its appropriate amplitude, defined by its capacitance rating. As the circuit is disconnected from the power source and connected solely to the resistance in its second state, the electrical energy would be consumed, discharging the capacitance. The defibrillator power circuit is illustrated in Figure 16.

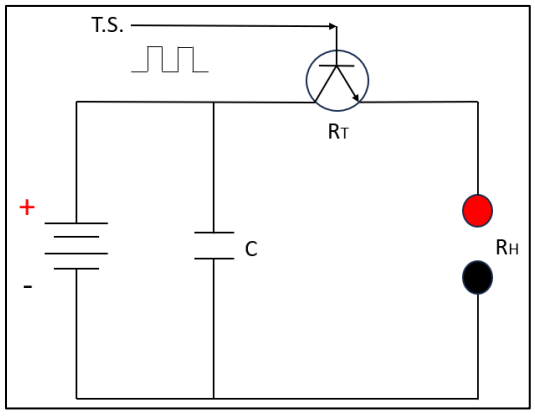

Figure 16 – Power circuit of defibrillator [67]

By measuring the voltage differential across the resistance and knowing the time it takes to discharge, the resulting resistance can be calculated. The following equation defined in Figure 17, mathematically describes the behaviors of the defibrillator circuit shown above [67]. In this equation, the voltage differential is represented by U_2 and U_1 in volts (V) respectively, T being the pulse duration in seconds (s), C being the capacitance in farads (F), and R in ohms (Ω) which is the resistance to be determined. A graphical example of this discharge behavior of known resistors, correlated with the circuit equation, is shown below in Figure 18.

$$\frac{U_2}{U_1} = e^{-(\frac{T}{RC})}$$

Figure 17 – Circuit equation for defibrillator [67]

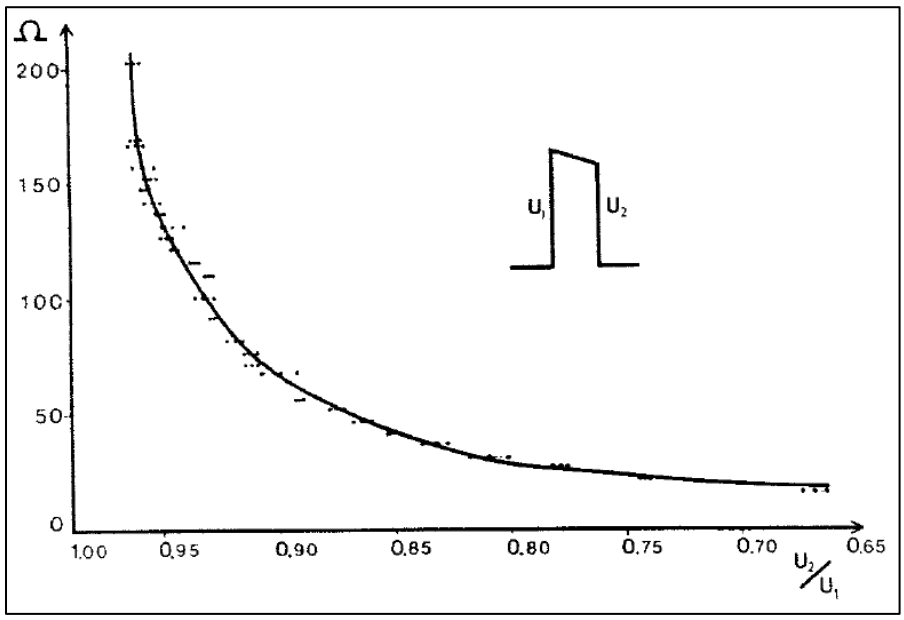

Figure 18 – Voltage drop correlation to resistance of known resistors [67]

With respect to current delivery type, as discussed earlier in the literature, Kugelberg noted that with either AC or DC current, the influence of the resistance will remain the same. This assumption was based on his observation from his earlier studies, that the measured decay signal of the capacitor discharge appeared strictly linear, and thus the myocardium should be regarded as pure resistance without any capacitive or inductive components [68]. He further went on to demonstrate the effectiveness of this measurement method via external defibrillation. Based on the aforementioned methodology, an electronic

circuit to simulate the defibrillation behavior was developed for this study. Components for this circuit comprised of a bench top DC power supply with a rating of 0-25V, an oscilloscope to measure the voltage decay, a three-prong switch to act as the control transistor to switch circuit states, a capacitor, wires, and a breadboard. A three-prong switch for a manual state trigger was selected as opposed to a signal generator, due to the intention to capture a single trigger instance. There was no need to fully simulate the cyclic charge and discharge behavior of an AED, given that each discharge cycle would look the same given the same resistance. However, if it was desired to replicate this behavior, a signal generator would simply take the place of the switch. In terms of component selection specifically, a 100µF capacitor with a power supply set at 5V was chosen. Given the limitations of the power supply and measurement equipment, it was not possible to completely replicate the specifications of a commercial AED. However, as our test model is based on voltage differential and the decay behavior, there was no explicit need to do so, provided that the objective was to compare resistance behaviors between defibrillator pad types. As such, to properly measure this pattern on the oscilloscope given a low power source rating, a relatively small capacitance was chosen. Figures 19, 20, and 21 illustrate the circuit diagram, physical circuit model, and setup created for this study.

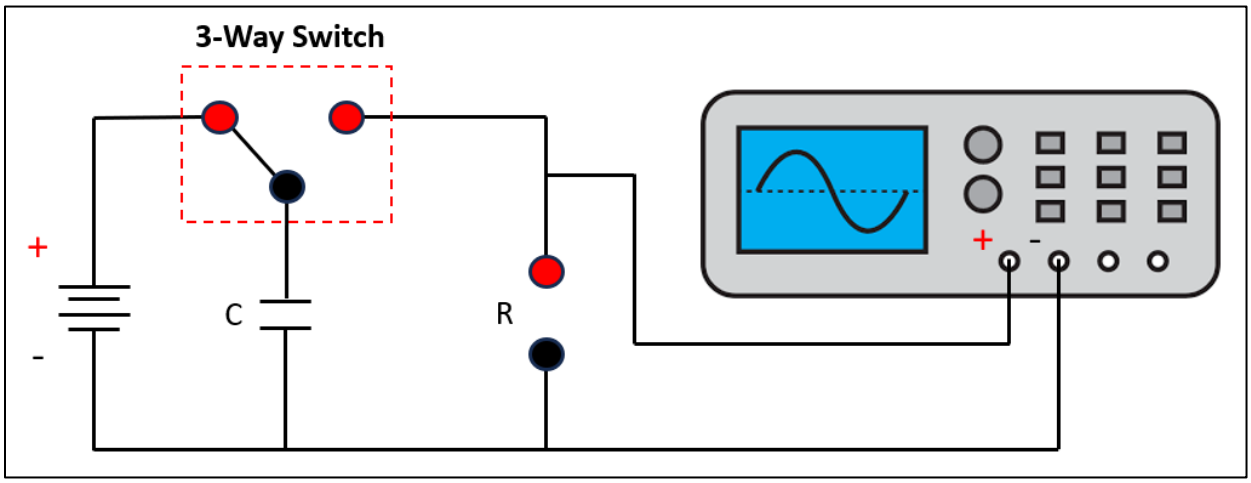

Figure 19 – Experimental test circuit diagram

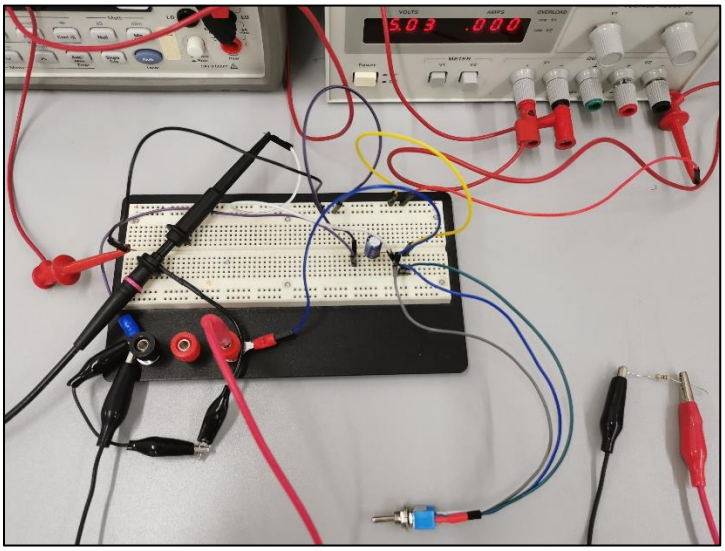

Figure 20 – Experimental circuit model

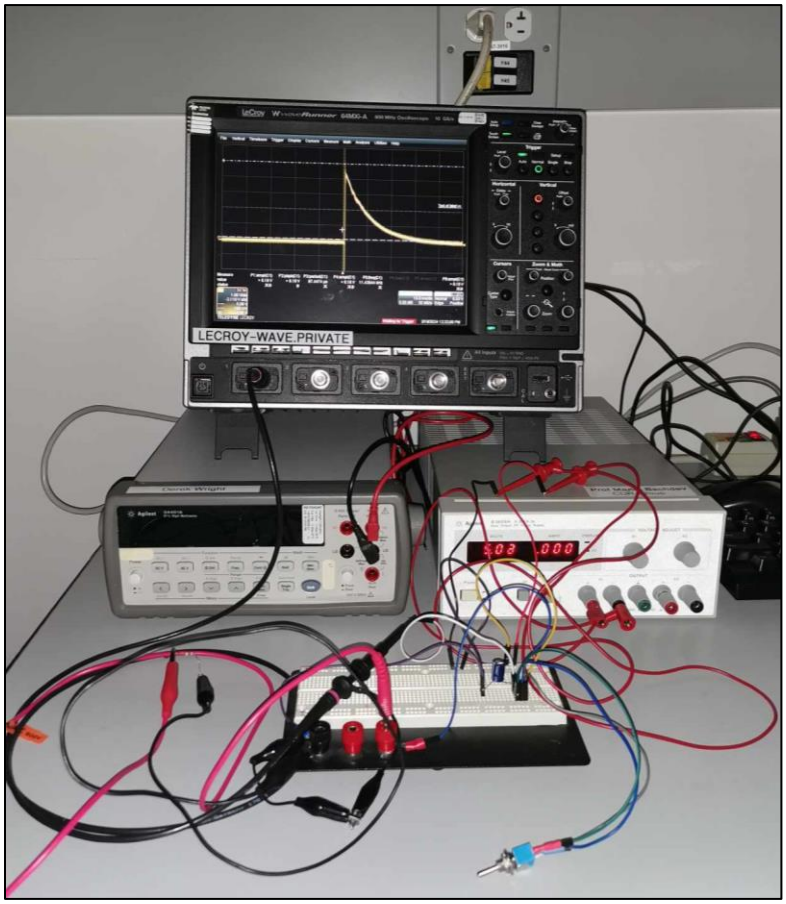

Figure 21 – Experimental model setup

Although the components and transistor mechanics differed from the study, the test circuit functioned identically to the behaviors defined in the circuit equation for a defibrillator. The three-prong switch controlled the capacitor charge and discharge behavior for a single cycle. With the switch set in state 1, the 100µF capacitor would be allowed to fully charge via the 5V connected power supply. Once the user triggered the switch to state 2, the capacitor would discharge through our resistor which was comprised of a microneedle pad on one side, a suitable test medium (be it an animal skin tissue or cadaver model), and a probe or equivalent measurement pad, to act as our ground to complete the circuit. An oscilloscope was connected in parallel to the resistor, to measure the voltage differential before and after the energy transfer through the medium.

The test procedure used to collect the data covered in this study is outlined as follows, with adjustments made as necessary between design iterations to account for new variables and limiting external factors:

1. Terminal 1 and Terminal 2 were connected using a combination of:
   a. Original Equipment Manufacturer (OEM) Pad
   b. Measurement Probe
   c. Microneedle Pad
2. Terminal 1 and Terminal 2 were placed on the test medium in either a surface configuration (both terminals on the surface parallel to each other on the skin) or in a through body configuration (terminals placed on opposite sides of the medium) depending on circumstance.
3. The center to center distance was recorded between the two test pads and remained consistent throughout the testing process.
4. SignaGel electrode gel was placed on the contact area between the test medium and test pad.
5. The oscilloscope would be set to record a single trigger and illustrate the decaying signal.
6. A single circuit charge and discharge cycle was manually initiated via state 1 to state 2 transition.
7. V1, V2, and T were recorded in accordance with the circuit equation.
8. Resistance was calculated based on known values, isolating the circuit equation in terms of resistance as shown:

$$R\ (ohms) = \frac{T\ (ms)\ \times\ 10^{-3}}{[C\ (\mu F)\ \times 10^{-6}] \times [\ln \frac{V1\ (volts)}{V2\ (volts)}]}$$

9. Steps 2 through 8 were repeated per dataset combination with adjustments to the terminals made as necessary.

3.2. Iteration 1

3.2.1. Design Process – V1

Before designing a prototype, an important set of criteria had to be laid out corresponding to the project objectives. In this research, beyond the intent of simply creating a concept for microneedle-based AED electrodes, there was an extended notion of creating a pad which could function with a redeveloped AED interface that could precisely control and monitor the optimal delivery of shock current, via the individual microneedles. With this thought in mind, the first criterion was for the pad to have individually connected microneedles so that the energy distributed could be controlled if this feature was integrated. Second, the pad had to be flexible in nature to conform to the shape of the body but at the same time be rigid enough to make sure the insertion force was evenly distributed. Third, although the length and number of needles was important, this factor could vary depending on the test medium, AED architecture, and other external factors, which would be challenging to control given the duration of this study. As such, for a proof of concept, it was more crucial to confirm the functions and effects of the microneedles rather than trying to iteratively perfect for a fixed condition, which may not reflect the elements in a real defibrillation setting.

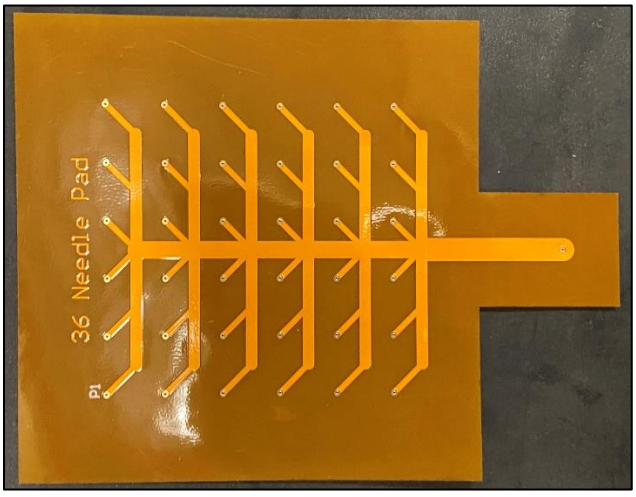

Figure 22 – Flex PCB

With these criteria in mind, a thirty-six holed (8cm by 8cm) flex PCB comprised of a polyimide substrate and single inner copper channeling, was developed as proof of concept. The flexible PCB was designed using Altium and was manufactured by PCBWay, a prototype and fabrication manufacturer located in Shenzhen, China. Disposable stainless steel scalp microneedles measuring 10mm in length, 0.3mm diameter, with a conical-shaped tip were selected as the microneedles. These microneedles were

manufactured by Natus located in California, USA. Based on this, the hole diameter of the flexible PCB was set to be 0.45mm to allow for enough clearance. For this design, the copper channeling was shorted together so that the microneedles would function as a single electrode, mimicking the behavior of a traditional pad, allowing for ease of testing. To address the first criteria, the design was simple enough so that if desired, a specified number of needles could be isolated from each other with dedicated electrical inputs. The manufactured flex PCB is illustrated above in Figure 22.

As the intention was to create a prototype that would conform to the human body, a flexible PCB was chosen as opposed to a conventional FR-4 laminate based rigid PCB. Furthermore, to shield the user from electrical currents and to introduce sufficient rigidity for good microneedle insertion, a combination of non-conductive polyimide (PI) shielding, and polytetrafluoroethylene (commonly known as Teflon) was used. Once the microneedles were inserted through the holes and electrically bonded to the exposed copper channeling, a Teflon layer would insulate the needles lengthwise, exposing only the desired tip length. This Teflon layer would also provide a mechanical bond for the needles, preventing the needles from being pushed out during insertion or remaining stuck on the body during removal. The PCB would then be sandwiched between two layers of semi-rigid PI shielding, to provide electrical isolation and prevent excess bending of the PCB substrate. A layered view of the completed flex PCB concept is presented in Figure 23.

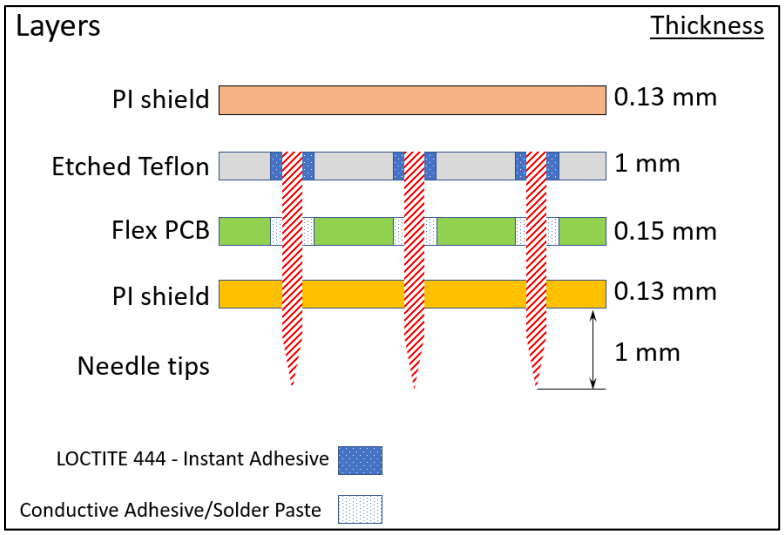

Figure 23 – Cross section view of Iteration 1

As the stainless-steel microneedles had to form an electrical bridge to the flex PCB, the initial approach was to use a silver-based solder paste or conventional tin/lead-based solder to form this connection. The 10mm microneedles, housed within a plastic casing compatible with a scalp electrode

harness, were removed and uniformly cut to the desired length via a makeshift needle mold, as shown below in Figures 24 and 25. With a preliminary investigation, it was suggested that a 1 – 2mm needle depth was enough to penetrate the high resistive epidermis layer. According to Shi et al. who performed a study on measuring skin thickness on the chest, they determined that the skin was roughly 1.5mm, a number including both the epidermis and dermis [69]. Although the chest anatomy of males and females are different, as this study focuses on the skin itself rather than the quantity of adipose tissue, 1.5mm was considered as the absolute maximum skin thickness to be expected. However, given the difficulty in cutting these microneedles to size, a more generous 5mm needle exposure was utilized as an initial proof of concept.

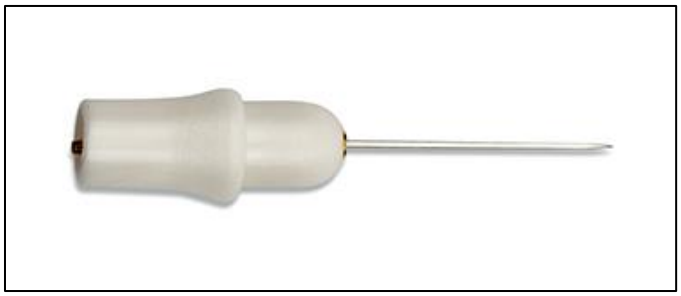

Figure 24 – Scalp microneedle

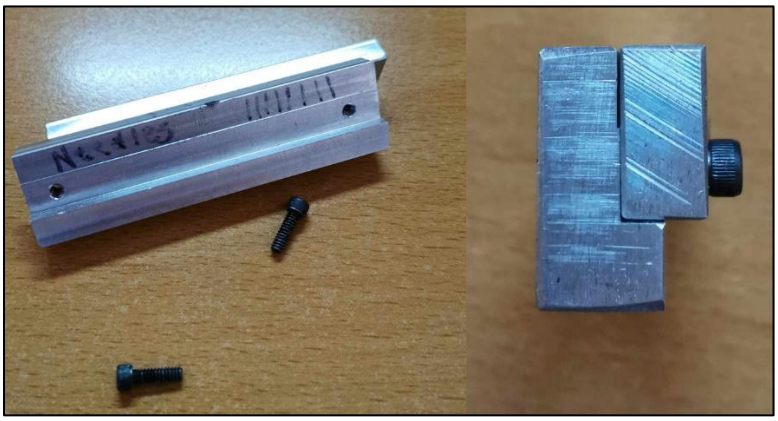

Figure 25 – Needle mold

With some initial trials using either solder or solder paste, there was difficulty in holding the stainless-steel microneedles in place while soldering to the copper PCB base. Due to the small surface area of the needles, which prevented adherence to the Teflon base and an equally small contact area to the pad, preventing a solid mechanical bond sufficient to bear load via soldering, a different attachment method had

to be used. Instead of securing the needles to a contrasting Teflon material through an adhesive, we opted to use a tungsten fusion weld technique to bond the stainless-steel needles with a similar metallic material. Stainless steel shims were cut into small squares and welded to needles. They provided each needle with a solid base of attachment, preventing the needle from being detached from the pad during the deployment and retrieval process. Once the needle joints were placed within each hole of the flex PCB, a silver (Ag) based solder paste was used to form the bridge between the needle and the pad. Additionally, a thin rubber layer was added in between the shims and the PCB, for better adhesion with the glue between layers and to prevent the shims from cutting into the PCB during application. The layered view and completed iteration 1 prototype are shown below in Figures 26 and 27.

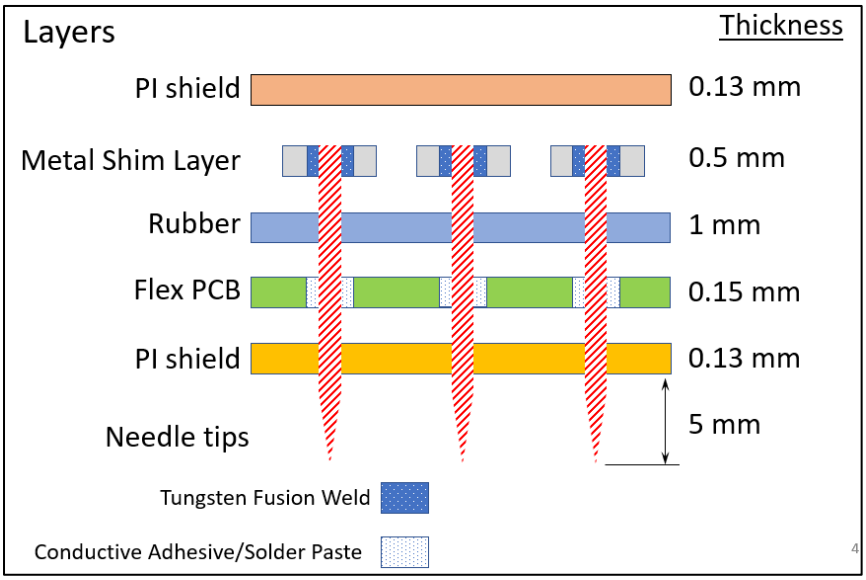

Figure 26 – Revised cross section view of Iteration 1

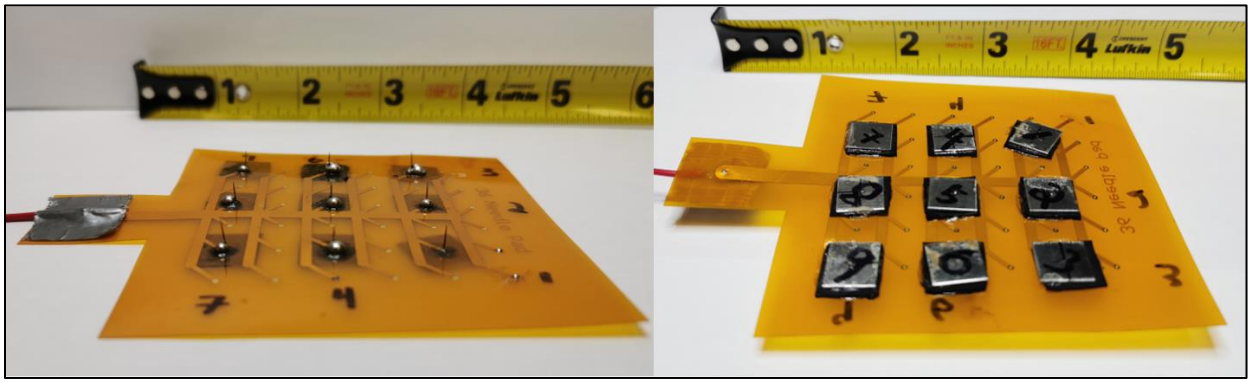

Figure 27 – Iteration 1 prototype

3.2.2. Test Methodology – V1

To verify the proper connection of the microneedles to the PCB, a basic connectivity test followed by a resistivity test were conducted as follows:

1. **Preparation & Visual Inspection:**

The required equipment, including a multimeter, test leads, a conductive surface like a metallic plate, and an insulator material, was assembled. Subsequently, a wire was soldered and affixed to the input side of the flex PCB. The connection points between all microneedles and PCB joints were inspected for any signs of damage or visually loose connections.

2. **Continuity Test:**

To perform a continuity test, the multimeter was set to continuity mode and the test leads were connected to the pad, one side to the input wire, and the other to the desired measurement point. Upon a successful connection, the multimeter would produce a beeping sound, indicating continuity. The initial measurement point would be taken from the solder joint, where the needles protruded from, and the second would be from the actual microneedle itself. Using a combination of the metallic and insulator plates, each microneedle was isolated separately from the conductive surface to obtain an accurate measurement.

3. **Resistivity Test**

Likewise, to perform a resistivity test, the multimeter was set to the appropriate resistance range for testing. The test leads were connected to the same points of interest as prior, with the initial point taken from the solder joint and the consequent measurement from the tip of the microneedles. To confirm a proper connection, the reading had to be within acceptable ohmic limits relative to the other properly connected measurement points.

4. **Documentation**

Lastly, the test results from the input to the solder joints as well as input to the tip of each microneedle were recorded. Any discrepancies in connectivity, or abnormalities in resistivity suggesting a questionable connection were recorded and investigated. The experimental setup for the connectivity and resistivity tests is shown below in Figure 28.

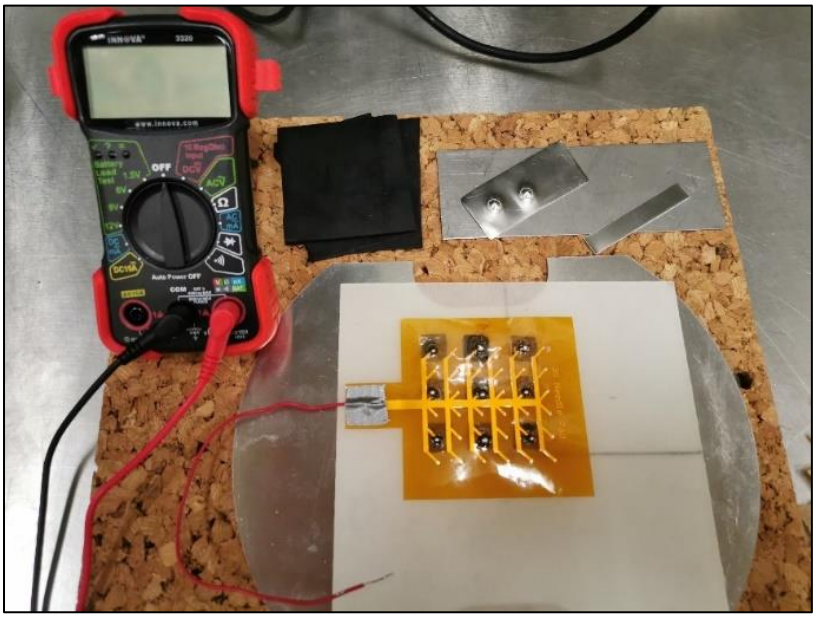

Figure 28 – Experimental setup (Iteration 1)

3.2.3. Experimental Results – V1

First, with the initial connectivity and resistivity testing between the solder joints and the pad input, the results were positive with all connections between 0.2 to 0.9 ohms. This confirmed that the solder was properly bonded to the to pad. Following this, the connectivity and resistivity tests were performed at each needle point, yielding unexpected results. The results were inconclusive as either some needles recorded a relatively stable reading, others fluctuating heavily, and some were unreadable indicating infinite resistivity and an open circuit. These values ranged between 3.5 ohms to indeterminate, according to the auto ranging multimeter. Upon diagnosis, the issue was that the Ag based solder paste failed to form a proper electrical connection with the polished stainless-steel needles. Despite forming a proper bond with the PCB, due to issues such as contact area and an indeterminable surface finish on the needles, neither a basic solder nor solder paste was able to bond properly with the needles themselves. Additionally, it was noted that with this iteration of the flex PCB, the exposed copper circular channels at the base of each hole were too small, preventing the solder from having a sufficient attachment point to the pad. This was noticeable as only a small amount of solder could be applied on the PCB and the needle weld being easy to remove, supporting the results of the previous electrical connection issue.

3.3. Iteration 2

3.3.1. Design Process – V2

To resolve the shortcomings in the first iteration, the first step was to revise the 36 holed flex PCB by adding more copper. Both the amount of copper internally as well as directly at the contact points between the needles and PCB was increased. This allowed a larger, more distributed amount of solder to be used to aid in mechanically fixing the microneedles in place. Second, to address the issues of adhesion and conduction, a crimped attachment approach was taken akin to how the microneedles were originally manufactured. Provided that the microneedles were meant to operate as a conductive component for subdermal monitoring, this notion suggested that a crimped approach should replicate the behaviors of the original microneedle. Since the 10mm microneedles were too long for our purpose and had to be cut from the blunt end, this meant removing the original crimped metal from the plastic assembly. Thus, once the 10mm needles were cut to size, a ferrule type connector was used as a direct replacement. Tin plated copper ferules approximately the diameter of the needles, were cut to 2mm sizes and crimped onto each needle. Subsequently instead of using solder paste, a conventional tin & lead alloy-based solder was used to connect the needles to the PCB. As there was now more space for the solder to adhere to, applying the solder manually was easier than using a liquid solder method. Lastly, as an observation from conventional AED pads, rather than using a rigid polyimide layer which would be difficult given the crimped protrusions, we opted to use an insulated foam layer instead. This would serve as an equally functional electrical barrier between the user and device and further improve pad flexibility. This iteration of the pad is illustrated below in Figures 29 and 30. All 36 holes were later populated with microneedles after initial testing confirming proper function.

Figure 29 – Iteration 2 prototype

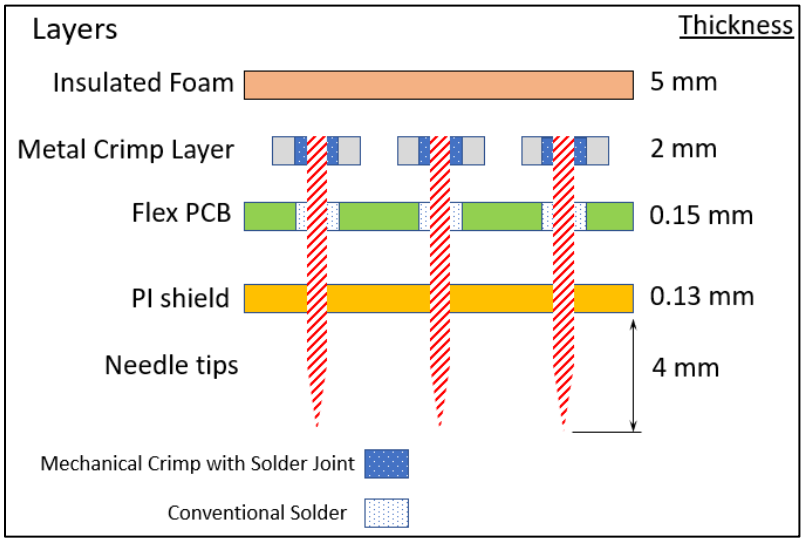

Figure 30 – Cross section view of Iteration 2

3.3.2. Test Methodology – V2

After initial connectivity and resistivity testing was performed to validate the connection between the pad input and the needle tips, this yielded positive results compared to the former. The resistance between the needle tips and the pad input were all measured to be in milliohms, which is negligible in terms of inherent electronic resistance and within acceptable limits. In hopes of further increasing the effect provided by the needles, all 36 needles holes were populated. As the construction of the pad was now validated, we moved onto evaluating the effectiveness of the microneedle pad.

The main experimental model as discussed in section 3.1 – experimental model was used. Terminal 1 was kept consistent as an electrical probe and terminal 2 was swapped between measurement pads. As the test mediums, initially an uncooked rotisserie chicken with the skin and meat intact and later pork belly were selected as animal test samples, as shown below in Figure 31. These skin samples were chosen due to their likeness in terms of thickness, density, and other similarities to human skin based off existing literature [70], [71]. The Phillips FR2 pads, sourced from AED Solutions Canada, were utilized as the OEM commercial pad, and compared to the needle pad, as depicted in Figure 32. With both skin samples being refrigerated or frozen in the case of the chicken, moisture content was relatively low and contrasting to a live body. As such prior to testing, tap water was added to the surface of both skin samples to reintroduce a bit of moisture for the samples to absorb, attempting to replicate a more realistic subdermal condition.

Furthermore, to attain consistent data, environmental temperature was considered. Both samples were left in room 20-21°C temperature for roughly 12-24 hours to allow the sample temperature to thaw and stabilize.

Figure 31 – Chicken & pork belly animal test samples

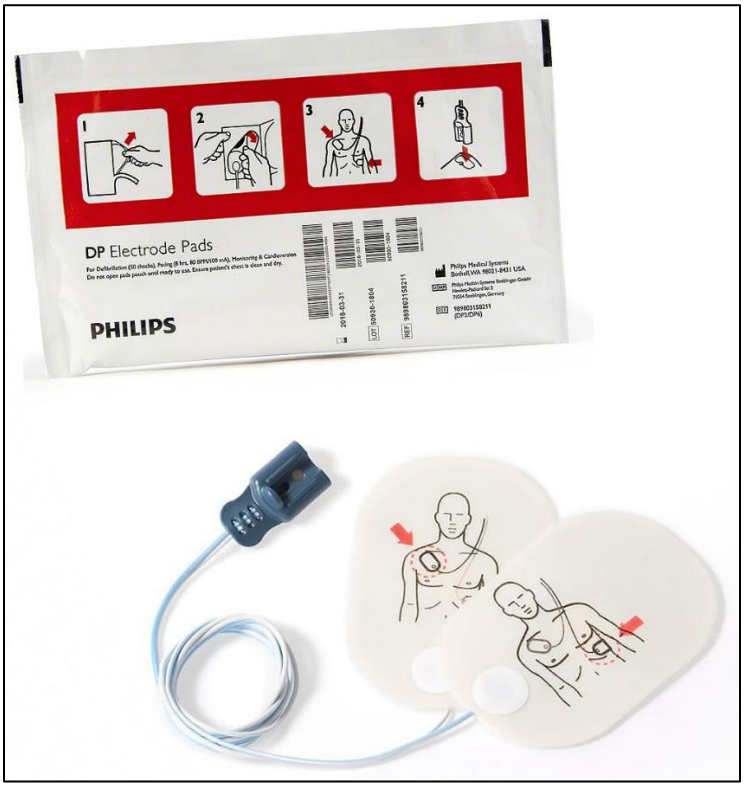

Figure 32 – Phillips FR2 adult defibrillator pads

Three main test variations were applied to the experimental model to account for possible errors and new results attained throughout the testing process. The first approach involved the comparison of the microneedle pad with a full OEM defibrillator pad. With those results, a second approach involved evaluating the microneedle pad against the OEM pad using an equivalent conductive area method. This method involved calculating the exposed area of the needles and revealing an equivalent amount of conductive space on the OEM pad, covering the additional space with a non-conducting material. Given the measured diameter of the needles being 0.26mm and exposed length to be 4mm, assuming a cylindrical shape without both circles for estimation, the equivalent surface area was 1.18 cm^2. Following a similar approach to evaluate microneedle effectiveness, the third approach utilizes a microneedle & OEM integrated pad versus a normal OEM pad. The notion behind this approach follows a study performed by a group of researchers from Rice University where they utilized needles as an add-on to a conventional pad [65]. By evaluating the microneedle pad as a part of the OEM pad against itself without the add-on, the intent would be to obtain results that show an increase in effectiveness as a part of the full pad. Although the outcomes may not demonstrate significant findings, they will serve as the foundation for modifications in design and additional experimental considerations. Each experimental dataset was repeated at least 3 times to obtain results and the average value was used to generate the graphs shown in the results.

3.3.3. Experimental Results – V2

As presented in section 3.1, the V1, V2, and T parameters used to calculate the resistance were attained from the oscilloscope. Like the literature, a decaying signal relative to time was observed. As the resistance decreased between the two measurement terminals, the signal would decrease faster and vice versa for an increase in resistance. An illustration of this behavior is shown below in Figure 33, a sample graph attained for this dataset. For this sample graph, the V1 would be 5.10V, V2 would be 3.52V, and T would be 10ms.

For test variation 1 using the full OEM pad versus the microneedle pad, it was immediately apparent that the flex PCB was not electrically comparable to a regular OEM pad due to the large discrepancy in metallic contact area as well as material composition. As discussed in section 2.2 – current electrode technology in AEDs, a regular defibrillator paddle uses a metal alloy combination such as tin, aluminum, and stainless steel depending on the manufacturer [19]. This conduit coupled with a conductive gel and adhesive border maximizes the contact area and energy transfer to the body. In comparison, the flex PCB is comprised of stainless-steel needles which are a worse electrical conductor and have far less metallic surface area compared to the metallic alloy film. A list of common conductive materials is shown below in Table 3, ordered based on their conductivity and resistivity as a reference to this point.

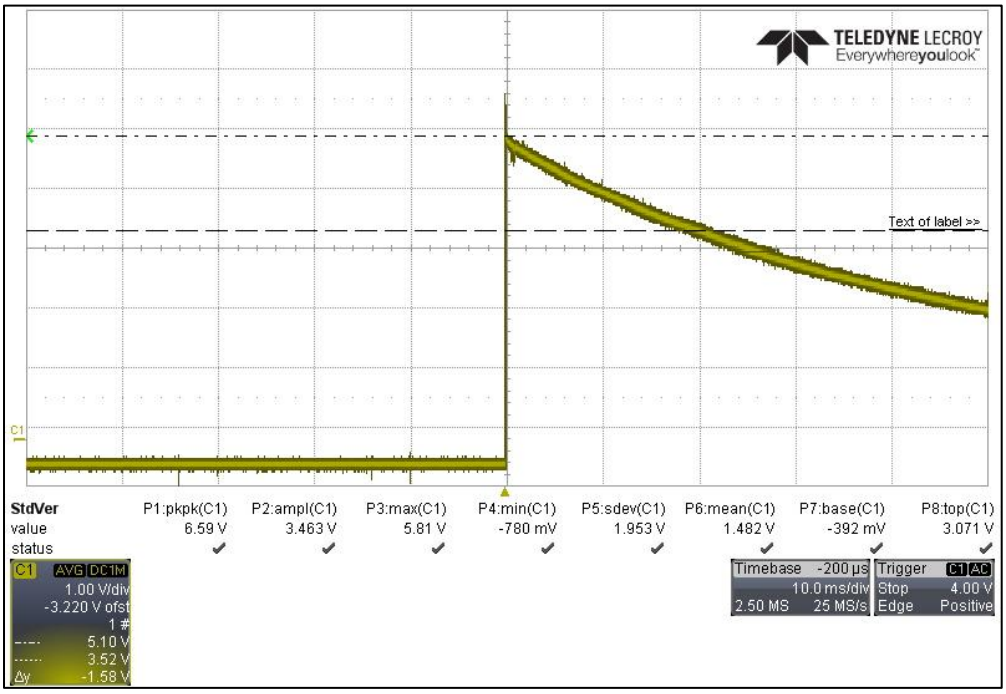

Figure 33 – Sample decay signal via experimental methods

Table 3 – Table of resistivity and conductivity at 20℃ [72]

Material	**Resistivity - ρ [Ω•m]**	**Conductivity - σ [S/m]**
Silver	1.59×10^{-8}	6.30×10^{7}
Copper	1.68×10^{-8}	5.96×10^{7}
Gold	2.44×10^{-8}	4.10×10^{7}
Aluminum	2.82×10^{-8}	3.5×10^{7}
Zinc	5.90×10^{-8}	1.69×10^{7}
Nickel	6.99×10^{-8}	1.43×10^{7}
Iron	1.0×10^{-7}	1.00×10^{7}
Tin	1.09×10^{-7}	9.17×10^{6}
Stainless Steel	6.9×10^{-7}	1.45×10^{6}

During testing on the chicken skin sample, there was a high degree of deformation and signs of separation between the skin and the chicken meat. This resulted in a large degree of variability during data collection and presented an unknown of whether the needles were having much of an effect due to the thin and near non-fat nature of the chicken medium as opposed to human skin. Additionally, as all inner organs and contents had been removed, a hollow bone cavity was the only thing which remained. This did not aid in a through-body connection, rather one which was merely on the surface as the path of least resistance. This notion was recognized much later in the iterative cycle as an issue once testing was performed on larger animal mediums and human cadavers. As such, whole chicken or chicken breast alternatives were not used again for future testing.

On the contrary, despite pork belly being a better test medium than chicken, the abundance of fat underneath the skin was noticeable. According to a study by Bouazizi et al. on the properties of biological layers within human tissue, fat emerged as the worse conductor, followed by skin, and then muscle [73]. Underneath the skin, the pork sample contained a mix between dense layers of fatty material and normal belly meat. These layers were not necessarily in sequence, although the fatty layers appeared closer to the outer skin surface rather than towards the inner side of the meat. Nevertheless, the acquired data was more consistent, showing repeatable trends. This data is presented below in Figures 35 and 36, where the error bars represent a 5% variability error. A 5% variability error was chosen to mirror the precision of the measurements, influenced by inherent fluctuations in the experimental process and unmanaged external variables. This selection aimed to encompass significant variations in the data observed across various experimental conditions and samples throughout the study, specifically isolating for the resistance. An illustration of how the probes were placed on the animal test samples is presented below in Figure 34.

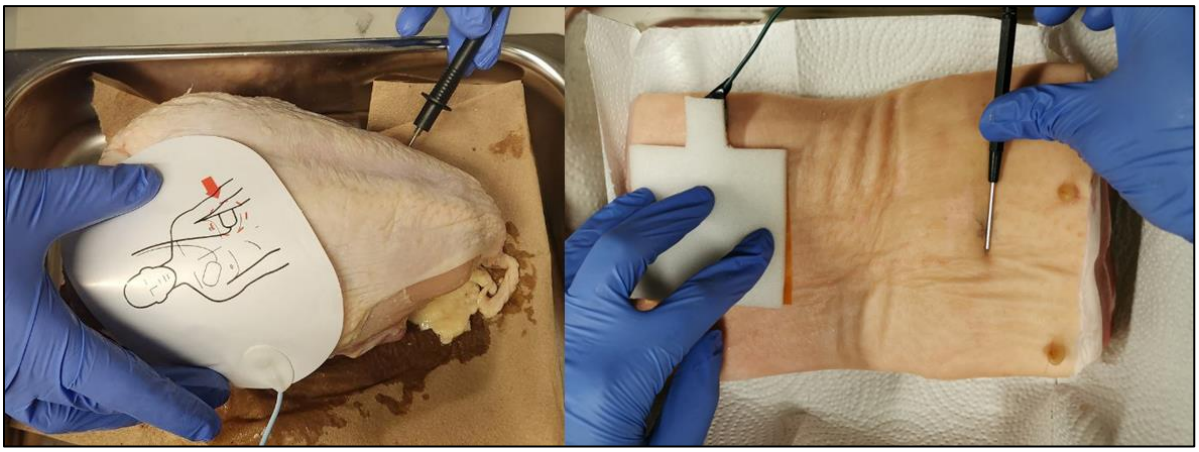

Figure 34 – Probe placements for animal skin samples (Iteration 2)

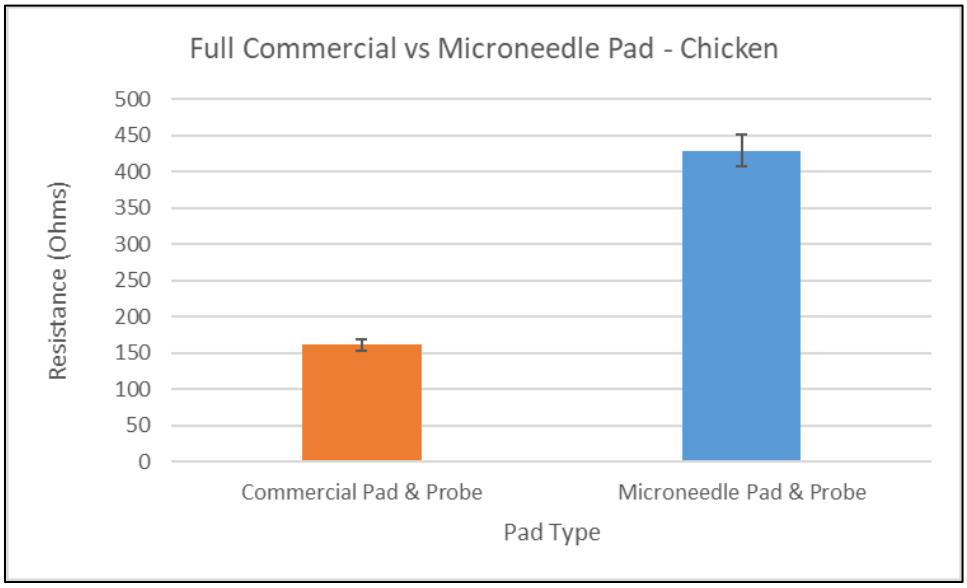

Figure 35 – Commercial vs. microneedle pad on chicken (Iteration 2)

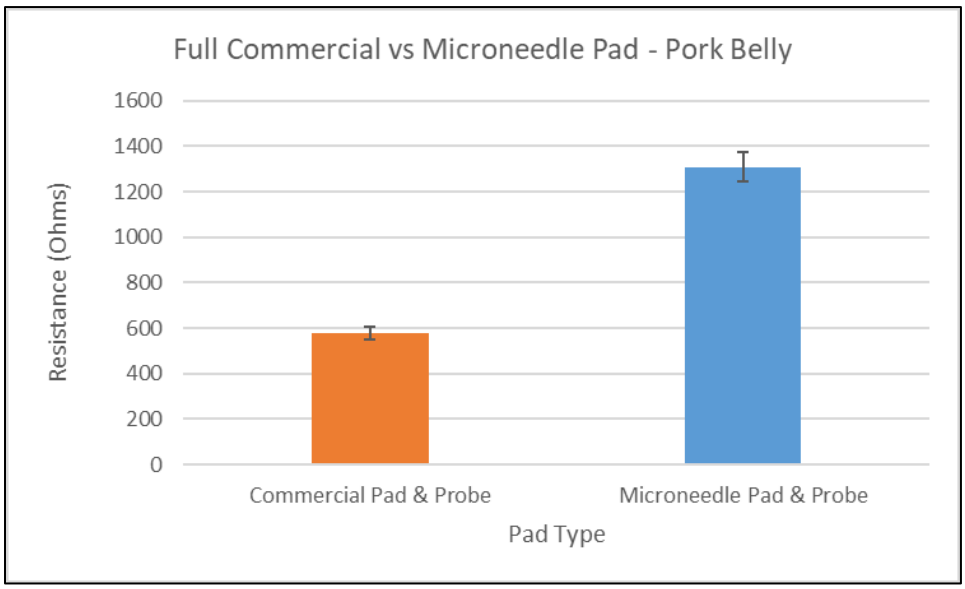

Figure 36 – Commercial vs. microneedle pad on pork (Iteration 2)

In the second test variation, to provide a better understanding of how the exposed metallic area influenced the results, an equivalent metallic resistance test was performed on the pork belly medium. The total surface area exposed by the microneedles calculated and an equivalent was then exposed on the OEM pad to provide a better comparison. Like the data acquired in the first test variation, the results still showed that the flex PCB had a much higher resistivity compared to either the full commercial pad or its equivalent

conductive area comparison. These results are shown below in Figure 37, highlighting a similar statistical trend as the first test iteration.

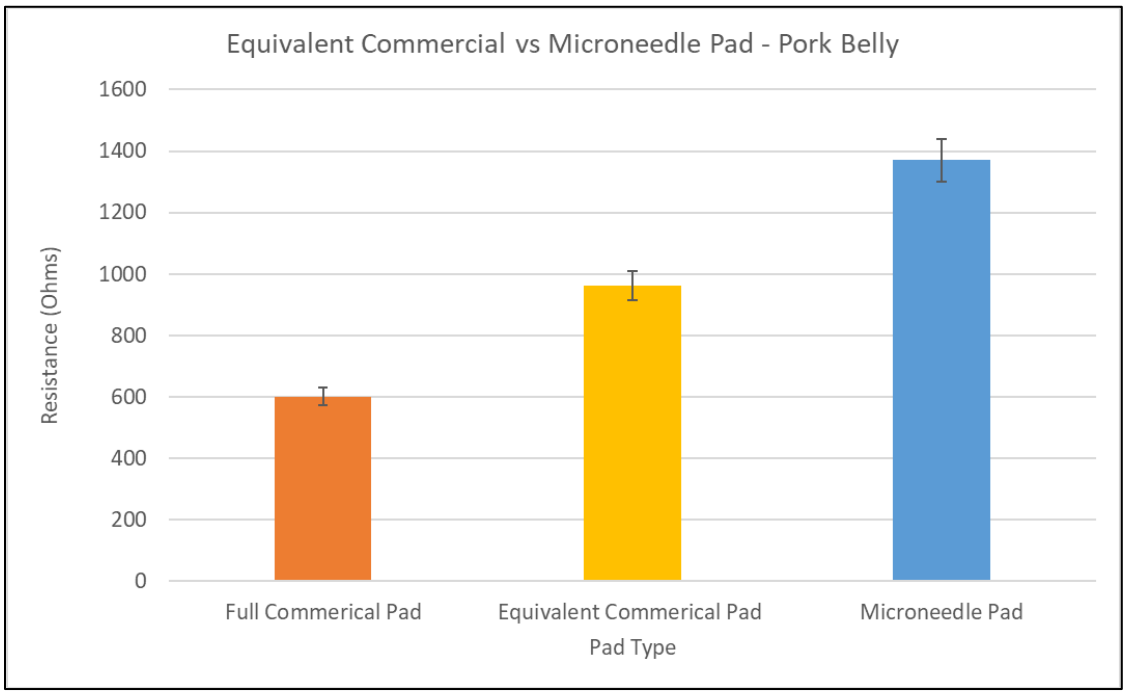

Figure 37 – Equivalent commercial vs. microneedle pad on pork (Iteration 2)

In the third test variation, it was of interest to see if the microneedles would still enhance the behavior of an OEM pad. By taking the flex PCB and puncturing it through an OEM pad, this would allow the pads to be electrically shorted together and function as a combined AED pad, as shown in Figure 38. The hypothesis was that the combined nature of the pads would allow the OEM pad to make use of the effect from the microneedles, reducing overall resistivity between the terminals. The test terminal was connected to the OEM pad wire harness while the other was connected to a probe. Tests were performed once again on a pork belly medium to evaluate the effect of the needles. Although there was an indication of a positive effect by the microneedles, roughly 5-10%, this was not a significant difference as this was within a 5% margin of variability error. Considering external factors such as measurement errors, temperature change, moisture, noise, and a lack of repeatable testing to confirm the results, many factors could have played a part in what was observed. As such, there was not necessarily any conclusive evidence to demonstrate that the needles had an effect in reducing the resistivity. Despite this, there was a need to further evaluate the outcomes as the combined method showed the most positive demonstration of functionality for the microneedles. As discussed earlier, provided that the added conductive area by the

microneedles were small compared to the overall size of the OEM pad, these results were not unexpected. The results for this test variation are illustrated below in Figure 39.

Figure 38 – Combined commercial needle pad (Iteration 2)

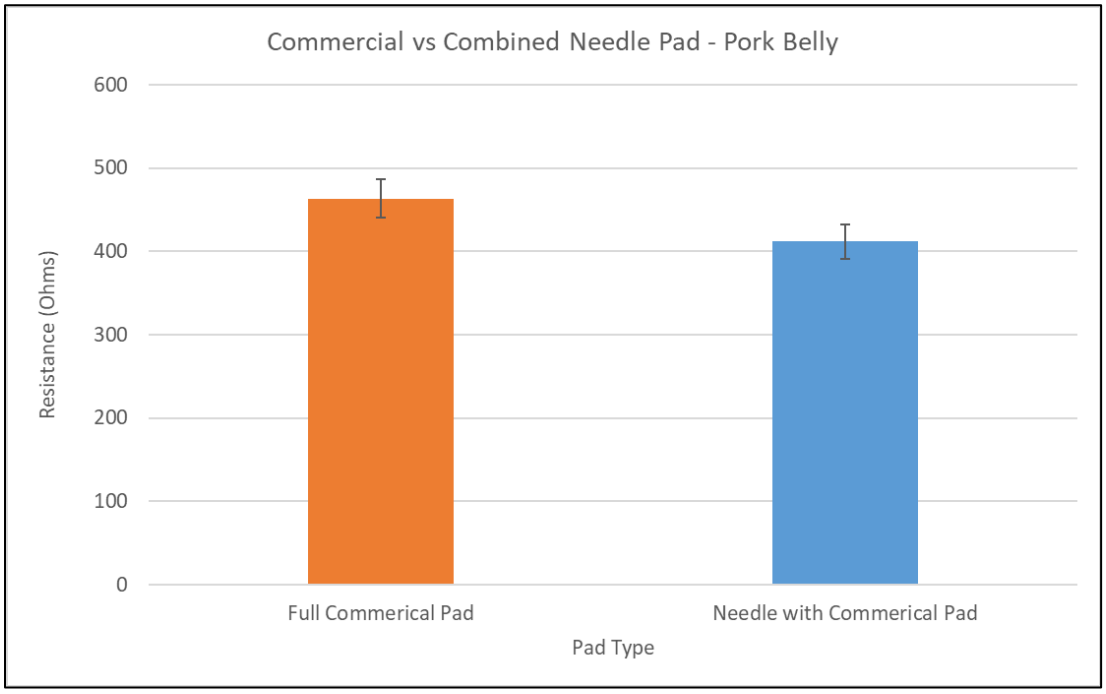

Figure 39 – Commercial vs combined needle pad on pork (Iteration 2)

3.4. Iteration 3

3.4.1. Design Process – V3

Stemming from the shortcomings of the previous iteration, the goal of iteration 3 was to revisit the combined microneedle OEM test method and see if it was possible to obtain significant results, proving positive microneedle functionality. To test the previous hypothesis of increasing metallic contact within the medium, a wooden nail bed was constructed to validate this notion. The dimensions of the nail bed were consistent to the flex PCB and 1.8mm diameter copper nails were inserted into the wooden frame. The same 4mm were exposed from each nail which were also consistent with the implementation of the flex PCB microneedles. With 61 needles inserted into the wooden base and once again assuming a cylinder approximation without the circles, the equivalent surface area was 13.8 cm^2. As a reminder, from the former design iteration with 36 microneedles, the equivalent surface area was 1.18 cm^2. In order to enhance metallic conductivity, copper nails were chosen as superior conductors compared to the typical alloy-based metallic films commonly found in conventional electrodes (see section 2.3), as illustrated earlier in Table 3. Although copper is not necessarily biocompatible for all internal medical applications, this iteration was solely created to validate a hypothesis with no manufacturable component in mind. By improving both the metallic contact and electrical conductivity of the material, the goal was to see a conclusive difference between a penetrated skin surface and one without the needles, functioning regularly on the surface. The constructed nail bed and its equivalent size comparison to iteration 2 is illustrated below in Figure 40.

Figure 40 – Iteration 3 prototype

3.4.2. Test Methodology – V3

Like the test methodology for the previous iteration, testing followed the sequence defined by section 3.1. Terminal 1 was kept consistent as an electrical probe and Terminal 2 was swapped between an OEM pad without the needle bed attachment and one with. Following the results from the previous testing, pork belly alone was used as the animal skin test medium. The OEM pad remained consistent and remained the Phillips FR2 defibrillator pads. As observed previously, temperature swings had a large impact on the internal resistance, where colder temperatures meant higher resistance and warmer improved conductivity. The test procedure for subsequent tests was adjusted to better address these effects, incorporating extra time for the medium to acclimate to room temperature. Moreover, the moisture content was demonstrated to have a significant impact on the readings. Despite applying tap water to the skin samples immediately before testing, it remained difficult to interpret the oscilloscope graphs at times due to high resistive readings. Considering the frozen and relatively dry nature of these animal test mediums, the internal moisture content influenced the readings much like temperature did. Samples with higher existing moisture exhibited faster signal decay, while those with lower moisture experienced prolonged decay. Of course, this is due to water being an excellent conductor of electricity compared to skin [74]. Additionally, literature has shown that leaner cuts of meat electrically conduct better than fattier kinds [75]. As such, a leaner cut of pork belly was selected as the test medium for these experiments, although the pork belly still contained a significant amount of fat due to the nature of where it is cut from. To improve our readings and more easily identify changes due to the needles, the animal skin medium was submerged in a saline solution (NaCl) for roughly 24 hours prior to testing, to improve moisture levels and test sample salinity. A 0.9% saline solution was created using household table salt and tap water to replicate the bodily fluid condition in a human body [76]. The saline dosing process of an animal sample is shown below in Figure 41.

Figure 41 – Saline dosing process

In short, based on the experimental methodology during iteration 2, additional factors were considered. Testing temperature remained consistent by placing the animal sample at room temperature for 24 hours at the minimum to allow for proper defrosting and stabilization. Furthermore, an effort was made to select a pork sample with a leaner cut rather than fatty. Lastly, a saline dosing bath was provided to the test sample prior to testing to improve salinity, overall conductivity, and mimic bodily fluid conditions. The primary experimental setup for iteration 3 is shown below in Figure 42.

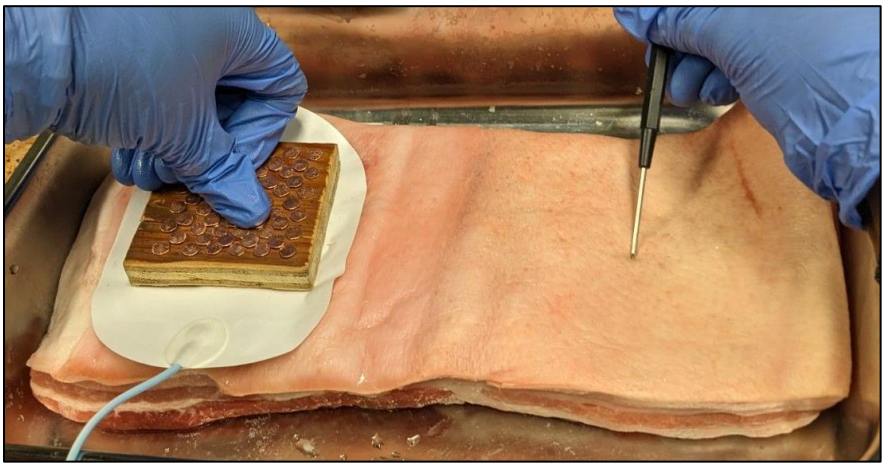

Figure 42 – Experimental setup (Iteration 3)

3.4.3. Experimental Results – V3

In this set of experiments, it was recognized that by having the measurement probe slightly pierced inside the skin along with not putting much pressure on the OEM pad, the results between trials were much more consistent. In order to maintain consistent pressure, the same experimenter was tasked with applying a uniform degree of pressure to the best of their abilities throughout the trials. Additionally, with a testing hypothesis to increase contact between the OEM pad and the nail bed beyond the thin alloy film, a set of trials were performed with the OEM pad placed on top of the nail bed to fully short the connections through the nail heads. However, in this configuration it was recognized that the surface of the OEM pad would not contact the test surface, increasing interelectrode resistance. Four distinct setup variations were explored within these results; the full OEM pad with a probe, combined needle pad flush & pierced with the skin, combined needle pad with needles just touching the surface & not pierced, and the OEM pad placed above the needle bed as just discussed.

From the results, it was observed that the OEM pad still performed the best followed by the needle OEM combination pierced, combined needle bed on surface, and OEM pad on top, in that order.

Particularly, it was unexpected that the needle OEM combination performed worse than the commercial pad alone. Unlike the trend from iteration 2, where the data suggested that the microneedles were positively affecting the interelectrode resistance, the results of this test suggested otherwise. With the hypothesis based on increasing needle density and a conductive material change thus improving conductivity, the expected results were to demonstrate a positive outcome beyond the margin of error. An overview of these results is presented below in Figure 43, with error bars illustrating a 5% variability error.

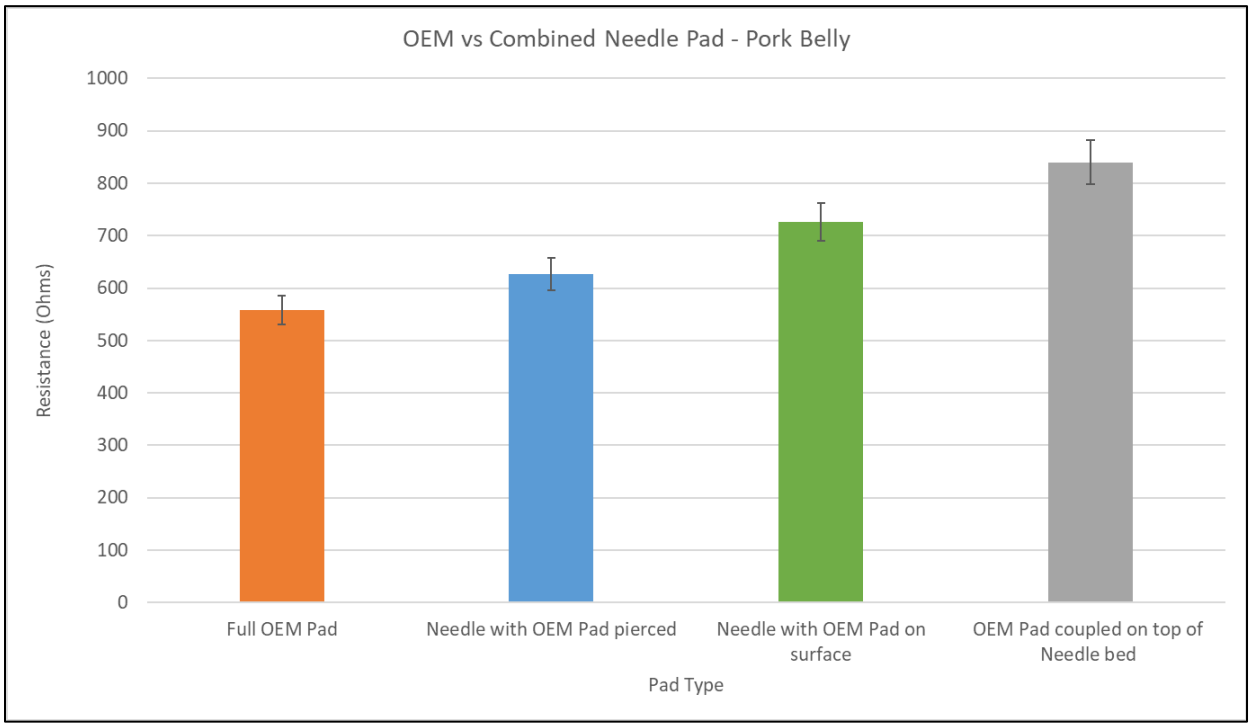

Figure 43 – Commercial vs combined needle pad on pork (Iteration 3)

A suspicion concerning the OEM needle interface arose following an investigation into the test equipment, setup, and procedure to identify any anomalies. To confirm this notion, a conductivity test between the nail bed and OEM pad was performed. One terminal of the multimeter was connected to the main lead of the OEM while the other rotated between each of the needle ends. Although not immediately apparent, this showed that there was an issue in the interface as some nails showed a good connection while others did not seem to be properly shorted to the alloy film. Despite some nails showing a good connection initially, the stability of these readings would change with slight movements in the needle OEM interface such as during pad application or removal. Unlike the flex PCB, the nail heads were not shorted together

via a robust conductive channel, rather they were reliant on a thin alloy film to form a strong electrical bond.

Second, although there was a notion to increase needle size, amount, and density within the same PCB area, this proved to be a negative aspect. Apart from the issue of the thin conductive film, the characteristics of these needles furthermore prevented a good connection. During the needle pad application onto the OEM pad, due to the increased diameter of these needles and density, this prevented the needles from easily piercing the alloy interface. Instead, additional force was needed to push the needle bed through and consequently, this caused the alloy film barrier to tear unevenly rather than in a symmetrical circular manner. Lastly, it was observed that the rigid wooden base of the needle pad may have prevented a good pad to surface connection. As the wooden base stiffened the OEM pad significantly between the pad's surface and test medium, an additional air gap may have been created. This air gap would further increase the skin impedance barrier as there would be parts of the pad not touching the surface, despite all needles being pierced. Whereas in comparison to the former iteration, the OEM pad would conform to the surface contours without much resistance from the microneedles. As observed in the results, when the surface of the OEM pad was not touching the test surface in the two test cases; when the combination pad was not pierced into the medium or when the OEM pad was placed directly above the needle bed, this drastically increased the skin impedance barrier. Thus, it is hard to ascertain how many needles were functionally connected to the system and whether the full OEM pad was touching the skin surface during testing, as with each test repetition the condition may have changed. With all these factors in play, further testing was required to validate the effectiveness of the subdermal needles and how the integration of microneedles on an OEM may be properly achieved.

3.5. Iteration 4

3.5.1. Design Process – V4

Although the third iteration provided many faults in both the construction and implementation of the needle pad, the notion to insert needles into a structure and shorting them together remained viable. Revisiting the idea of maintaining a flexible base to promote good surface interaction, a flexible TPU base was created, designed using SolidWorks. This rectangular needle base measured 6cm by 8cm and was created using additive manufacturing. 0.5mm diameter 12mm long nickel-plated steel sequin pins, used for fabric or hobby purposes were selected as the needles. In comparison to the stainless-steel scalp microneedles which were 0.26-0.3mm in diameter, these microneedles were far more accessible and could be purchased in large

quantities without any issue. These needles were inserted into the base, spaced evenly every 5mm for a total of 165 inserted needles in an 11 by 15 pattern. The spacing between these needles was relatively generous to minimize the tearing behavior in the alloy barrier during needle application. As these needles were quite thin, much thinner than the 1.8mm copper nails used in the third iteration, tearing would not be an issue. To increase conductivity, nickel plated steel needles were selected as they are more conductive than regular stainless steel needles, as per the table defined in section 3.3.3 [72]. Two separate sets of microneedle pads were created, one with 6mm of exposed needle and the other with 1.5mm as per the skin thickness according to literature. As such, the thickness of the TPU base was adjusted accordingly to these specifications. To resolve the connectivity issue, copper tape was used to electrically short all 165 needles together on both sides of the base and conductive electrode gel was applied to the skin surface to eliminate any air gaps during testing. The construction process and the completed pads are illustrated in Figures 44 through 47.

Figure 44 – Flexible TPU nail base

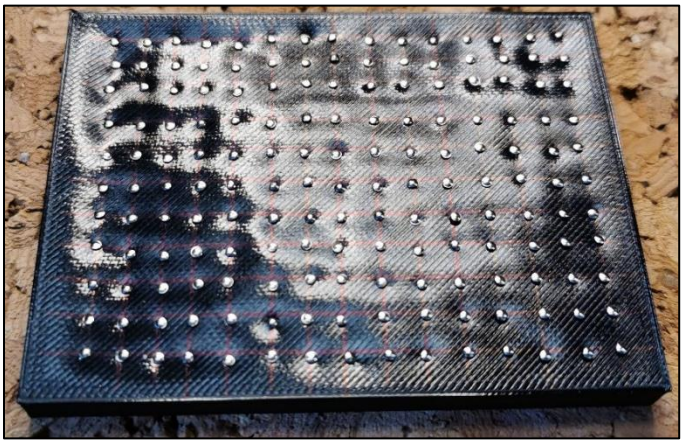

Figure 45 – Nail insertion method (Iteration 4)

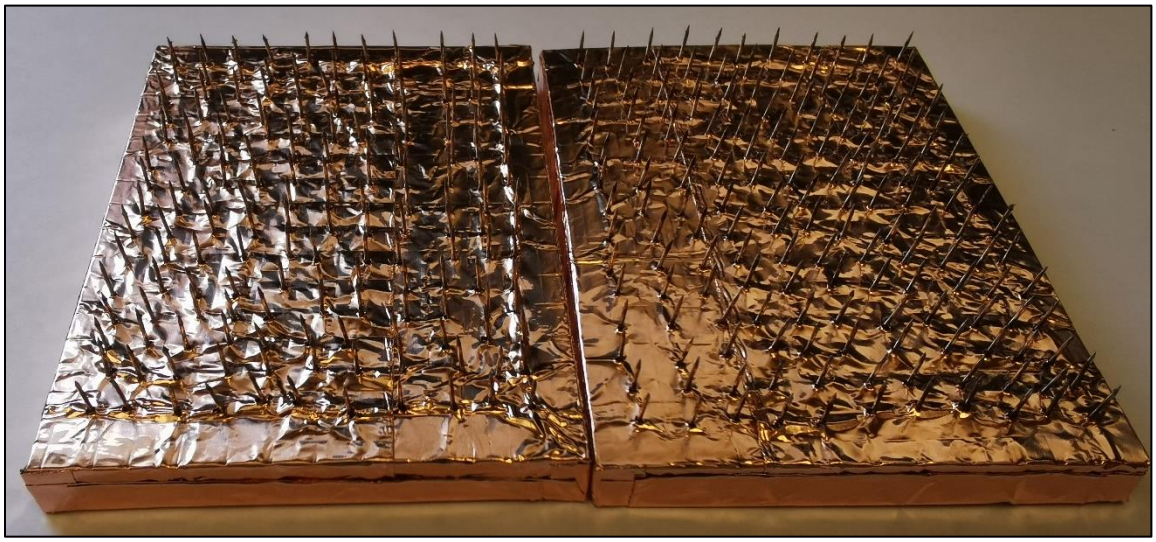

Figure 46 – 6mm pad variant (Iteration 4)

Figure 47 – 1.5mm pad variant (Iteration 4)

As illustrated, this method mimicked the construction of a commercial OEM pad where an alloy film is embedded inside a conductive gel layer. With confidence that this iteration would yield positive outcomes, the microneedle pads were created with the notion that testing them individually would be possible. Like the first two iterations, the microneedle pads would be isolated as test variations in a comparison against the commercial pad. Unlike prior, the conductive area of this iteration was much greater and more comparable to that of a commercial pad. With the same cylindrical approximation assumptions as prior, the conductive area with both needles and the copper base touching the surface was estimated to be 63.55 cm^2 for 6mm needles and 51.89 cm^2 for 1.5mm needles. Due to the Phillips FR2 commercial pads

being discontinued making it difficult to source, the Physio-Control Quick-Combo adult defibrillator pads were sourced from AED Solutions Canada and selected as the replacement OEM pad. These pads had an estimated conductive area of 112.7 cm^2 and were slightly larger than the former pads which were around 95 to 100 cm^2. The OEM pads are illustrated below in Figure 48.

Figure 48 – Physio-Control Quick-Combo adult defibrillator pads

3.5.2. Test Methodology – V4

With prior experience using the probe as the second terminal in the previous iterations, it was both difficult to stabilize and keep consistent throughout the trials. With a slight change in probe depth or orientation, this would alter the readings as it would need to be manually held in position. As such, due to the availability of materials, a second set of identical pads were used in place of the probe for each test variation. Like prior, the experimental model was used as the basis of comparative testing between the OEM pad, a combined OEM needle variant, and the needle pads themselves. As mentioned earlier, for the test medium it was recognized that despite pork skin being a viable substitute for human tissue, the abundance of fat content did not contribute to the accuracy of the readings nor was it similar to a human chest model. As such, an alternative whole duck animal sample was used in parallel to the pork belly. Like the chicken model, the whole duck sample would have its skin intact, despite being hollowed out. However, given the larger animal sample and characteristics of the skin, there was a generous layer of lean meat for the needles to puncture into despite the hollowed-out body cavity. Both animal samples were treated with the same

0.9% saline bath and defrosted, if applicable for a minimum 24 hours at room temperature before testing. This duck sample is shown below in Figure 49.

Figure 49 – Whole duck test medium

To evaluate the proper functionality of the needle pads, the 6mm needle pads were used. As always, the first test variation evaluated the OEM pads themselves, followed by combined OEM needle pad, and finally the needle pads themselves. Once the 6mm needles were punctured through the pad, the exposed needles would be closer to 4mm, identical to previous iterations, as illustrated in Figure 50. Because of the internal wire harness connection of the OEM pad, it was observed that the needles could not fully puncture to the same degree in a small area at the center of the pad, as illustrated.

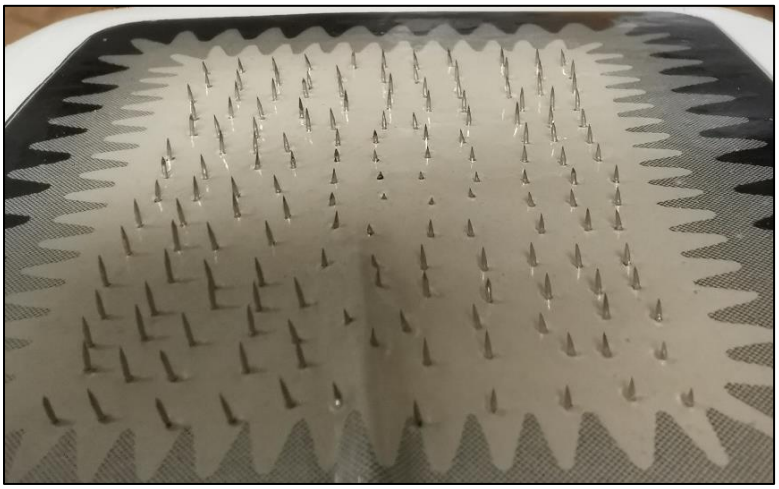

Figure 50 – Combined OEM needle pad (Iteration 4)

In both animal test samples, the center-to-center distance of the pads were kept consistent at roughly 15cm apart. The pads were placed as far apart as possible on both samples and a gap was left in between the pads to avoid the conductive gel touching both sides. For the duck sample, the pads were placed on the meatier chest side of the sample for better pad to surface interaction. The pad placement locations for the animal samples are shown below in Figure 51 and 52.

Figure 51 – Pad placement pork sample (Iteration 4)

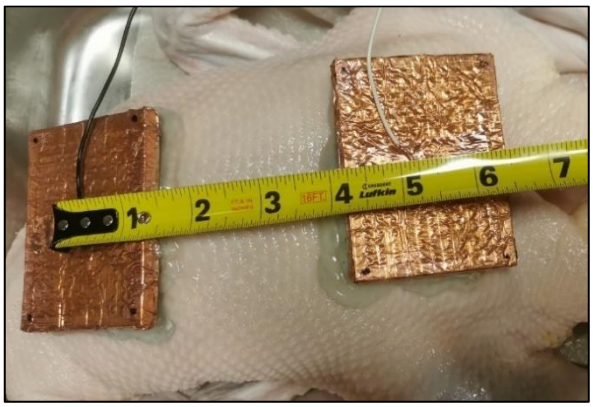

Figure 52 – Pad placement duck sample (Iteration 4)

Based on the results shown in the next section, the needle pads demonstrated sufficient functionality to reduce the skin-impedance barrier in animal models. Thus, the next step was to perform testing on human tissue. Being unable to acquire a chest skin sample from an unembalmed specimen at the time, a human unembalmed thigh sample was used. The thigh sample was part of an intact human leg, encompassing the majority of the femur and extending down to the toes. This sample was frozen prior and defrosted for 24 hours or more prior to testing, to allow both inner and outer tissue to acclimatize to room temperature. The male thigh specimen was average in terms of a lean-to-fat ratio and the donor's cause of death was COVID-19. Prior knee dissection was performed on the sample, but the leg remained intact with the thigh portion

untouched. Otherwise, there were no abnormalities observed on the human leg. The pads were placed on opposite sides of the thigh, with one pad placed medially on the inner thigh and the other placed laterally on the outer thigh. The surface center-to-center distance of the pads was roughly 18cm apart. Three test variations were used for this sample, the equivalent masked area OEM pads, 6mm needle pads, and 1.5mm needle pads. The 1.5mm needle pads were created after testing on animal models for the sole purpose of testing on human tissue, where the exposed depth of the needles conforms with literature. As the specimen already contained a decent level of moisture internally, the saline bath was not necessary nor practical. As the human leg was harvested without embalming or treatment, the original blood and bodily fluids were preserved within the cadaver medium and subsequently frozen. To prevent any changes to the internal moisture content, the thigh area was not immersed in saline solution. However, just prior to testing, a saline absorbed gauze would be wrapped around the thigh for several minutes to increase levels of surface moisture. The pad placement location for the human thigh sample is shown below in Figure 53.

Figure 53 – Pad placement human thigh specimen (Iteration 4)

3.5.3. Experimental Results – V4

In the animal skin tests, there was a meaningful reduction in resistance via the needle pads. For the pork belly sample, based on the average value of the OEM pads as a benchmark value, there was roughly a 10% improvement via the combined configuration and a 7% improvement via the needle pads alone. As observed, both needle variants demonstrated positive effects as a result of the needles beyond a 5% standard variability error. Although the combined OEM pads demonstrated slightly better results in this instance compared to the needle pads alone, both needle variants were similar in magnitude and were within 5% of each other as shown in the graph below. Likewise, for the duck sample, there was roughly an 11% improvement via the combined configuration and a 15% improvement via the needle pads. This set of data

was significant as the magnitudes were outside of the 5% variability error. Once again, both needle pad variants were similar in magnitude, with the needle pads alone being slightly better than the combined variant. With the whole duck specimen, this demonstrated the needle pad's ability to conform to the surface with no issue due to the flexible TPU base. Additionally, the density of the needles was not an issue as most, if not all needles were able to puncture through the animal skin samples as the data suggests. The results are summarized below in Figures 54 and 55, with error bars indicating a 5% variability error.

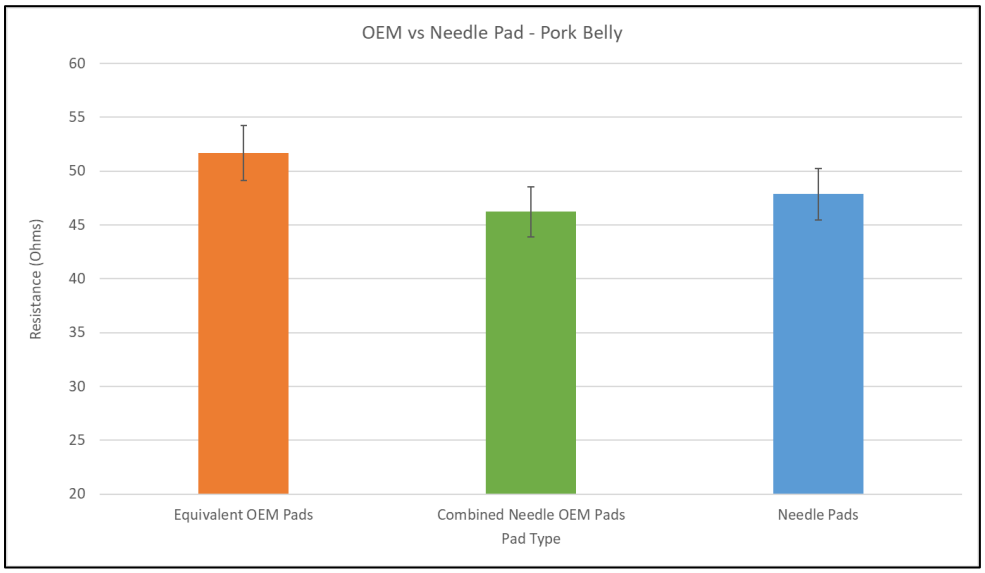

Figure 54 – Commercial vs needle pads on pork (Iteration 4)

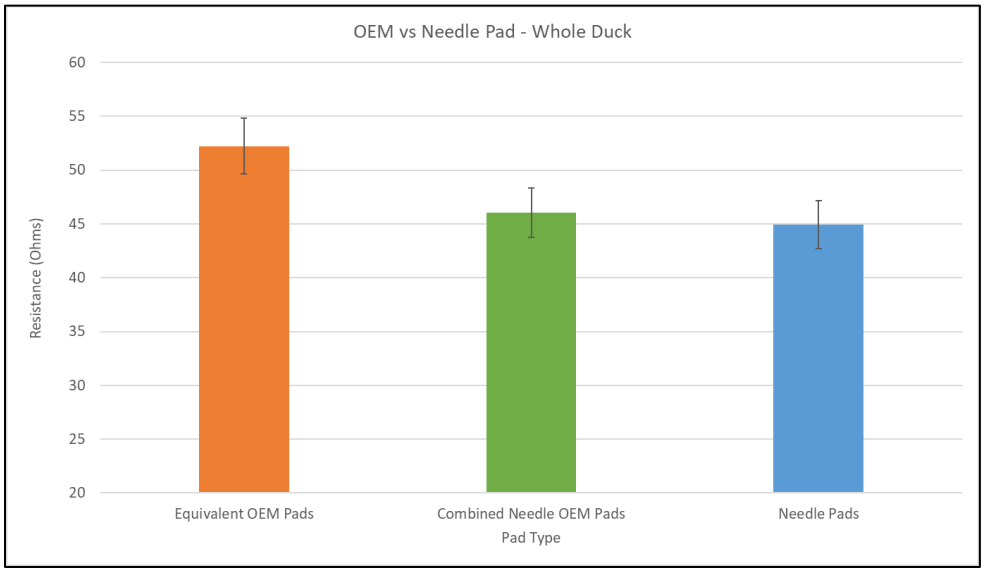

Figure 55 – Commercial vs needle pads on duck (Iteration 4)

Due to similarities in performance between the combined needle variant and needle pads alone, the next step was to validate the functionality of pad needles on a human tissue. Despite the conductive area of the needle pads being roughly 50% the amount on a conventional pad, the results on the animal samples demonstrated the immediate effectiveness of the needle pads, with the combined effects of the conductive material change and the needles of course. With the human thigh specimen, there was roughly a 13% improvement via the 6mm needles and a 22% improvement via the 1.5mm needles. Although one would think that the increased depth of the needles would be beneficial in improving conductivity, in this instance, due to the shape of the surface and skin characteristics of the human thigh after being frozen, it was clearly observed that the 6mm needles had a hard time piercing the surface during application. Hence, as demonstrated by the results, the 6mm needle pad did not fully conform to the surface and prevented a degree of needles not breaking the skin barrier. In comparison, although this issue may have also arisen with the 1.5mm pads, it was observed that there was not as much skin resistance preventing puncture given needle depth. With the needle tips positioned closer to the base surface, theoretically, this minimized the horizontal swaying of the needles during application, although this aspect was not readily observable. As per this notion, the 1.5mm pads were noticeably easier to puncture into the surface, encountering less resistance from the skin pushing back along with the reduced penetration depth. Nevertheless, both needle variants exceeded the 5% margin of variability error to validate the effectiveness of the needles. The results are illustrated below in Figure 56.

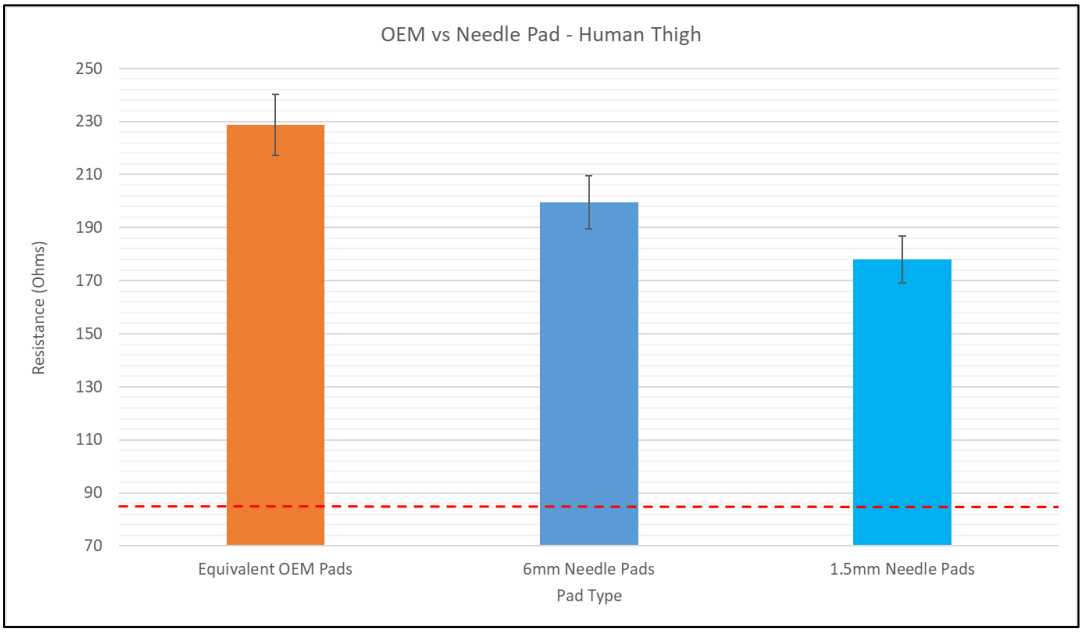

Figure 56 – Commercial vs needle pads on human thigh (Iteration 4)

Given the nature of the human thigh, unlike the animal samples from prior, there was a much higher degree of internal resistance. With the skin, muscles, fat content, human fluids, and bone there are many more internal obstacles for the current to pass through from one terminal to the other terminal of the pads. Due to this, the degree of improvement should be relative to just the effects of the skin as there is no way to overcome all internal aspects of the human body, nor the variability of it between different human specimens. Referring back to the project objectives, the goal of this project is to demonstrate the effectiveness of a microneedle-based defibrillator pad in overcoming the skin resistance, not the highly independent nature of the internal composition from person to person. As such, to further compare the effectiveness of the needle pads, the skin layer was removed from the thigh specimen, leaving behind as much content not pertaining to the skin as possible. The thigh sample is illustrated below in Figure 57.

Figure 57 – Thigh sample skin removal (Iteration 4)

As observed above, the location of the removed skin samples corresponded to where the test pads were placed during experimentation. The yellow layer left behind is the fatty layer which covers the inner muscles of the thigh. Once the skin was removed, the OEM pads were placed in these two cutouts and the resistance was measured. The measured value removes the resistance imposed by the skin and considers the rest of the internal resistance only. This value is marked in red dashes on the graph above and signifies a 63% improvement from the OEM pads on the surface after skin removal. This demonstrates that although the needle pads are bypassing some resistance, approximately 22% provided by the skin as measured, it does not bypass all of it and further efforts could be made to optimize the needle pads to approach this baseline value in this current pad iteration.

3.6. Iteration 5

3.6.1. Design Process – V5

With success in validating the effectiveness of subdermal needles and factoring necessary design conditions; using sufficient needle density, ensuring good surface interaction, and proper needle depth, the next step involved developing a prototype with functioning microneedles. This circles back to the initial goals of this project to produce a functional microneedle-based defibrillator pad. With the rather difficult manufacturing process and hard to maintain uniformity of the scalp microneedles in the first two iterations, a different manufacturing process was needed. Based on literature discussed in Chapter 2 with developing functional microneedle electrodes such as with Mahony et al., a commercial bulk micromachining method was selected to produce a set of microneedle arrays using a metallized silicon substrate [40], [77]. With the nanofabrication of these needles outside the scope of this research, the needle arrays were developed in partnership with the Waterloo Institute for Nanotechnology.

The notion behind this prototype was to integrate a set of microneedle arrays, while retaining the proven flexible nature of the needle base to encourage surface conformity. By nature, the silicon wafer substrate is a brittle material and lacks any form of flexibility unlike the ductile nature of most metals [78]. To balance the flexibility of the pad while maintaining a degree of rigidity to support the needles during pad application, the notion was to design a set of needle clusters which could then be placed separately on the pad, allowing pad flexibility in the non-substrate areas between. Given the limitations of a 1mm thick (100 crystal orientation) silicon wafer, the maximum manufacturable needle height was approximately 0.7mm. For prototype purposes, this should be sufficient to overcome any needle displacement in skin indentation due to physical skin characteristics. Although 0.7mm does not bypass the 1.5mm average skin thickness of a human being, 0.7mm would theoretically be enough to fully pierce the epidermis layer of the skin which ranges between 0.05mm to 0.15mm thick and likely to pierce the stratum corneum layer which ranges between 0.01mm to 0.03mm, as discussed earlier. Unlike prior where the design consideration was to verify the functionality of the needles, hopefully piercing both epidermis and dermis layers of the animal samples, 0.7mm was sufficient based on project objectives to reduce the majority of inherent skin resistance via the epidermis, as discussed in Chapter 2. While it is feasible to manufacture longer needles using a thicker silicon wafer, constraints related to equipment, resources, and overall production time rendered this option impractical. Additionally, to produce a defibrillator pad with sufficient microneedle clusters within resource constraints, only a single pad was created versus a pair.

The process flow to manufacture the needle arrays are detailed as follows:

1. **Substrate Preparation:**

A 1mm thick silicon wafer, featuring a 100 crystal orientation and measuring 4 inches in diameter, underwent cleaning to remove debris and dust using acetone with ultrasonication for 5 minutes. This step was crucial, as the bulk micromachining process employed to manufacture the microneedles would be constructed directly perpendicular to this surface.

2. **Needle Mask Pattern Preparation:**

A 48mm-by-48mm mask was created using KLayout, an integrated circuit layout editor. This mask consisted of 9 microneedle clusters, each with a 2.2mm needle pitch (the center-to-center distance between needles) and contained 25 needles per cluster. Since the final microneedle height determined the mask size, the needle pitch or spacing between needles on the mask needed to be approximately three times the final height of the needle to guarantee the proper creation of all needles and ensure overall stability. As such, the density of the microneedle array was maximized within the constraint of a 0.7mm needle height. This mask pattern is illustrated below in Figure 58, where white indicates the exposed silicon and red indicates the masked areas of the wafer.

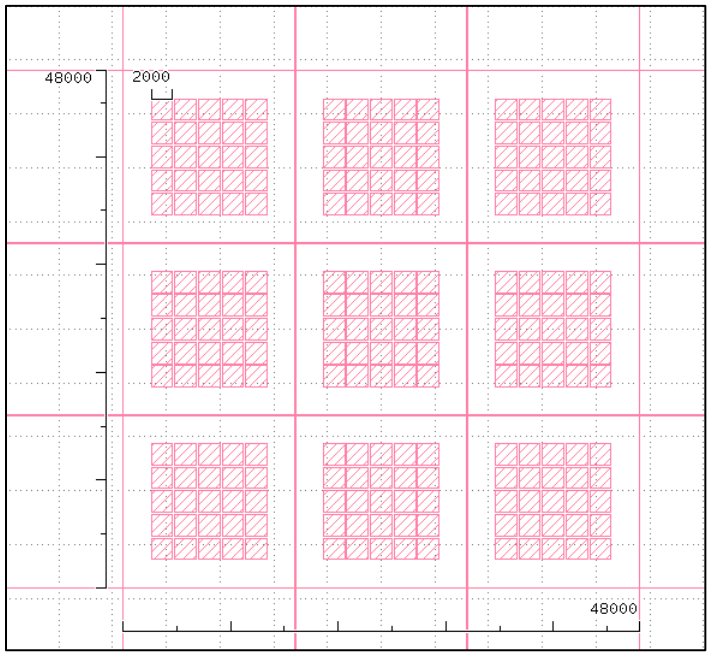

Figure 58 – Microneedle mask pattern (μm)

3. Low Pressure Chemical Vapor Deposition (LPCVD)

A 200nm silicon nitride layer was deposited on both sides of the silicon wafer via an LPCVD process deposition. The silicon nitride (SiN) layer was used as the main masking material for the microneedle pattern. Figure 59 illustrates the silicon nitride layer following its application onto the wafer.

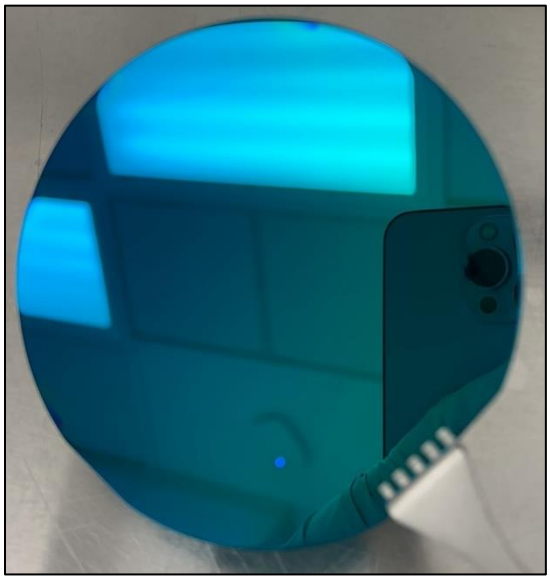

Figure 59 – LPCVD SiN deposition

4. Patterning

An AZ nLOF 2035 photoresist was deposited onto the wafer and UV-lithography was utilized to pattern the resist according to the previously defined mask pattern. The photoresist functioned as the mask of the SiN layer, safeguarding the areas marked in red from being etched away. Following the photoresist lithography, reactive ion etching (RIE) was used to etch away the unprotected areas of the SiN layer, forming the masked pattern.

5. Mechanical/Blade Dicing

An AZ P4620 photoresist was deposited onto the wafer via spin coating to protect the SiN mask layer during the dicing process. The dicing dimensions for each cluster were 1.6cm by 1.6cm and were mechanically diced, resulting in final clusters measuring approximately 1.3cm by 1.3cm. The AZ P4620 (thicker) and nLOF 2035 (thinner) photoresists were then removed using acetone following dicing. The diced wafer and remaining SiN mask layer, in green is illustrated below in Figure 60.

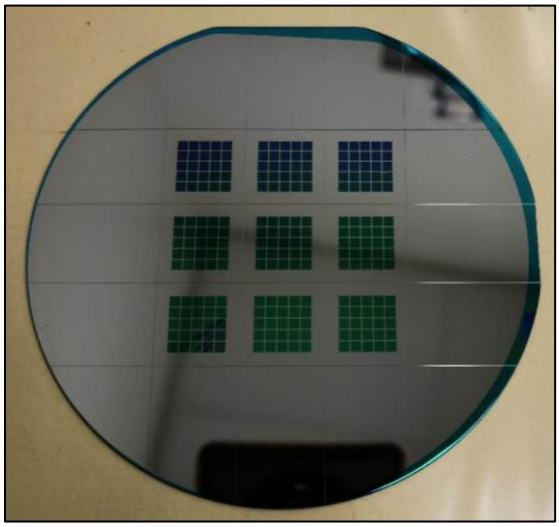

Figure 60 – Silicon wafer sample after dicing

6. Wet Etching

A 29wt% potassium hydroxide (KOH) solution at 80℃ was used to etch the pattern for approximately 10 hours. The remaining SiN material was fully removed during the etching process as the needles were formed. The desired needle height, 700 microns, was defined by the etching rate divided by the growth rate. In the case of these microneedles, the etch rate averaged around 72 microns per hour, totaling 10 hours to achieve the desired microneedle height. A scanning electron microscope (SEM) image of the etching process is shown below in Figure 61, with the microneedle on the verge of being fully formed.

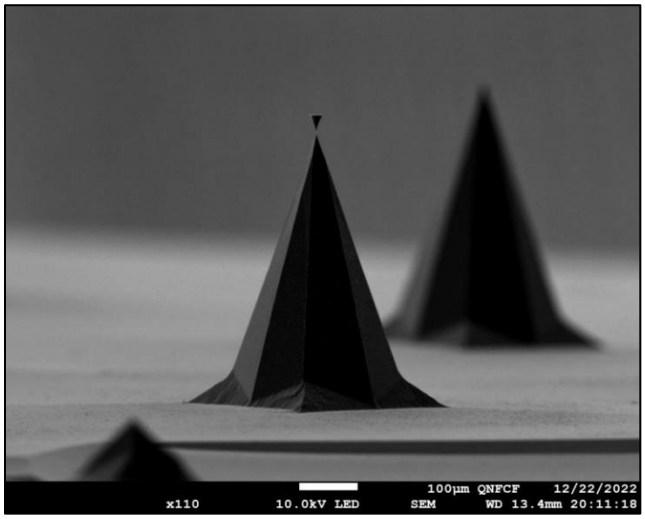

Figure 61 – Etching of microneedles

7. Cleaning

The needle arrays underwent an RCA cleaning process for 5 minutes at 75℃ to remove contaminants on the wafer surface. The RCA-1 clean recipe was as follows, H_20 (43%): NH_4OH (27%): H_20_2 (30%) at a 5:1:1 ratio. The wafers following the RCA cleaning process are depicted below in Figure 62.

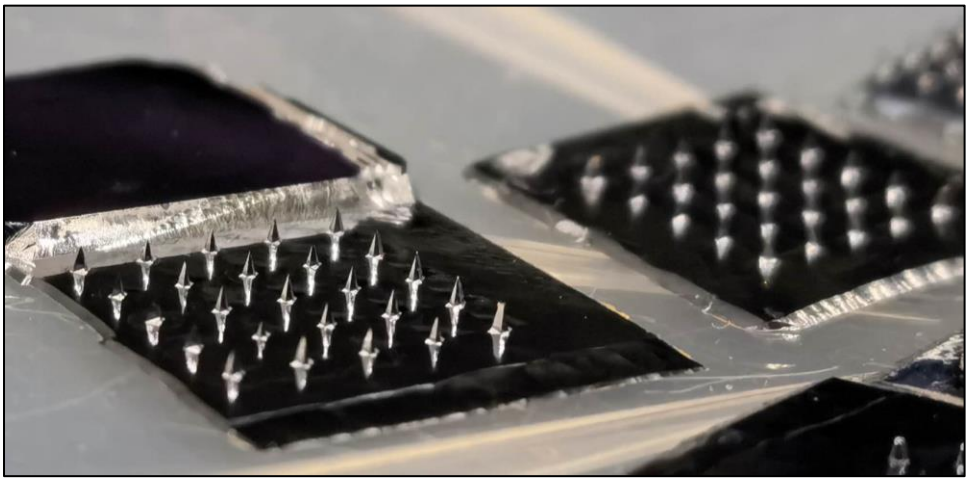

Figure 62 – Microneedle arrays after RCA clean

8. Metal Deposition

Two metallic layers were deposited onto the silicon arrays through e-beam evaporation: a 50nm titanium (Ti) base layer to enhance adhesion, followed by a 50nm layer of gold (Au). The images of the 8 completed needle arrays/clusters are shown below in Figure 63. Unfortunately, one of the nine clusters was damaged during manufacturing and was not received.

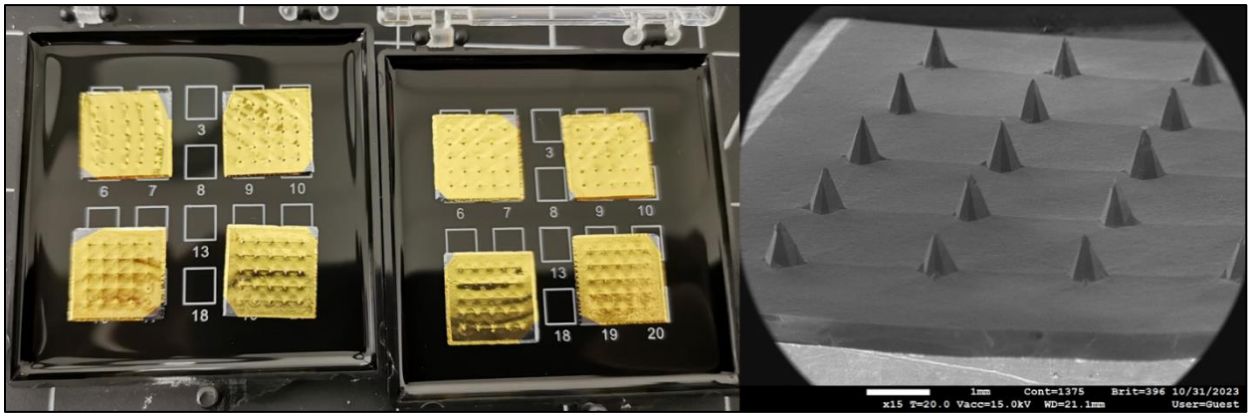

Figure 63 – Completed microneedle clusters

After the microneedle clusters were completed, SEM images were taken to measure the dimensions of the needles. All needles were confirmed to have an average height of 700µm (0.7mm) and a needle tip diameter of 3µm (0.003mm), as shown in the following images below in Figures 64 and 65.

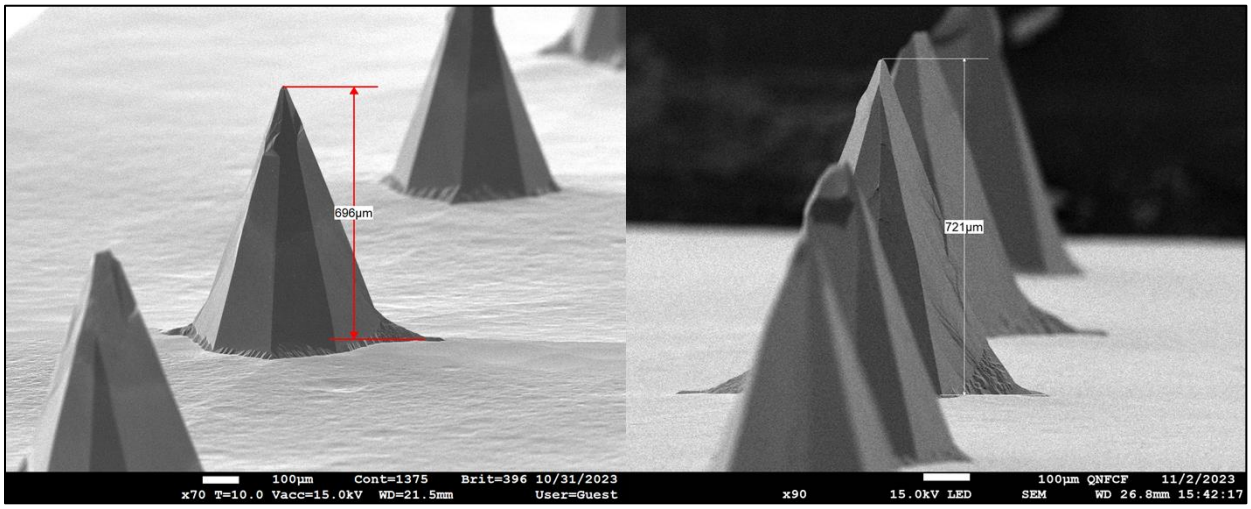

Figure 64 – SEM images of microneedle height measurement

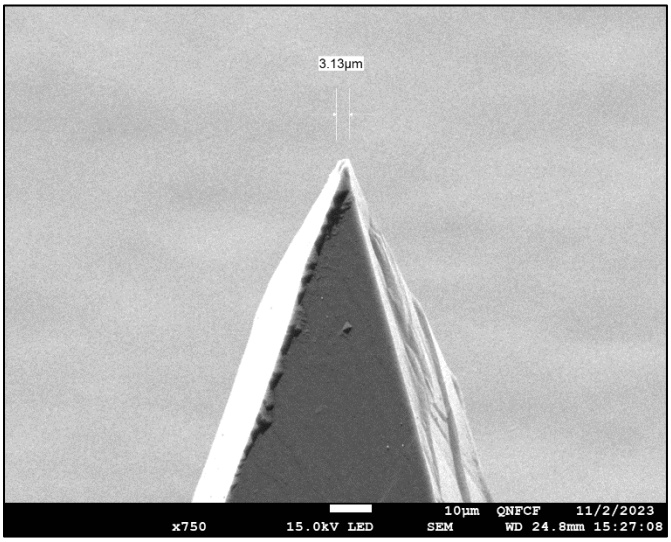

Figure 65 – SEM image of microneedle tip measurement

After the microneedles were produced, they were attached using double-sided tape onto a flexible TPU base measuring 5cm by 8cm, slightly smaller than the needle base used previously. The TPU base was designed to maximize flexibility so excess material was removed from the needle base. To account for the thickness of the electrical wiring between the microneedles, the clusters were elevated off the surface of

the base, creating a cavity. The design and particularly depth of the cavity was key to encourage surface interaction between the microneedle clusters and the skin while preventing the wiring harness from causing any disturbances. This attachment process is illustrated below in Figure 66.

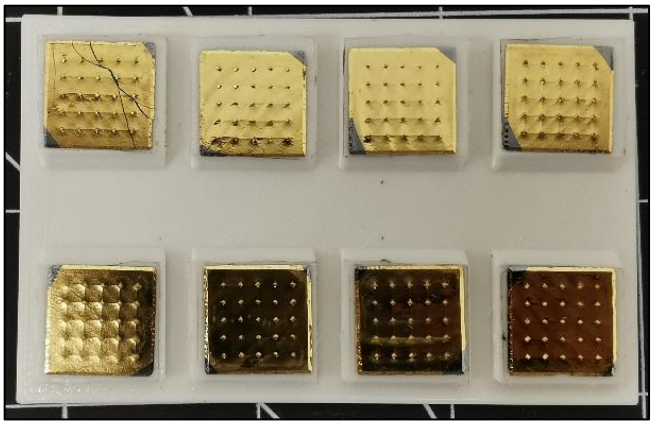

Figure 66 – Microneedle cluster attachment

As the metallic coating was only applied to one side of the needle array due to the process restriction of e-beam evaporation, wiring of the clusters could only be done using the surface. Despite some degree of interaction between the wiring and the microneedles which is not ideal, this proved to be the only manner for which a consistent connection could be formed. Various methods were attempted including using conductive copper taping or wiring just on the sloped edges, but they did not pass the basic electrical resistivity test. In addition, once the surface of the clusters had gotten saturated from the skin sample or electrode gel, the adhesives would begin to fail, disconnecting whatever connection was properly connected. Hence, it was determined that by running a wire from one side of the pad across the surface of the cluster, this would ensure a stable connection due to sufficient contact area and furthermore, vertical forces during pad application would ensure good wire to pad surface contact. As such, to minimize the wire interference, a relatively thin 24-gauge electrical wire was connected to each microneedle cluster. The wire was not tinned to allow ductility and promote surface conformity with the clusters. Each side of the wire was held in place via conductive copper tape and each cluster was connected separately with an individual wired connection. As per the project motivation, with the notion for future work in individual control of microneedle clusters, each cluster was connected separately as per this concept. This would also allow the evaluation of any number of these clusters during experimentation if so desired. Lastly, the wires were connected to a terminal block to function as the microneedle pad lead for experimentation. Following each experiment session, the old copper tape would be removed and replaced with a fresh set to ensure continued

adhesion of the wires. Resistance testing would be performed prior to each testing session to ensure all pads were properly connected to their wire harness. With the wire harnesses properly connected to the terminal block, the system resistance from the terminal to each cluster ranged between 0.9Ω – 2.3Ω. The completed prototype of the fifth iteration is illustrated below in Figure 67.

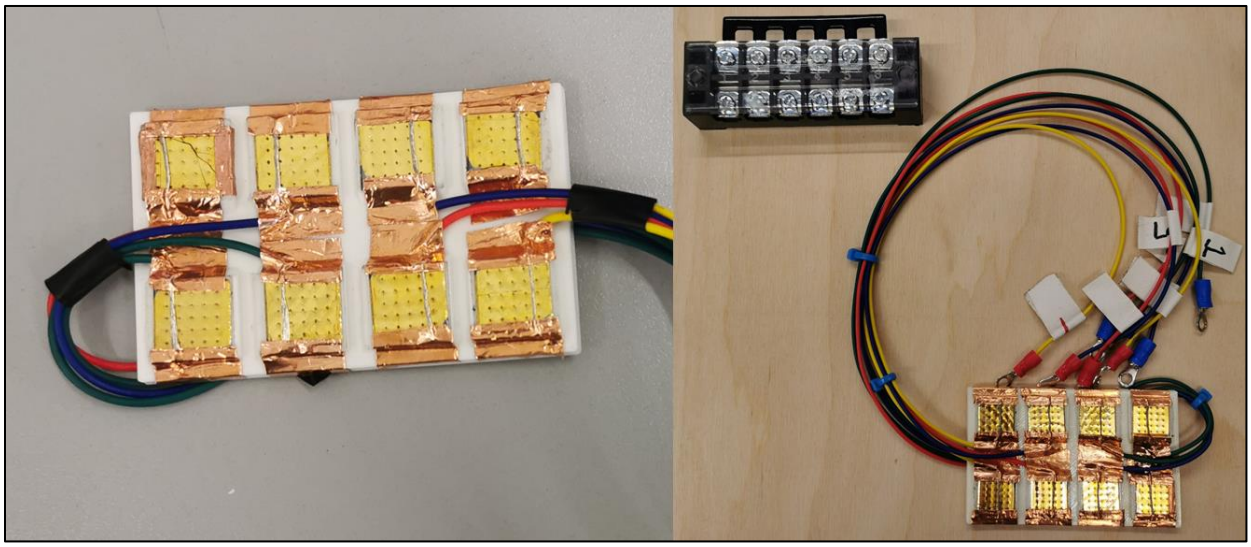

Figure 67 – Microneedle pad prototype (Iteration 5)

3.6.2. Test Methodology – V5

Using the experimental model, three separate cadaver mediums were used to evaluate the microneedle pads. First, a set of experiments were run using the human thigh sample from the last iteration. The OEM pads, Physio-Control Quick-Combo adult defibrillator pads were compared against the microneedle pad, with the other terminal remaining consistent as OEM pad. Similar to the last iteration, the skin layer at the test surface was removed to isolate the effects presented by the skin and revaluated using the set of OEM pads to determine a comparative OEM baseline value. Following this experiment, a second set of tests were run using the removed skin alone. The two human thigh skin samples were placed approximately 15cm apart from center-to-center on a conductive steel plate, substituting in as the internal resistance within a test medium. As an alternative method to measure the effects of the pads on the skin without the noise created by the high internal resistance of the human body, this would yield more conclusive results. The same test pad variants would be used on the skin and the OEM baseline value would simply be when the skin was removed off the conductive plate. An equivalent surface area equaling to 8 microneedle clusters was masked off for the OEM pad. As we saw earlier in the first several iterations, when the microneedle pad had

substantially less conductive surface area than the OEM pad, it was difficult to verify the effects of the needles. By removing all the values lower than the typical baseline and substituting in a conductive plate with low inherent resistance, the effects of the microneedle pad can be better observed. The test setup of this experiment is illustrated below in Figure 68.

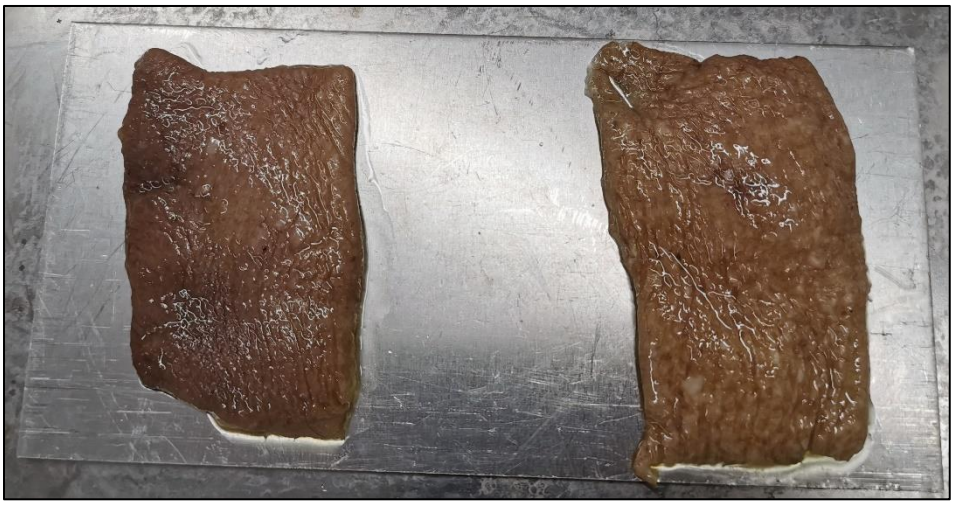

Figure 68 – Human thigh skin sample evaluation

Second, in collaboration with the Human Anatomy Dissection Laboratory at the University of Waterloo, a newly deceased fully intact unembalmed human cadaver body was acquired. This body was never frozen prior and was kept in a refrigerated morgue condition between 2°C (36°F) to 4°C (39°F) for several days leading up to the experiment. The body was left to acclimate to room temperature for roughly 26 hours prior to testing and bringing the internal resistance to more recordable levels. Although it was not possible to raise the inner temperature of a cadaver body to normal biological temperatures around 37°C (98.6°F) [79], letting the inner body acclimate to a warmer temperature would prove beneficial to observing the decay behavior of the signals with pad variations. The donor was a 90-year-old male weighing 51kg /112lbs and the cause of death was COVID-19 & advanced dementia. Identical testing sequences were performed by evaluating the effects of the OEM pad versus the microneedle pad. To characterize the behavior of the microneedle clusters, the number of clusters were incrementally connected to the terminal block, increasing from 1 to 8 number of clusters. This test sequence would demonstrate the functionality of the needle pad, validating the increased effect of the needles with each incremental microneedle array. The pads were placed diagonally on the frontside of the chest, one placed above the right nipple below the clavicle on the sternum and the other placed below the left nipple towards the side of the chest laterally. Due to the use of an adult cadaver body, the anterior-lateral pad placement method was used rather than an

anterior-posterior method commonly used for children [80]. The center-to-center location between the pads was approximately 33cm/13inches apart. The pads were placed on the cadaver as shown in Figure 69.

Figure 69 – Full body cadaver pad placement (Iteration 5)

Third, as it was not possible to remove any skin from the full body cadaver, chest skin was harvested from a different cadaver. This cadaver was also an unembalmed specimen but was frozen prior. After defrosting the body, two pieces of chest skin were harvested from the general area described above for adult pad placement, minimizing the amount of lipids extracted. The harvested skin samples are shown below in Figure 70.

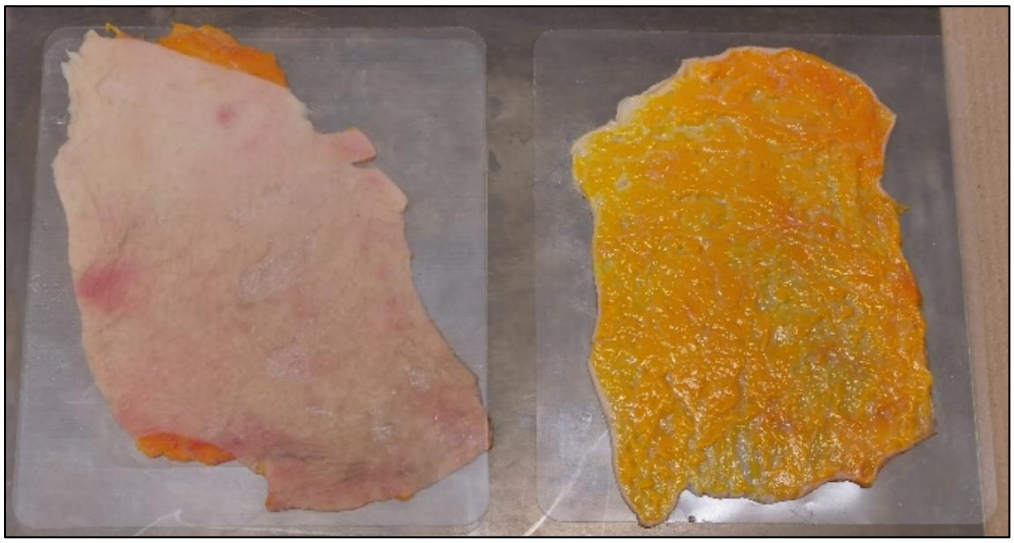

Figure 70 – Harvested cadaver chest skin (Iteration 5)

Using a caliper and two sheets of clear plastic, the skin thickness was measured to be 1.2mm, a value in line with the thickness of human skin as previously described according to literature. The donor was a 96-year-old female weighing 39kg / 86lbs and the cause of death was a combination of heart failure, pneumonia, and dementia. The skin was placed on a conductive steel plate with a center-to-center distance of approximately 18cm / 7inches apart. The interelectrode resistance was measured in the same manner as the previous set of experiments, incrementally increasing the number of microneedle clusters. Furthermore, to gather more data and confirm the validity of the results, this test was run again with a minor procedural adjustment on a separate day. To provide a better one-for-one comparison against the OEM pad, similar to the test methodology in iteration 2, an equivalent OEM characterization was performed. The equivalent conductive surface area was calculated for 2, 4, 6, and 8 number of microneedle clusters and likewise, the matching surface area on the OEM was exposed. Transparent plastic sheets were cut to sizes and were placed over the surface of the OEM pad in incremental order to mask the equivalent 2, 4, 6, and 8 cluster areas. The experimental setup as well as the constructed OEM masks are shown below in Figures 71 and 72. The table defining the conductive surface areas of each pad variant is detailed below in Table 4.

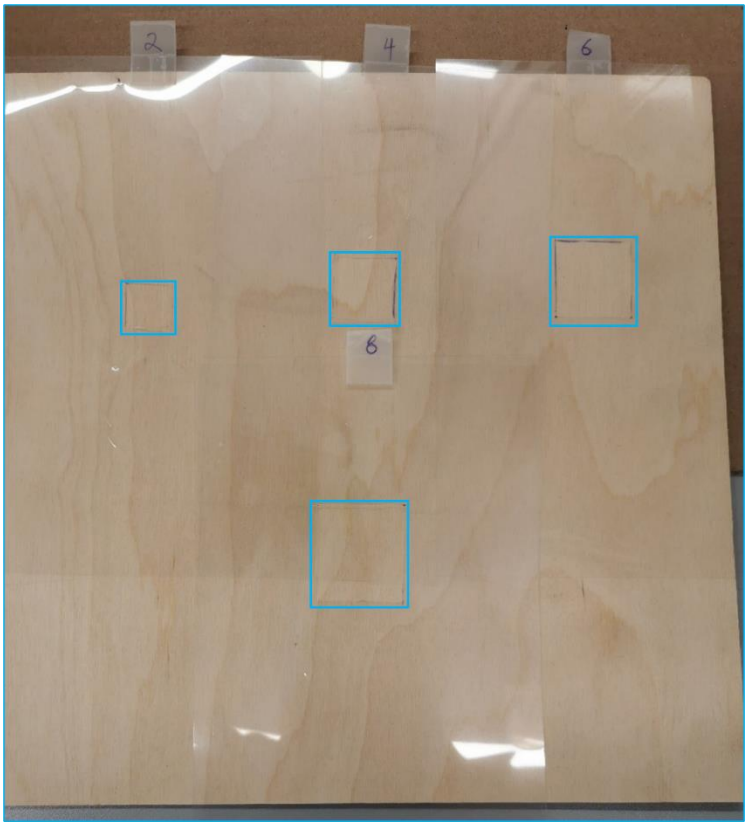

Figure 71 – OEM masks for equivalent cluster areas

Figure 72 – Cadaver chest skin sample evaluation (Iteration 5)

Table 4 – Estimated conductive surface areas of pad variants

Pad Variant	**Dimensions (cm)**	**Estimated Conductive Surface Area (cm^2)**
OEM Pad (Quick-Combo)	9.8 x 11.5	112.70
1# – Needle Cluster	1.3 x 1.3	1.69
2# – Needle Clusters	–	3.38
4# – Needle Clusters	–	6.76
6# – Needle Clusters	–	10.14
8# – Needle Clusters	–	13.52
~67# – Needle Clusters (Equivalent OEM)	–	113.23

3.6.3. Experimental Results – V5

For the human thigh sample, there was approximately a 5.5% improvement via the microneedle pad compared to an equivalently masked OEM pad. Relative to the OEM system baseline, where the skins were removed and the OEM pads were placed directly on the lipid layer of the thigh, a 6.5% reduction was observed. Although the measured median resistance values between the equivalent OEM and microneedle variations are similar in magnitude within a 5% variability range, four separate repetitions were performed to ensure accurate results. Additionally, it can be observed that the percentage reduction via the microneedle pads is very similar to the OEM baseline value after the skins were removed from the thigh. Due to the high internal resistance of a cadaver medium, similarities in the results were to be expected. The results of the human thigh evaluation are illustrated below in Figure 73, with error bars illustrating a 5% variability error.

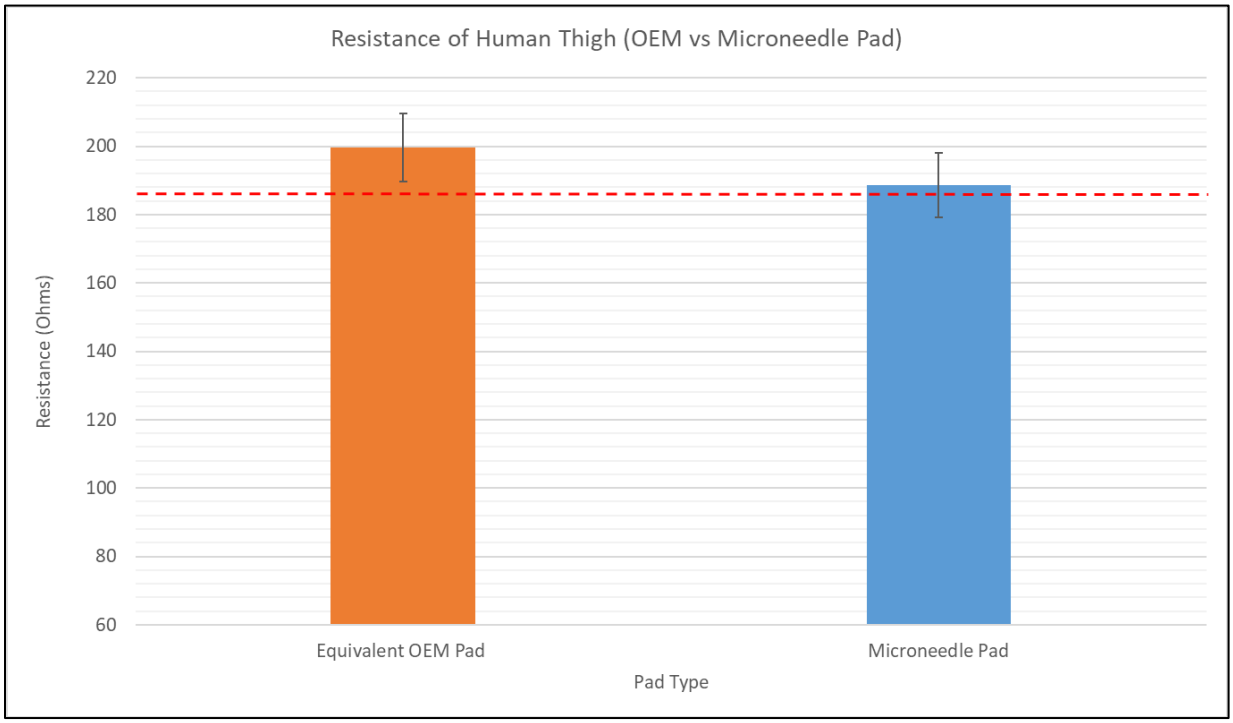

Figure 73 – OEM vs microneedle pad on human thigh (Iteration 5)

Likewise, for the human thigh skin evaluation on a conductive plate, a 17% improvement was observed via the microneedle pads compared to an equivalent OEM pad. Regarding the OEM system baseline, this time removing the skins from the plate and measuring the resistance via two OEM pads, there was a 37% improvement. Immediately, it can be observed that relative to the skin itself, there was a higher degree of improvement comparing one pad to the other. The magnitudes of both pad variations are outside

of the 5% variability error. Unlike the cadaver test on the full human thigh, there remains a 20% difference between the OEM baseline and the existing microneedle pad which could be improved with design revisions and other design factors. In either test, the improvement trend favors the microneedle pad versus an equivalent OEM counterpart and validates proper function of the pad design as was intended. The results of the human skin thigh evaluation on a conductive plate are illustrated below in Figure 74.

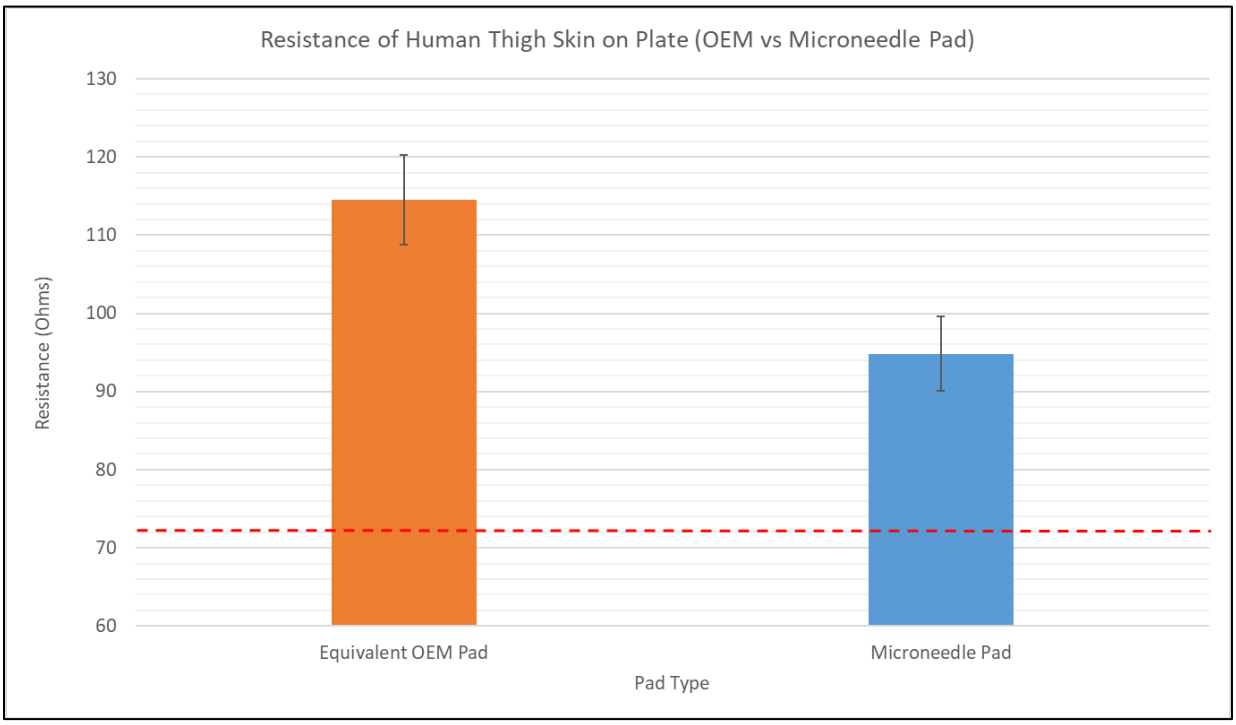

Figure 74 – Pad resistance comparison of human thigh skin on plate (Iteration 5)

To further demonstrate the functionality of the microneedles, a pad characterization evaluation was performed on a full human body cadaver, simulating the most realistic use case for a defibrillation medium. No baseline value was measured relative to the skin removed, as mentioned in the test methodology. From the results, using the full OEM pad as the comparison, it can be seen that the OEM pad has a lower interelectrode resistance versus the microneedle pad. Given that the entire microneedle pad is close to 9x smaller than the conductive surface of the Quick-Combo OEM pad, this result was to be expected and provides good context in comparison. Additionally, it can be seen that with each cluster connected to the system, a relatively noticeable rate of improvement is observed as we increase the number of clusters. As seen in the full thigh sample, due to the high inherent resistance in a cold cadaver body relative to the skin, which is of room temperature, slight changes in pad variations may not always result in the most noticeable

effects in terms of resistance. Particularly, in the middle number of clusters between 3 to 6, there does not immediately appear to be a drop-off. Factoring in the 5% variability error and after checking that the microneedles were properly connected; the data suggests that it was simply hard to evaluate the differences between cluster additions rather than being complete outliers in the data. Furthermore, looking at the dataset in its entirety, the progressive trend from one cluster to eight remains sound. The results from the full body pad characterization are shown below in Figure 75, with error bars illustrating a 5% variability error.

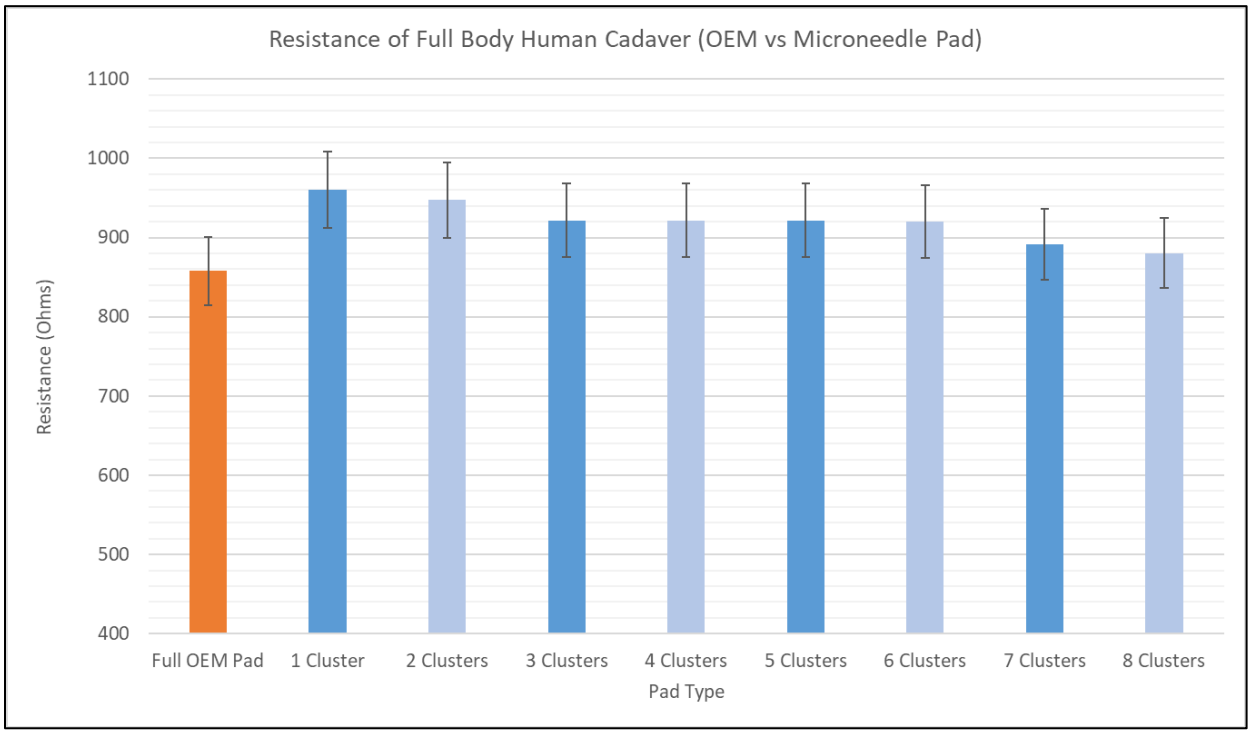

Figure 75 – Microneedle pad characterization of full body human cadaver (Iteration 5)

Lastly, the pad characterization experiments were performed on human cadaver chest skin using a conductive plate. The OEM baseline value with the skin removed and the OEM pads on the conductive plate are highlighted by dashed red lines on the graphical results. For the first evaluation, it can be observed that the distinctive trend in degree of improvement via each additional microneedle cluster is more pronounced than on the full body, reflecting the results from the human thigh evaluation. For the second test, the results also demonstrate the same progressive trend for both equivalent OEM and microneedle pad clusters. The implications of these results are discussed in the next chapter. The results from the first and second human chest skin pad characterization on a conductive plate are shown below in Figures 76 and 77, with error bars illustrating a 5% variability error.

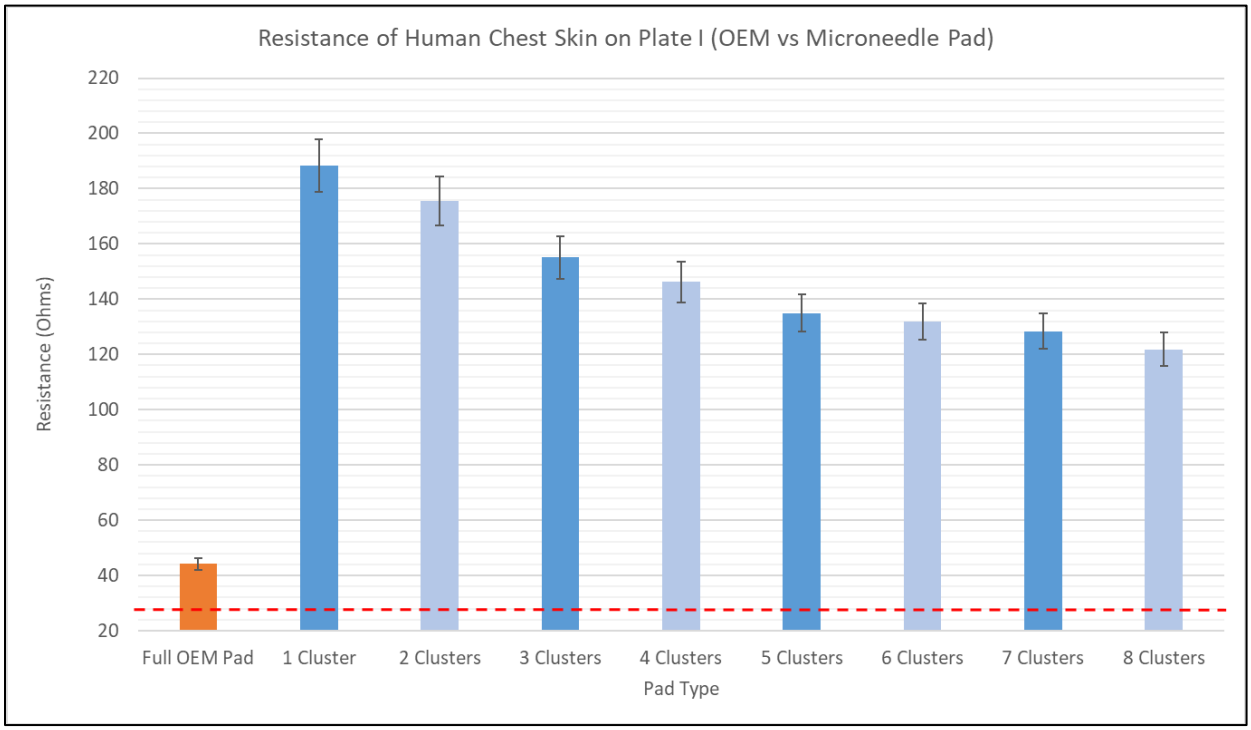

Figure 76 – Test #1 microneedle pad characterization of human chest skin on plate (Iteration 5)

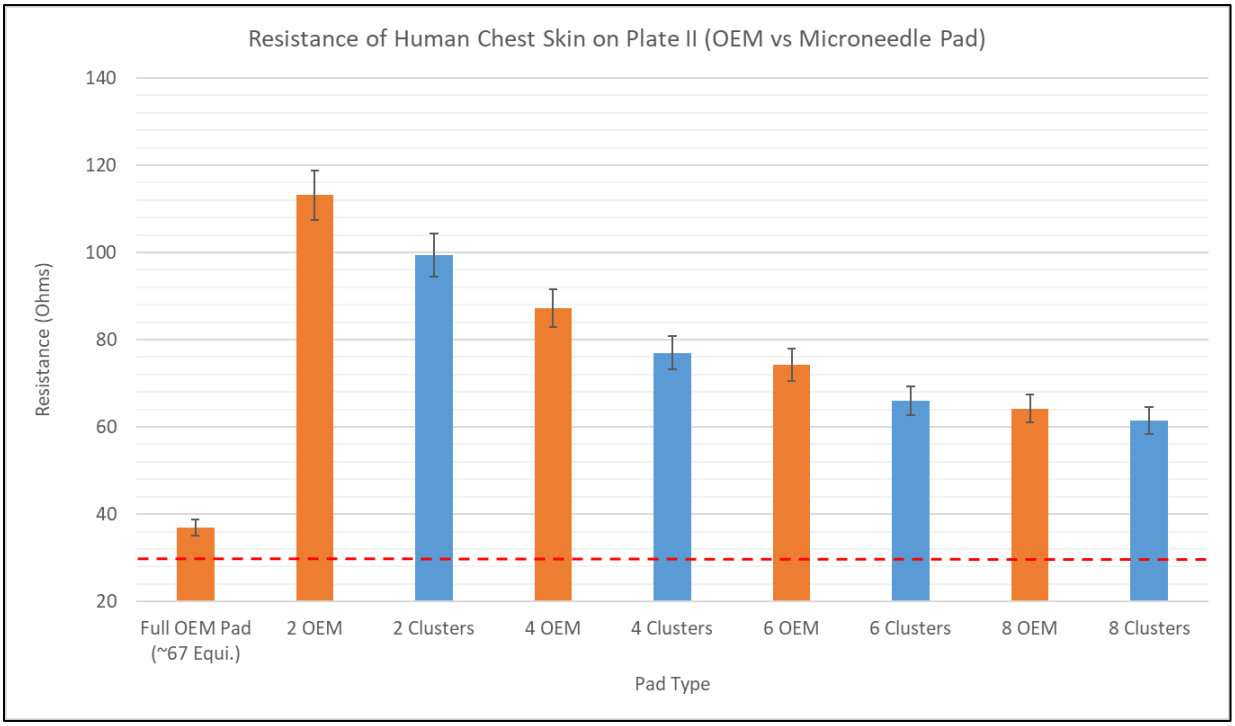

Figure 77 – Test #2 microneedle pad characterization of human chest skin on plate (Iteration 5)

Chapter 4

4. Discussion

The present study examined the necessity of improving the portability of AEDs by integrating microneedle-based electrodes, specifically their potential capabilities to improve the electrode-skin interface. This was accomplished by creating a set of operational MN electrode prototypes and then assessing their efficacy in decreasing the electrode-skin resistance in comparison to a conventional AED pad. It was hypothesized that a functional AED MN pad, demonstrating proper connectivity and resistivity characteristics, would exhibit a meaningful reduction in resistance. By addressing this aspect, it would allow for a reduction in the size and specifications of essential electrical components, thereby significantly decreasing the weight of an AED, and potentially enhancing cost-efficiency for both manufacturers and consumers. In this chapter, the results of the experimental methodology are discussed and validated in comparison with previous literature. Due to the limited availability of literature specifically on the development of MN electrodes for AED applications, only secondary comparisons and validations were conducted. Additionally, the implications and possible sources of error in the experimental process were discussed. A preliminary biocompatibility and safety assessment was conducted to validate the construction of the final iterative design of the MN prototype. Lastly, the insights and potential impact of this study were identified and are presented in this chapter.

4.1. Iterative Design & Experimental Methodology

In Chapter 3, a series of microneedle pad designs were iteratively developed and evaluated via an experimental model. This experimental model, derived from a study by Kugelberg, utilized a DC powered parallel resistor-capacitor circuit, otherwise known as a parallel RC circuit [67]. This circuit depicted the behavioral dynamics of a cycle involving charging and discharging an AED during defibrillation. Through this process, we quantitatively measured the inter-electrode resistance across various test mediums, including animal test samples and human cadaver mediums. As seen in literature, this was not the only method to evaluate the inter-electrode resistance, as an AC powered parallel RC circuit was also a viable option for the evaluation of biopotential electrodes, as depicted in Chapter 2. For this method, a range of frequencies from low to high were provided as an input, with results illustrating the associated inter-electrode impedance as a result.

There were several reasons why the experimental methodology was based on the former DC model rather than the later AC model for this study. As noted prior, modern AEDs typically utilize a DC power source via a biphasic waveform, where the current provided is one of low frequency. As the AC model analyzes the behavior of the electrodes under a dynamic high-frequency nature, the relevant measurements for AED applications would only pertain to the lower-frequency range. The AC RC circuit model considers the impedance of the electrodes as a function of frequency, considering both resistance and capacitive components of the load component, while possibly incorporating any inductive elements. This scenario refers to section 2.4 – microneedle technology overview, where literature illustrated the differences between a microneedle electrode and a conventional wet electrode for the electrode-skin interface, the load component of the electrical system [41]. Specifically, it was discussed that the untreated stratum corneum layer (top layer) possessed both a resistive and capacitive component, where the viable epidermis underneath was purely resistive. In comparison, the DC RC circuit model simplifies this behavior by treating the entire inter-electrode resistance, including the epidermis as purely resistive. At low frequencies, the impedance (Z_c) of the capacitor in the load itself would be high because the capacitive reactance (X_c) is inversely proportional the frequency (f) according to the formula $X_c = \frac{1}{2\pi fC}$, where C represents the capacitance [81].

As frequency (f) decreases, the capacitive reactance (X_c) increases by this relation. Furthermore, at extremely low frequencies, the reactance approaches infinity, effectively acting as an open circuit. Thus, at low-frequency signals, the capacitive components can be considered as open circuits, with the component impedance being negligible. As the capacitor and resistive component of the load are connected in parallel to each other, the current will only pass through the inter-electrode resistive component, comprised of the skin and the test medium. Similarly with a DC circuit model where the frequency is 0 Hz, the capacitor acts as an insulator or open circuit [82]. Hence, as noted by Kugelberg in his study, with either AC or DC current, the influence of the inter-electrode resistance would be the same as the current will only pass through the purely resistive component of the inter-electrode interface at low frequencies [68]. Therefore, a DC parallel RC circuit model was chosen for this purpose, aiming to comprehend the effect of capacitor charging and discharging on the overall electrode-skin resistance and evaluate electrode quality.

An iterative electrode design process was employed when developing AED MN electrodes as it allowed for continual refinement and improvement in the electrode design. As outlined in Chapter 2, the experimental literature on microneedle (MN) electrode development was primarily focused on monitoring biopotential signals and applying biofeedback stimuli. Each of these investigations employed different

fabrication methods, materials, electrode specifications, and experimental approaches to evaluate the efficacy of their microneedle (MN) electrode. They assessed various aspects such as the enhancement of biopotential signal strength, reduction of signal noise, or measurement of electrode-skin impedance. Although similarities were noted across the studies, the results diverged notably, with none specifically conducted on transthoracic human skin, which corresponds to their intended application area. Additionally, there was a lack of literature on the development of microneedle electrodes for AED applications, as this study represented a novel venture. Given the production of diverse microneedles through various fabrication techniques, particularly with variations in microneedle array specifications, and deviating resulting performance, it was crucial to determine what would be effective for AED applications. It was essential not only to illustrate the proposed advantages of microneedles but also to determine which fabrication technique would be suitable for a distinct application compared to literature, with a focus on transthoracic skin placement. Most notably, an AED microneedle electrode would have considerably larger dimensions compared to those utilized for other electrode applications discussed in the literature.

Therefore, five unique prototypes were developed iteratively, with concise justifications provided in Chapter 3, following the results of each design. A concise recap of these justifications will be revisited, highlighting key points. Due to the absence of experimental studies focusing on the effectiveness of MN electrodes in reducing electrode interface resistance in transthoracic human skin, the initial three iterations were designed to investigate this concept, culminating in a significant outcome achieved in the fourth and fifth iteration. The first iteration involved a flexible PCB with microneedles attached to predetermined positions through soldering and subsequently welding, both aimed at establishing a reliable electrical connection. The result of this iteration revealed that the pad failed both the initial connectivity tests and resistivity tests, indicating inadequate connections with the microneedles. For the second iteration, a modified flexible PCB was employed to improve needle adhesion, coupled with a crimped attachment method to securely affix the needles. In both iterations, solid prefabricated subdermal scalp microneedles, measuring 0.3mm in diameter, served as the primary needle component. The main challenge posed by these prefabricated microneedles was that constructing the electrode around their specifications to achieve the desired height, density, and thickness would prove challenging, making it difficult to guarantee uniformity across the pad. Thus, the exposed needle height using prefabricated microneedles was adjusted to be approximately 5mm. Meanwhile, owing to the significant variance in conductive surface area between the microneedle pad and a conventional AED pad, the outcomes were unfavorable, with no evidence of a reduction in resistance.

The objective of the third iteration was to improve the conductive properties of the penetrated electrode component by employing larger, more conductive nails to validate this principle. The intention was to create a more accurate comparison with the conventional by augmenting the conductive surface area of the subdermal component. Nevertheless, excessive emphasis on augmenting the conductive surface area within the same pad area led to a high density of needles, impeding proper electrode-skin contact and conformity, thereby yielding comparable inadequate outcomes. For the fourth iteration, prefabricated solid needles were once again employed, capitalizing on the shortcomings identified in the third iteration. More precisely, hobby needles (sequin pins), measuring 0.5mm in diameter, were chosen for their affordability, accessibility, and suitability for prototyping purposes. The needles were evenly spaced apart, with ample room left between them to prevent any concerns regarding complete penetration into the test medium. Considering the shorter manufactured length of these needles, the needle height was set at approximately 1.5mm, reflecting the average skin thickness as reported in the literature. The outcomes of this iteration showed promising effects, indicating a decrease in resistance in both animal and human thigh test mediums. Since solid hobby needles (sequin pins) were utilized in creating this electrode prototype, it became necessary to conduct additional assessments regarding the functionality of a microneedle electrode, especially considering the minimally invasive nature of the needles. Furthermore, in line with the objectives, it was imperative to develop a functional prototype that closely resembled an electrode capable of direct integration with an AED as a commercial product.

Therefore, the fifth iteration of the electrode prototype was crafted using one of the several traditional solid microneedle fabrication methods, namely bulk micromachining. Unlike pre-manufactured microneedles used for other applications, this fabrication method enabled precise control over needle density, thickness, number of needles per array, and uniformity in needle height, without compromising the thickness of the overall electrode. The manufactured needles measured 0.7mm in height with a needle tip diameter of 3μm (0.003mm). Eight clusters with 25 needles per array were affixed to a thin flexible TPU base. While other conventional methods could have been chosen for manufacturing the microneedles, this method was the most accessible for prototyping purposes, with the possibility of exploring other methods in future endeavors. To assess the functionality of this electrode, a pad characterization evaluation was conducted, measuring the effect of each microneedle cluster in comparison to a full conventional electrode. The outcomes of this test were not immediately evident, as further extrapolation would be necessary to directly compare equivalently sized pads. Similar to the issue encountered in earlier iterations, this arises from the significant difference in conductive surface area between the fifth iterative microneedle pad and a

conventional AED pad. The extrapolated outcomes of this experimental model are discussed in the following section.

4.2. Implications of Experimental Model

To achieve a more quantitative comparison of electrode performance, a line of best fit using common trendlines was overlaid onto the microneedle results from cluster-to-cluster, extrapolating the necessary number of MN clusters required to match the performance of the conventional electrode. Utilizing the equation derived from the line of best fit, the extrapolated cluster performance for an equivalently sized OEM pad, approximately 67 clusters (refer to Table 4), was determined. The x axis represents the number of clusters, and the y axis represents the projected resistance. The intersection points between this curve and the horizontally drawn line, which is the measured resistance of a baseline value, illustrates the equivalent comparison. As the fifth iterative MN electrode design had a conductive area approximately one-eighth the size of a conventional pad, it became imperative to extrapolate the performance of a full-sized MN AED pad that would be used in real-life scenarios. Utilizing an extrapolated approach enabled us to derive relevant data by projecting the performance curve through observed MN cluster results. By utilizing relatable data consistent with the specifications of AED electrodes, we were able to draw meaningful conclusions regarding the quantitative and qualitative impact of microneedle AED electrodes.

As a start, we will first discuss the results of the full body human cadaver, as shown in the next figure. The line of best fit for this set of data was a power curve trendline, which illustrates that the resistance decay is exponential proportional to the increase in number of MN clusters, as illustrated via the data. As mentioned in the previous section, due to the high internal resistance of the cold human cadaver, the degree of change may not have been immediately noticeable, particularly in the middle number of clusters from 3 – 6. However, with a variability error, limited datapoints for extrapolation, and possible sources of error from external factors, these data points were not removed as outliers. Using the extrapolated power curve, the intersection point, relating to the resistance of the full OEM pad, was 26 number of MN pad clusters (43.94 cm^2 estimated conductive surface area). This indicated a 61% reduction in estimated conductive surface area to reach the same level of performance as a single OEM pad. With the equivalent MN area comparison at 67 clusters, there was an estimated 4% reduction in resistance. As a reminder, the experimental results of Iteration 5 represent the results of a single MN pad and an OEM pad as its counterpart, while the comparison is the use of two OEM pads simultaneously. The extrapolated results of the full body human cadaver test are illustrated below in Figures 78 and 79.

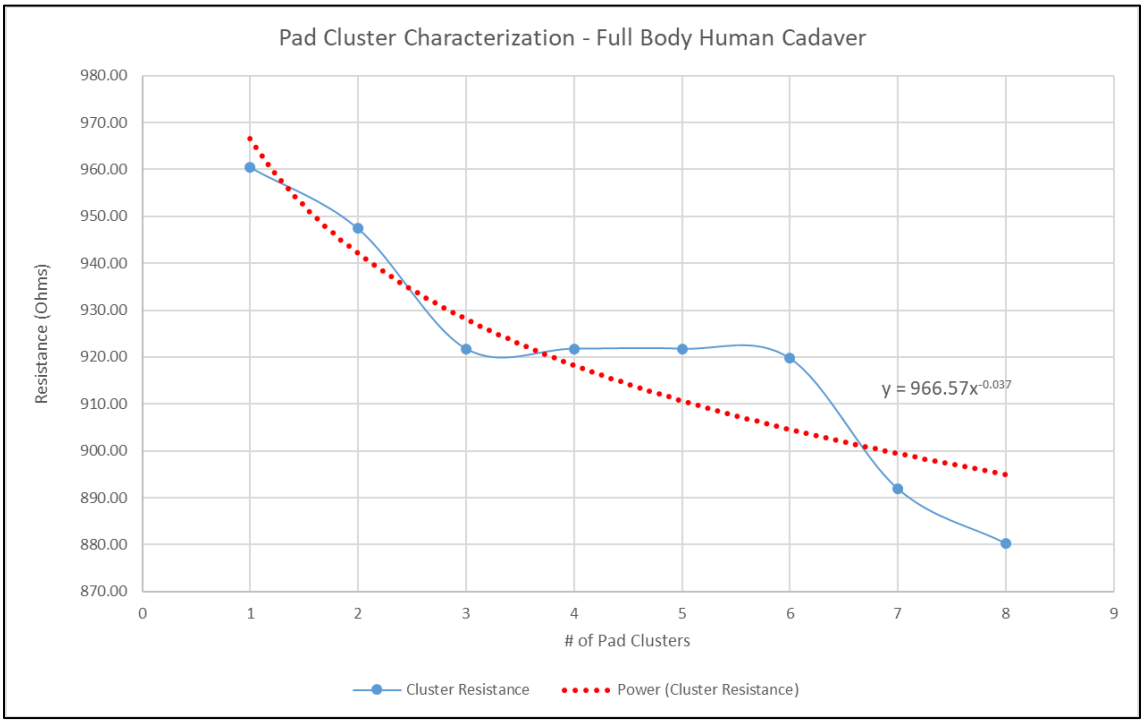

Figure 78 – Pad cluster characterization on full body human cadaver

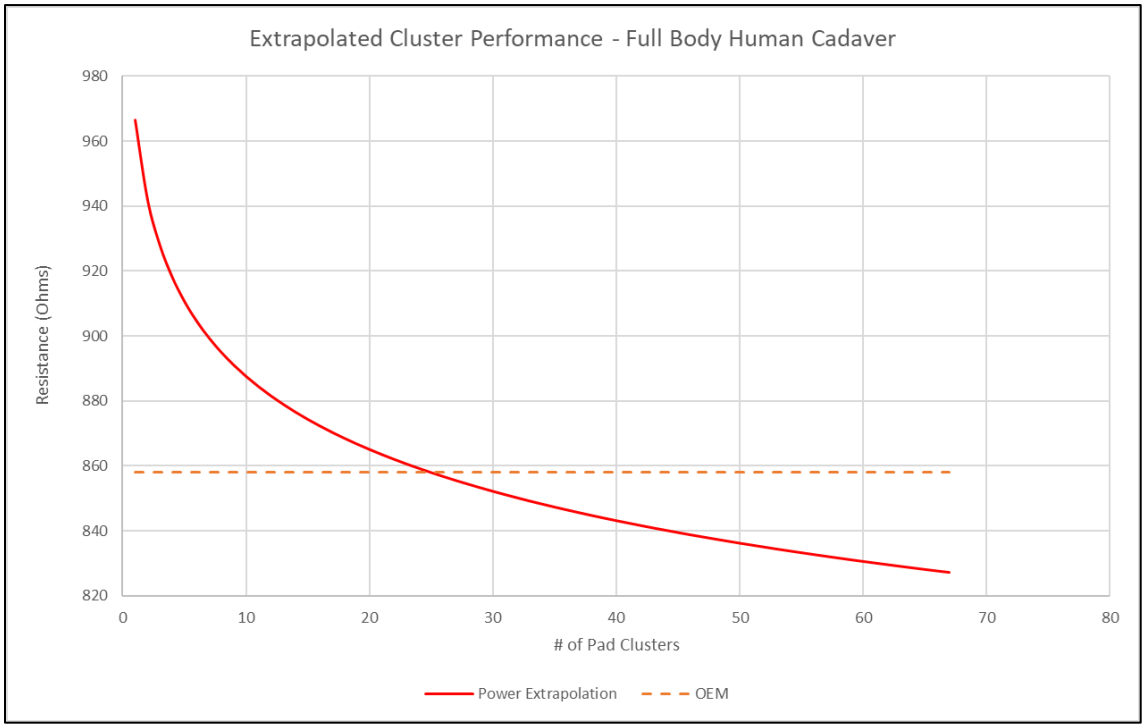

Figure 79 – Extrapolated cluster performance on full body human cadaver

As observed from these results, there are several limitations to discuss. First, other data trendlines such as a logarithmic trendline may also appear to fit the 8 MN cluster datapoints, which will result in a different approximation for the extrapolated performance of an equivalently sized MN electrode. As the actual performance curve is unknown, we can only estimate the behavior of the MN electrode with each added cluster based on projected characteristics, including a shifting slope pattern, an improved reduction in resistance, and a resistance baseline that cannot be exceeded with any further MN clusters. Knowing these characteristics, this provides sufficient evidence to eliminate certain trendlines including, linear due to the ever-changing slope and fit with the data, polynomial since there is no point of inflection, and exponential as the data does not appear to rapidly decay and accelerate with added clusters [83]. Although the actual performance curve may be a combination of different trendlines, the best current approximation uses a single trendline pattern. Based on elimination, this pattern is best represented by a power or logarithmic non-linear relation, where they exhibit an asymptotic behavior; the notion that the trendline approaches but never quite reaches a certain baseline value.

Second, the precision of the approximation may be uncertain. Although a trendline best suited for the data was chosen based on the aforementioned characteristics, this trendline is limited by the initial data points used to generate it. With the limitations of the MN pad, 8 consecutive datapoints are used to extrapolate the 59 consequent values, which make up the equivalent surface area of a conventional pad. As the 8 cluster datapoints represent a small portion of the overall data range, estimations are required for the following data points. Specifically, the trendline may not precisely represent the point at which the data plateaus, where the microneedles no longer provide additional benefit within a given surface area. The power or logarithmic trendlines are both sensitive to outliers, as they can disproportionately influence the placement of the trendline, thereby affecting the precision of the data extrapolated.

Third, the MN clusters may exhibit a reduced marginal return of adding additional surface area versus a conventional pad. As the curve is extrapolated from an early subsection of the data range, collected experimentally, it is uncertain whether the predicted consequent values would be reflected in reality. Although the function of the trendline is representative of the initial 8 data points, there is insufficient data to conclude that the function will continue as is, providing additional benefit per increment, with additional MN surface area. As such, to address many of these limitations and better exemplify the rate of reduction in resistance, additional testing was performed using human cadaver skin on a conductive surface. By removing the inherent transthoracic impedance and isolating for the skin resistance alone, the effects of the MN pad is better observed. The extrapolated results of this test are shown below in Figures 80 and 81.

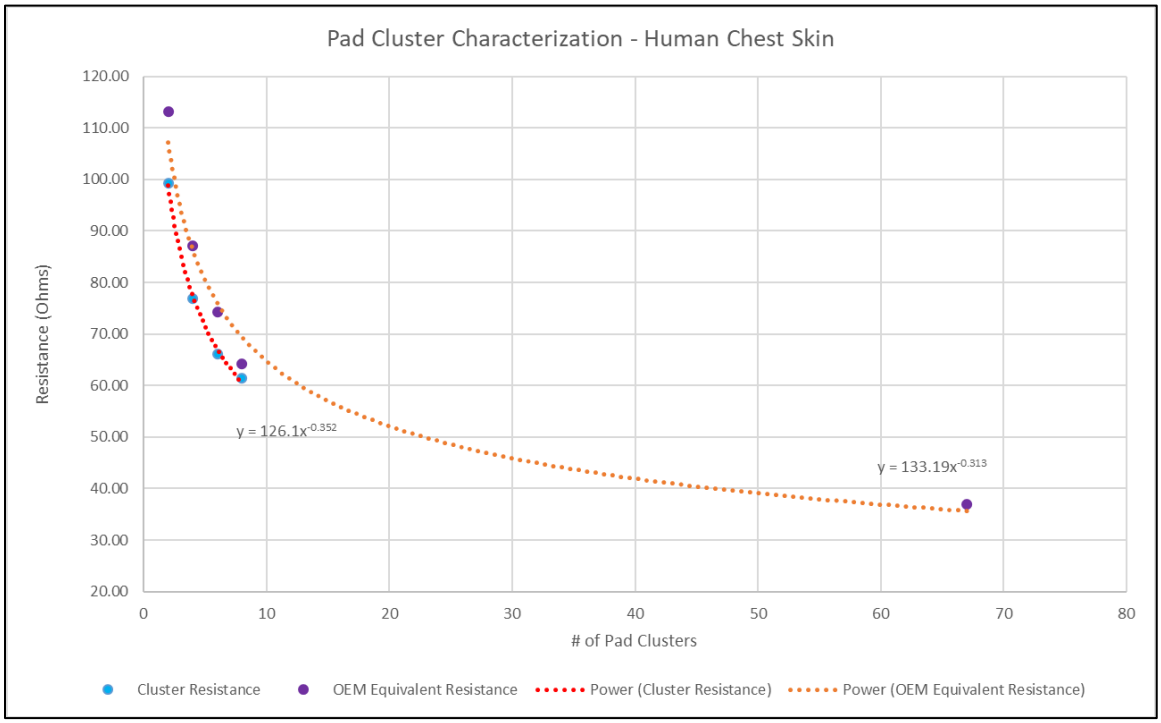

Figure 80 – Pad cluster characterization on human chest skin

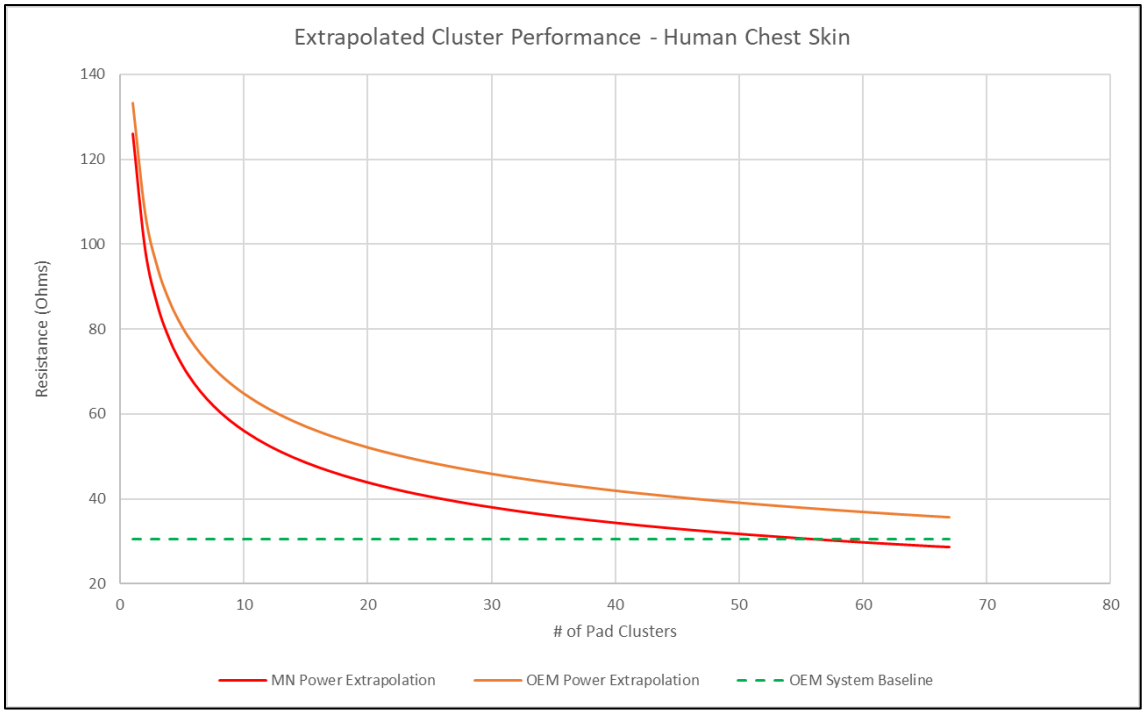

Figure 81 – Pad cluster characterization on human chest skin

Unlike previous tests where the difficulty in experimentation was always to extrapolate the performance of the MN pad to obtain a homogenous comparison with a conventional pad, this experiment utilized a controlled comparison approach. This approach referred to comparing both pads under identical, reduced equivalent surface area conditions (2,4,6,8 cluster equivalents), and increasing them in the same manner for the next dataset comparison. This ensured that any observed differences were directly attributed to the variable, the degree of resistance, being tested. In a like-for-like comparison, this also ensured that any observed differences were not due to disparities caused by the superimposed trendline and extrapolated function, as both datasets would be privy to the same inferred performance conditions to create the full scope of the data range. For the OEM pad, there was an added benefit of being able to measure the resistance of the full pad, otherwise known as the 67^{th} equivalent cluster. Likewise, the OEM system baseline value was measured using two OEM pads on the conductive plate itself.

This extrapolated experimental approach addresses the aforementioned limitations of an unknown performance curve for the full data range, uncertain precision, and a possibility for reduced marginal return with a MN pad versus a conventional, with varying degrees of justification. With the observed direct cluster comparisons, both pads illustrate similar trendline characteristics, specifically using a power trendline that best fits both datasets. The measured data showcases that between intervals, the rate of change is consistent and that they do not behave in an unpredictable manner, with increased marginal return with each added increment. Using an averaged dataset consisting of at least four separate repetitions per increment, there were no observed outliers that indicate the trendlines differ from the MN pad to OEM or vice-versa, nor any indication that the trendlines exhibit a sudden change in relative marginal return, if either trendline intersects the other at any point within the recorded data range. Thus, within our resource constraints, it is reasonable to assume that the extrapolation of this data would suggest that the two trendlines continue to behave in a similar manner, across the full range of the data. This provides a certain degree of confidence that for a like-for-like basis, it is reasonable to expect that the consequent 59 consecutive cluster datapoints perform according to this extrapolation, justifying the precision of the approximation. Likewise, by observing the trendlines defined by the full range of the data, the margin of return follows a similarly defined pattern. As there was no indication of a diminished relative return between the two pads in our observations, it is viable to assume that the pattern of separation is consistent throughout. Specifically at the projected end of the data range, despite the plateaued behavior of both pads, the relative marginal returns remain justified.

Therefore, the extrapolated results of the experiment illustrate that an equivalently sized, 67 microneedle clustered electrode exhibits an improved reduction in human transthoracic skin resistance versus a conventional AED electrode. Specifically, an equivalently sized MN electrode will further decrease resistance by an average of 20% versus an OEM alternative. Additionally, results indicated a 46% reduction in estimated MN electrode surface area (36 clusters) to achieve identical performance as a full-size OEM electrode (67 cluster equivalent). As mentioned prior, the experimentation and results specifically address the scenario when a single OEM pad is replaced with an equivalently sized MN pad. These results demonstrate the relative improvement an MN electrode would provide versus a conventional AED wet electrode, using an equivalent area-to-area comparison. However, due to resource constraints, the effects of two MN electrodes versus a pair of OEM electrodes were not evaluated as part of the scope of this set of experiments. With additional resources, further experimentation can be performed to confirm the accuracy of these extrapolated results as well as the additive benefit provided by a second MN electrode.

4.3. Sources of Error in Experimental Methods

Within the experimental methods to sample the observed data, there are several sources of error that may have arisen. First, the selection of the transthoracic skin samples and human chest cadavers may not fully represent a diverse living population. Specifically, the epidermal thickness of both samples may not conform to an average living human specimen, where the device would be deployed. Although the total skin thickness of the harvested transthoracic skin sample was measured to be an average thickness according to literature, this does not necessarily mean the composition of the layers reflect that. Additionally, both cadaver skin samples may not provide the appropriate level of distinction between male and female genders. Although testing was performed on both cadaver mediums, demonstrating similar trends in margin of return per cluster increment, the cadavers themselves may not appropriately represent the gender differences, such as amount of lipids as well as the skin thickness differences between the two cohorts. As untreated cadavers begin to decay almost immediately post-mortem, the cadaver skin mediums may not fully represent the electrical characteristics from an equivalent living human being. Although refrigeration of both samples was used to delay the decomposition process, these samples were subsequently left at room temperature for an extended duration during the experimental process.

Second, measurement error and measurement bias are factors to consider. As the main test methodology utilized a set of derived readings from an oscilloscope, this presents a possible degree of human error. Specifically, as this required manual intervention to record the point at which the decaying

waveform reached the desired time interval, inaccuracies and imprecise measurements of this component could lead to erroneous results. Additionally, as the experimenters are aware of which electrode is being used, this could influence their behavior during data collection such as an applied variability in pressure or hand placement, impacting skin contact which could lead to bias. To minimize these biases, test variations were repeated multiple times in a nonsequential manner, obtaining an averaged set of results.

Third, the standardized test procedure may not have accounted for unforeseen external factors. Similar to the development of the MN electrode iterations, the test procedure was iteratively revised to account for any prior unforeseen test factors. Despite the general test methodology having been based on literature, as the process was adapted to fit an array of test mediums, various external factors had to be considered. Specifically, these factors included the consideration of temperature, test medium moisture, skin condition, and preservation methods. However, upon reflection of the experimental methodology, other factors including the post-mortem interval, skin integrity, and anatomical cadaver variability, may present a degree of inconsistency in the data.

Lastly, the MN prototype design of iteration 5 may have contributed to the degree of variability in the results. As reported by Tezuka et al., the density, length, shape, and size of a microneedle array can result in varying degrees of needle displacement on the surface of the skin [63]. As the needles are positioned on the skin, there may be a portion of needles that do not penetrate into the skin, rather causing skin indentation instead. Especially in these experiments, the degree of penetration from MN cluster to cluster may vary, additional to the differences in skin conformity with each cluster position. As briefly mentioned earlier in the construction of the MN electrode, due to design limitations, the connecting wire that runs atop the base of the MN clusters would also influence the degree of penetration per needle array. To address the conductive aspects of the MN electrode, surface cracking caused by repeated experimentation on the microneedle prototype, may also influence the number of microneedles connected per cluster. As this was a known issue during experimentation, conductive copper tape was used to ensure the fragments remained connected to their associated wire harness, minimizing the variability between microneedle arrays to the fullest extent of our capabilities.

4.4. Comparison with Literature

Apart from some of the qualitative and design aspects which were briefly discussed in the previous sections, including sources of error and safety, the quantitative comparisons and associated novel contributions will be discussed in this section. The observed and extrapolated MN results, relative to their ability to reduce

skin resistance, presents a good contrast with literature. In Tang et al., who performed a comparison between the conventional versus MN electrodes in a biofeedback application, the study concluded that a pair of MN electrodes further reduced resistance by approximately 88% in the low frequency range and 27% in the higher frequency range [64]. In comparison, the results of our extrapolated experimentation yielded a 20% improvement via a single MN electrode versus an OEM AED pad.

The differences between these results can be explained by examining the test methodology, MN design, and pad applications within their respective fields. The design of their polyimide MN array utilized 500 – 600 μm needles and a tip diameter of 20 μm, whereas our study used silicon based 700 μm needles and a tip diameter of 3μm. As their conductive coating, copper was selected as opposed to gold, the more electrically conductive material. Comparing test methodologies, Tang et al. utilized a parallel RC circuit model with a varying AC sampling frequency as their input, while this study utilized a consistent DC voltage input through a similar parallel RC circuit model. As discussed previously for typical AED applications, a DC power source is provided using a low-frequency biphasic current. Thus, despite the differences in experimental methodology, it is important to acknowledge the results particularly in the low frequency range.

For their test medium, they utilized a living human arm from voluntary participants which differs from the transthoracic cadaver mediums used in our study. As skin thickness and layer composition vary from human to human, especially in different body locations, this aspect is important to consider when evaluating the improved effectiveness of MN electrodes relative to the degree of puncture. In regard to their results, the study performed a comparison using a pair of MN electrodes versus an equivalently sized pair of conventional electrodes, unlike the single pad comparison for our study. Experimentation to evaluate the effects of a single MN electrode pad versus OEM pad comparison was not performed.

It is also important to note that the size of a conventional biofeedback wet electrode is much smaller than that of an AED electrode, with differing design architecture. As conventional AED electrodes are built to transfer a high degree of electrical energy during defibrillation, the chosen pad materials would need to be robust to prevent degradation. Additionally, these electrodes are designed to maximize conductivity and minimize adverse reactions caused through defibrillation. On the other hand, the transfer of electrical energy is quite low in biofeedback-based electrode applications. As such, the design of these electrodes may prioritize other factors including long-term function, quality of life, and the use of less-expensive materials which may be sufficient in these applications.

Due to these differences, it is only viable to acknowledge the trend, where an equivalent MN electrode demonstrates significant improvements versus a conventional electrode. It is also important to recognize the viability of different MN materials and their construction, specifically the need to investigate their impact towards improving the electrode-skin barrier, in their specific application. On the other hand, the study performed by Rice University offers a better applicational comparison, as their study focuses on the evaluation of a needle-based attachment for AED electrodes. In this study, they concluded a 70% reduction for a post-mortem ovine model and a 5% improvement for pork tissue, using the combined needle-AED pad combination [65], [66].

Likewise, differences between these two studies will be briefly discussed. Rather than the development of a microneedle electrode to replace conventional pads, Rice opted to design a needle-based attachment instead. Due to this nature, testing was only performed with either a combined pad or an OEM pad itself. Similar to Tang et al., the comparison utilized two different pairs of electrode variations, one with the needle attachment and the other as normal. Likewise, they utilized an AC based parallel RC circuit model versus the steady DC model used in our study. For their test mediums, data was only collected on animal skin samples, specifically an ovine carcass and a piece of pork tissue. It is unclear what the specifics of their test methodology were, pertaining to test setup and details concerning the test mediums. Regarding the results, a unique observation was made which is similar in nature to the results of our study. As discussed in the iterative design process, pork skin is widely used as a test substitute for human skin. However, as observed through the results of various tests, due to the substantial lipid layer and thickness composition of the pork belly skin, the interelectrode conductivity within the test medium was greatly hindered. Similar to iteration 4, where experiments were performed using a combined needle pad variant, results illustrated a 10% improvement in pork but increased to 22% with the human thigh specimen. Similarly, the inter-electrode resistance results from their study indicated a minor 5% improvement in the pork sample compared to a significant 70% improvement in the ovine model, suggesting that the latter served as a more consistent skin substitute for human skin.

Due to these differences, particularly in test mediums as well as design methodology, only secondary comparisons can be made. Similar to Tang et al., Rice demonstrated a consistent trend, where the benefits of a needle-based device were observed. The design of their needle prototype was relative to the full size of an AED pad and experimentation on animal test mediums demonstrated significant results. As a contribution to literature, the experiments performed in our study further demonstrate this trend and illustrate significant results, using an extrapolated MN electrode comparison on transthoracic human skin.

Additionally, the specifications of a microneedle electrode, particularly length of needles, are consistent with those used in other microneedle electrode applications. By directly evaluating one of the primary aspects of electrode performance on a relatable test medium, this provides valuable data for future studies to build upon and optimize.

4.5. Biocompatibility and Safety Considerations

A preliminary biocompatibility and safety assessment of the microneedle electrode prototype was performed, to ensure the prototype design and material selection adhered to basic regulatory standards. Specifically, this assessment would determine whether the composition of the electrode causes any unwanted effects such as adverse reactions or tissue damage, upon application to a normal human skin sample short-term.

First, the biocompatibility of the prototype electrode will be addressed. Biocompatibility typically refers to the ability of a material not to trigger adverse reactions including inflammation, immune responses, or toxicity when introduced with biological systems. Specifically for electrode applications, this would refer to any form of skin irritation, sensitization, allergic reactions, inflammation, or corrosion. As presented in the design of the pad, the primary materials in contact with the electrode-skin interface are a gold-titanium film coated onto a silicon substrate. Although the use of this electrode would not be for long-term applications, it is still important to consider the immediate effects resulting from skin contact and puncture [84].

Titanium is widely used in the manufacturing of medical implants and is regarded as the most biocompatible metal due to its stable and inert nature when exposed to an oxidizing media [85]. Additionally, it has excellent corrosion resistance and mechanical properties, which are important to sustain the reliability of implants. Likewise, gold is also considered a biocompatible material often used in dental applications, pacemakers, and stents, as a coating which is inert and does not react biologically in the human body [86]. However, it is important to note that the biocompatibility of gold particles can vary depending on the purity of the material, as gold alloys may contain other metals which may not be biocompatible. In our application, the purity of gold was close to 100% and was mixed in equal concentrations with titanium, both of which are biocompatible materials. While both materials have been widely used in medical implants and applications without adverse reactions, it is still possible, although rare for individuals to have allergic reactions or sensitivity to these metals. According to a study on the rarity of metal allergies, metal hypersensitivity is seen in 10 – 15% of the general population, more often in women than in men [87].

Specifically, this thesis addressed the long-term use of biocompatible surgical clips commonly made from nickel or titanium. For future experimentation, other biocompatible conductive materials may be explored.

Second, the potential electrical safety concerns with the MN electrode will be discussed. A traditional AED electrode is designed to handle a high degree of electrical energy in short intervals, thus generally safe. As testing was not directly performed to evaluate electrical safety of the MN electrode prototype, by applying high degrees of current through the microneedle clusters, we can only justify this aspect with what was performed experimentally and through literature. Throughout the experimentation process, low levels of electrical energy were applied to the pad, with no observable physical degradation. As the inherent system resistance of the pad was measured to be quite low in the ohmic scale, the resistance in opposition of the applied current would also be relatively low. As the purpose of the electrode is to function as a conduit rather than a barrier for electrical energy transfer, this characteristic is desired. Furthermore, as gold is a good conductor of electricity, with a low inherent electrical resistance, it further promotes this characteristic. Hence, the second aspect in terms of safety for the patient is to address the consequent effects of applying a high degree electrical energy to the skin. With conventional AED electrodes, due to the use of low-frequency high currents in a very short amount of time, this presents undesirable effects which includes pain, redness, and burns. As discussed, the design of MN electrodes mitigates this effect as the majority, if not most of the electrical energy is sent through the largest electrical barrier of the skin, the epidermis. By bypassing the skin, the current will flow through the path of least resistance, rather than through the surface level contact between the electrode-skin interface. As discussed in literature for feedback applications, this permits the use of a lower required input energy to achieve the same level of performance.

Lastly, the general safety concerns of the use of MN electrodes will be discussed. As per literature, the design of the microneedle prototype electrode with respect to length and size conforms to what has been proven prior. The application process is designed to be painless, as the depth of the needles do not come in contact with the pain receptors or nerves in the dermal layer, piercing only the top stratum corneum layer in the epidermis. As the penetrated microneedles do not touch the sensory layer of the skin, the MN electrode evades any form of pain sensation by the user. Due to the penetration of the skin, a greater risk of infection may initially appear to be a concern. An MN AED electrode would be intended for single-use and thus, properly sterilized beforehand, minimizing this risk. Additionally, because the microneedles do not contact the blood vessels in the dermis, the risk of infection would stem from a form of diffusion similar to standard skin contact, rather than offering pathogens direct internal access through the bloodstream.

However, it is important to recognize that the penetrated epidermis may present a diminished barrier against pathogens, requiring less diffusion at the points of contact. Contrary to the use of conventional wet electrodes, sufficient surface preparation including hair removal, would not be necessary. Similarly, conventional skin preparation techniques present their own increased risk of infection if not performed properly. Nevertheless, the single-use nature of the device with proper sterilization of the surface and pad will minimize the risk of infection. Further experimentation is necessary to confirm the electrical safety of the electrode as well as any undesirable effects such as pain.

4.6. Impact of AED Microneedle Pads

With the iterative design and experimental results of the AED microneedle pads, there are various degrees of impact which pertains to the motivations of this study, the need to enhance the portability of AEDs while further optimizing the efficiency and delivery of shock energy.

First, the microneedle electrodes demonstrate the ability to improve the efficacy of AEDs. Through experimentation and extrapolated outcomes, a single equivalent microneedle electrode was able to improve the electrode-body interface by at least 20% versus a conventional AED electrode. As discussed in Chapter 2, literature has suggested that by using a pair of MN electrodes, the resulting outcomes will be further improved, with future testing required to evaluate this impact. As microneedles have been shown to create a more optimal and reliable contact with the body, this enhances the two main capabilities of an AED electrode. Not only will the shock energy be more effectively delivered through the body with an improved electrical conductivity, but in addition, as shown in literature, the detection of ECG waveforms will also be more stable, by attenuating the signal and reducing the impact of surface noise. Furthermore, by reducing the skin-electrode barrier, more current will be able to reach the heart muscles via the same level of electrical energy, in less amount of defibrillation cycles required for patient resuscitation. Alternatively, less energy from an AED will be required for the same defibrillation current to reach the heart muscles.

Second, enhancing the overall energy efficiency of AEDs can reduce their weight and increase their portability. Although there are many traditional public settings such as malls or schools which do not necessarily require an increased device portability, there remains a strong market in remote or public rural areas where an increased level of portability would be extremely beneficial. Based on our extrapolated results, one perspective is that the size of a single conventional AED pad can potentially be reduced by at least 46% (refer to section 4.2) through the use of MN electrodes, while still achieving comparable performance with the same shock energy. As the microneedle electrodes would be designed to be

compatible with existing AED architecture, allowing for seamless integration, the immediate packaging of the device could be reduced.

On the other hand, with the improved delivery of shock energy, there would be less of a requirement to provide as much initial shock energy as well, as less energy is dissipated by the electrode-skin barrier. By focusing on this aspect, the electrical framework, encompassing high-voltage components such as the capacitor, transformer, and battery, as well as associated control components including the charging circuit and relays can be scaled down in specifications and consequently in size. By adjusting the scale of the electrical framework as needed, it could potentially reduce the overall cost of an AED, making it more economical for production and purchase. As previously discussed, a singular AED pad of equivalent size, resembling the iterative prototype design, would decrease human transthoracic skin resistance by an average of 20% compared to the conventional pad. While additional testing is necessary to confirm this aspect, it can be inferred that employing a pair of MN electrodes could yield an incremental advantage, resulting in a projected further reduction in resistance ranging from 30 to 40%. This estimate is fairly conservative and rational since the pair of microneedle pads would be applied to the same individual, ensuring comparable electrode-skin contact surfaces for both. As such, given that both pads contribute to improving the electrode-skin interface, the overall skin resistance can be further diminished. In contrast to prior experiments where the current had to pass entirely through one side of the skin, using a surface-mounted OEM pad as the second probe, employing two MN pads would allow for direct current flow between electrodes, creating a bypass and an improved path of lesser resistance. This behavior is depicted in the subsequent simplified DC circuit model representation of the electrical load, as shown in Figure 82.

As per our discussion in section 4.1 and consistent with the equivalent circuit models presented in literature, the impedance of the capacitive elements in the skin was considered negligible at low frequencies and thus excluded for interpretation purposes. A simplified electrical load of an AED is comprised of the resistance in the skin (R_{skin}), interior transthoracic body resistance (Rt), and resistance in the heart (R_h). As the current from an AED needs to traverse the skin twice, entering through one pad and exiting through the other, the circuit model includes two skin resistance (R_{skin}) elements. The resistance of the heart is comprised of the heart muscles and tissues, necessitating an adequate amount of defibrillation current for successful resuscitation. The remaining transthoracic resistance, excluding the skin and heart, is represented by the resistance Rt. As outlined in Chapter 2, the cumulative skin resistance constitutes a significant portion of transthoracic impedance, although there is no precise overall estimate available. Since the MN electrodes directly reduce the resistance of the two skin components, the major resistive component in the load, it can

be inferred that they also meaningfully decrease the overall transthoracic impedance of the body. Based on our previous estimate range, it can then be argued that there may be a reduction in the overall electrical load of approximately 35%. In order to contextualize this estimate within the internal framework of the AED electrical architecture, a simplified circuit model featuring a scaled back electrical load is presented below in Figure 83.

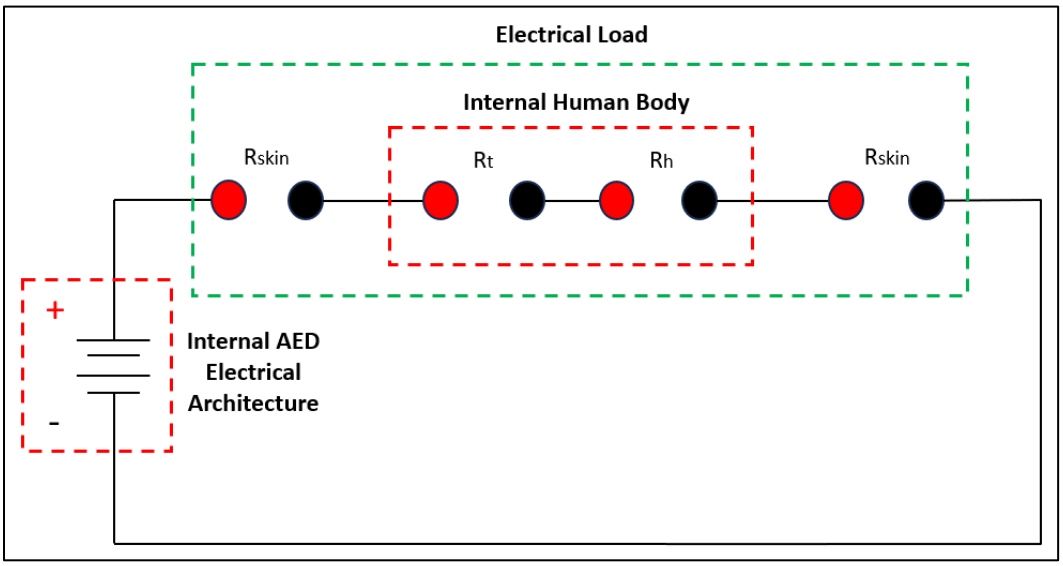

Figure 82 – Simplified DC circuit model of the AED electrical load

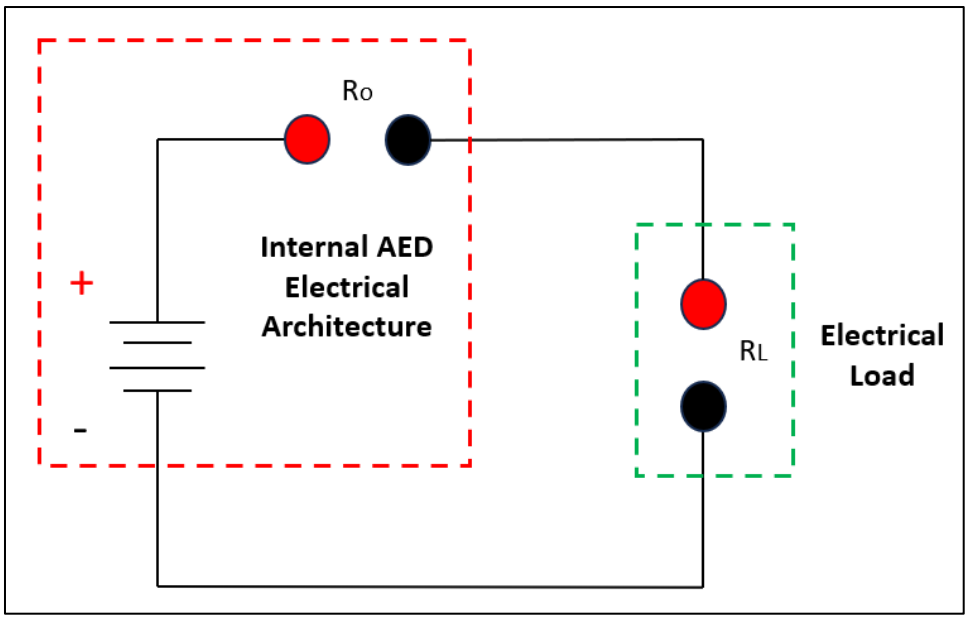

Figure 83 – Simplified overview of the circuit model for an AED system

The highlighted green area represents the electrical load, encompassing all elements depicted in the previously presented simplified model of the AED electrical load, focusing on the electrode-body interface. For the internal AED electrical architecture, which is highlighted in red, the resistive elements comprised of high-voltage components and circuit control devices are represented by R_o. With the load reduced by approximately 35%, we anticipate a proportional decrease in the energy supplied by the power source in the AED, as indicated by the series circuit model depicted above. Therefore, significant electrical components responsible for supplying this energy and constituting the majority of an AEDs weight, notably the battery, capacitor, and transformer, can be scaled down proportionally to achieve a maximum performance decrease of 35% compared to previous levels. Given the diminished requirement for supplying a high level of energy, the device's energy production capabilities can be downscaled accordingly. Since the composition of commercial AEDs is not openly disclosed and varies significantly between manufacturers, estimating the proportional weight decrease of these components can be challenging. Nevertheless, it can be inferred that by downsizing the major electrical components in both specifications and dimensions, the casing, which also contributes significantly to an AEDs weight, can likewise be substantially reduced. If we generously assume that a 35% decrease in performance corresponds to a similar decrease in the weight of a component and considering the average weight of an AED is 4.75 pounds as discussed in Chapter 2 [1], this will result in a reduced weight to approximately 3.1 pounds as an illustrative model. To provide some context in terms of common household items, this reduction in weight would be akin to carrying one less medium sized pineapple on person, which typically weighs around 2 pounds. However, additional research will be necessary to validate these speculations. By integrating these aspects into a potential new AED model, specifically for deployment in the AED use market where portability is key, the overall packaging and price for a traditional AED could be significantly reduced.

Finally, enhancing the portability of AEDs can lead to improved patient outcomes. Through the preliminary biocompatibility and safety evaluations, the usability and comfort of the microneedle electrodes have been shown to be comparable to a conventional electrode. As the needles are deep enough to puncture the epidermis, and significantly reduce the skin impedance, while not deep enough to cause any pain or bleeding, the comfort of the patient is not compromised. Additionally, despite the minimally invasive nature of microneedle electrodes, the likelihood of skin irritation or allergy is comparable to the conventional. As the microneedles do not come in contact with the bloodstream within the dermis, pathogens do not gain direct access to the body beyond typical skin diffusion. However, it was acknowledged that there might be a diminished barrier at the points of contact. With a microneedle electrode, ensuring a good electrode-skin

connection is not as reliant on skin preparation compared to a conventional AED electrode, where it is essential. With the use of lower shock energy and less dissipated energy on the skin surface, the risk of burns and redness will also be minimized. Additionally, there will be an increased level of safety due to the reduction in shock energy for both the patient and responder. The usability of the microneedle electrodes will remain consistent with the conventional designs, using a flexible substrate material, and featuring a robust adhesive component to ensure stable adherence of the pad to the skin during device operation. By increasing the portability of an AED, we can further increase accessibility, enable a more diverse audience to gain access to a defibrillator, and ultimately improve the rate of survival for individuals who suffer from SCA.

4.7. Summary

This chapter covered an array of topics crucial to the integration of microneedle-based electrodes for AED applications. First, the rationale behind the experimental methodology and iterative design process for the five developed microneedle prototypes was examined. Using the experimental results, we were able to draw meaningful conclusions through an extrapolated method of comparison. This method was necessary to create a direct comparison between the small-scale nature of the prototype MN pad and a conventional electrode, approximately eight times the scale in terms of conductive surface area. Significant results which were consistent and properly justified were obtained, with a 20% reduction in resistance through the electrode-skin barrier and a 46% reduction in conductive surface area necessary to match the performance of a conventional electrode. The design and experimental limitations were briefly discussed. Possible sources of error contributed by measurement error, external factors, and the variability of the data was provided. A brief biocompatibility and safety evaluation was conducted, evaluating the current design of the pad and potential issues which may arise from a microneedle electrode. The quantitative metrics of this study were compared with literature either directly or in a secondary manner by evaluating trends, differences, and limitations. The potential contributions to literature were also discussed, particularly the application of an MN based AED electrode evaluated on a human transthoracic medium. Finally, we completed the cycle by examining the overarching influence of microneedle-based electrodes with regard to the project's motivation. With an improvement in energy delivery efficiency, there is an increase in the intended portability aspect of an AED, resulting in enhanced patient outcomes.

Chapter 5

5. Conclusion

5.1. Summary

The objectives of this study involved assessing the viability of MN electrodes through the creation of a functional proof of concept compatible with existing AED architecture, examining the potential functional advantages or drawbacks offered by this prototype, and quantitatively determining its impact. After examining diverse literature pertaining to the current architecture of AEDs and advancements in MN electrodes in other applications, constraints were identified and taken into consideration into the development of a functional prototype. Subsequently, an experimental methodology was formulated to assess it effectively. Using this methodology and within the parameters of this research, it was theorized that an effective microneedle pad design would necessitate a strong electrical connection extending from the wire harness to the tip of each needle. Experiments conducted on human or animal skin substitutes were expected to reveal a notable decrease in resistance compared to conventional methods.

After five main MN electrode design iterations comprising of animal testing on chicken, pork, and duck as well as human cadaver testing, acquiring skin samples from the thigh and chest, significant findings were established. The electrode design consisted of 8 separate microneedle arrays assembled on top of a flexible base, roughly one-eighth the size of a conventional pad. Due to resource limitations, an equivalently sized electrode could not be manufactured, with only one electrode having been made. To resolve this, an extrapolated experimental approach addressed these issues by generating a predicted performance curve based on observed incremental equivalent area comparisons via the MN and conventional pads. Since the observed data displayed comparable trendline characteristics, showing increasing marginal returns per increment without any sudden changes in relative marginal returns between the two pad types, it was justifiable to assume that the subsequent predicted data points would behave as anticipated. As such, the extrapolated results illustrated that, in a one-to-one comparison between pads, an MN electrode offers an average reduction in resistance by at least 20% through the electrode-skin barrier and a 46% decrease in conductive area required to achieve the performance level of a conventional pad. While a functional evaluation was not conducted to confirm the integration of the MN electrode with an AED interface, particularly for receiving ECG waveforms and executing defibrillation, literature indicated positive outcomes in these areas. However, future testing would be necessary to validate these functionalities. An initial assessment of biocompatibility and safety determined that microneedle electrodes, specifically the

current iteration of MN electrodes are generally safe, with included features that enhance safety compared to conventional methods.

As we complete the cycle by revisiting the project's motivation, the design and development of microneedle electrodes for AED applications have a profound impact on the field. By harnessing the potential of MN electrodes, AED efficacy can be significantly enhanced by diminishing energy dissipation on the skin, thereby augmenting inter-electrode conductivity, and reducing the requisite shock energy for patient resuscitation. Based on a 20% reduction achieved by a single MN electrode pad and a series of reasonable assumptions, it was hypothesized that the electrical components responsible for supplying the shock energy could be scaled down proportionally, potentially resulting in a maximum performance decrease of 35%. As the demand for supplying high levels of shock energy decreases, the AEDs capabilities to deliver such defibrillation energy could be appropriately downscaled. As a result, the AED architecture can be redesigned since there is no longer a necessity to administer such high levels of shock energy. Through the utilization of smaller specification electrical components for high-voltage control, there is an overall reduction in AED size, enhancing portability. Additionally, a decrease in the electrical framework may lead to greater affordability in both the production and acquisition of an AED. Ultimately, AEDs will become more readily available to a broader audience, thereby enhancing patient outcomes, and improving the survival rate for sudden cardiac arrest.

5.2. Future Work

Although the proposed objectives were met, the current study presented several limitations which encourage future design improvements and additional experimental studies to be performed.

1. MN electrodes with varying needle height, density, conductive material, and other fabrication methods should be explored. The goal would be to pinpoint a set of characteristics that will enhance the pad's performance while also considering design considerations for manufacturing.
2. The subsequent version of the microneedle electrode should employ an improved technique for connecting the needle clusters and the wire harness, preferably on the non-contact side of each cluster. This will minimize any possible disturbance preventing full puncture into the test medium.
3. A secondary microneedle electrode of the same version should be produced to enable experimental comparison between two sets of MN pads versus a pair of conventional pads. Furthermore, future MN electrodes should closely match the size of an OEM pad to enable a more direct comparison without requiring extrapolated analysis.

4. Conducting a functional ECG measurement using the MN pads will be essential, as it serves as a critical AED device metric for identifying whether a patient has a shockable heart rhythm. The MN pads should exhibit performance metrics equivalent to those of a conventional AED electrode, with indications of an enhanced signal-to-noise ratio.
5. An assessment of external energy using a manual defibrillator should be conducted to compare heat generation between an MN electrode and a conventional pad. This quantitative analysis measures the risk of electrical burns during defibrillation. The pads should exhibit lower resulting surface temperatures compared to their counterparts when delivering the same level of shock energy.
6. Experimental testing should encompass a range of human test subjects (cadaver and living if possible) to gather data on the influence of gender, skin composition, and efficacy across different age groups, including adults and youth.
7. User studies should be conducted to gather feedback on the comfort and usability of MN electrodes, iteratively refining the electrode design to enhance usability.
8. Additional research is warranted to establish the correlation between the reduction in resistance at the electrode-skin interface and the consequent decrease in the required performance capabilities of an AED, along with its direct impact on the intended portability aspect as a result of a heightened device efficiency.

Letters of Copyright Permission

ELSEVIER LICENSE

TERMS AND CONDITIONS

Apr 12, 2024

This Agreement between Mr. Dominic Tung ("You") and Elsevier ("Elsevier") consists of your license details and the terms and conditions provided by Elsevier and Copyright Clearance Center.

License Number: 5766670315883

License date: Apr 12, 2024

Licensed Content Publisher: Elsevier

Licensed Content Publication: Sensors and Actuators A: Physical

Licensed Content Title: A 3D printed dry electrode for ECG/EEG recording

Licensed Content Author: P. Salvo, R. Raedt, E. Carrette, D. Schaubroeck, J. Vanfleteren, L. Cardon

Licensed Content Date: Feb 1, 2012

Licensed Content Volume: 174

Licensed Content Issue: n/a

Licensed Content Pages: 7

Start Page: 96

End Page: 102

Type of Use : reuse in a thesis/dissertation

Portion: figures/tables/illustrations

Number of figures/tables/illustrations: 1

Format: electronic

Are you the author of this Elsevier article?: No

Will you be translating?: No

Title of new work: Design and Development of Microneedle Pads for Automated External Defibrillators (AEDs)

Institution name: University of Waterloo

Expected presentation date: Apr 2024

Order reference number: N/A

Portions: Reuse "Fig. 8. ECGs from (a) dry and (b) wet electrodes" for reference as an illustrative example of electrode performance for thesis.

ELSEVIER LICENSE

TERMS AND CONDITIONS

Apr 12, 2024

This Agreement between Mr. Dominic Tung ("You") and Elsevier ("Elsevier") consists of your license details and the terms and conditions provided by Elsevier and Copyright Clearance Center.

License Number: 5766680057071

License date: Apr 12, 2024

Licensed Content Publisher: Elsevier

Licensed Content Publication: Sensors and Actuators A: Physical

Licensed Content Title: Long term biopotential recording by body conformable photolithography fabricated low cost polymeric microneedle arrays

Licensed Content Author: Alok Kumar Srivastava, Bhavesh Bhartia, Kingsuk Mukhopadhyay, Ashutosh Sharma

Licensed Content Date: Dec 1, 2015

Licensed Content Volume: 236

Licensed Content Issue: n/a

Licensed Content Pages: 9

Start Page: 164

End Page: 172

Type of Use: reuse in a thesis/dissertation

Portion: figures/tables/illustrations

Number of figures/tables/illustrations: 1

Format: electronic

Are you the author of this Elsevier article?: No

Will you be translating?: No

Title of new work: Design and Development of Microneedle Pads for Automated External Defibrillators (AEDs)

Institution name: University of Waterloo

Expected presentation date: Apr 2024

Order reference number: N/A

Portions: Reuse "Fig. 5. ECG data of the Dry and the wet gel based electrodes" for reference as an illustrative example of electrode performance for thesis.

CCC LICENSE

TERMS AND CONDITIONS

Apr 12, 2024

This is a License Agreement between Dominic Tung (“User”) and Copyright Clearance Center, Inc. (“CCC”) on behalf of the Rightsholder identified in the order details below. The license consists of the order details, the Marketplace Permissions General Terms and Conditions below, and any Rightsholder Terms and Conditions which are included below.

License ID: 1472884-1

ISSN: 1347-4065

Type of Use:

Publisher: IOP Publishing on behalf of the Japan Society of Applied Physics (JSAP)

Portion: Image/photo/illustration

LICENSED CONTENT

Publication Title: Japanese journal of applied physics : JJAP online

Author/Editor: Institute of Pure and Applied Physics

Date: 01/01/1962

Language: English

Country: Japan

Rightsholder: IOP Publishing, Ltd

Publication Type: e-Journal

URL: http://www.ipap.jp/jjap/index.htm

REQUEST DETAILS

Portion Type: Image/photo/illustration

Number of Images / Photos / Illustrations: 1

Format (select all that apply): Electronic

Who Will Republish the Content?: Academic institution

Duration of Use: Life of current edition

Lifetime Unit Quantity: Up to 499

Rights Requested: Main product

Distribution: Canada

Translation: Original language of publication

Copies for the Disabled?: No

Minor Editing Privileges?: No

Incidental Promotional Use? No

Currency: CAD

NEW WORK DETAILS

Title: Design and Development of Microneedle Pads for Automated External Defibrillators (AEDs)

Instructor Name: Naveen Chandrashekar

Institution Name: University of Waterloo

Expected Presentation Date: 2024-04-23

ADDITIONAL DETAILS

Order Reference Number: N/A

The Requesting Person / Organization to Appear on the License: Dominic Tung

REQUESTED CONTENT DETAILS

Title, Description or Numeric Reference of the Portion(s): Fig. 8. Distribution of the threshold voltage on the arm.

Editor of Portion(s): Japanese journal of applied physics

Volume / Edition: 55

Page or Page Range of Portion: 06GP15

Title of the Article / Chapter the Portion is From: Information transfer using wearable thin electrotactile displays with microneedle electrodes

Autor of Portion(s): Mayuko Tezuka et al

Issue, if Republishing an Article From a Serial: 6

Publication Date of Portion: 2016-06-06

References

[1] Avive, “Guide: AED Size and Weight Dimension - Avive AED.” Accessed: Mar. 04, 2024. [Online]. Available: https://avive.life/buying-aed/aed-size-weight/

[2] - AED.com, “How Much Do AEDs Typically Cost?,” AED.com. Accessed: Mar. 17, 2024. [Online]. Available: https://www.aed.com/blog/how-much-do-aeds-typically-cost/

[3] M. Neyman, “Latest Statistics,” Sudden Cardiac Arrest Foundation. Accessed: Mar. 02, 2024. [Online]. Available: https://www.sca-aware.org/about-sudden-cardiac-arrest/latest-statistics

[4] J. Chrispin, “Cardiac Arrest.” Accessed: Mar. 02, 2024. [Online]. Available: https://www.hopkinsmedicine.org/health/conditions-and-diseases/cardiac-arrest

[5] Y. Heyer, D. Baumgartner, and C. Baumgartner, “A Systematic Review of the Transthoracic Impedance during Cardiac Defibrillation,” *Sensors*, vol. 22, no. 7, p. 2808, Apr. 2022, doi: 10.3390/s22072808.

[6] L. W. Andersen, M. J. Holmberg, K. M. Berg, M. W. Donnino, and A. Granfeldt, “In-Hospital Cardiac Arrest,” *JAMA*, vol. 321, no. 12, pp. 1200–1210, Mar. 2019, doi: 10.1001/jama.2019.1696.

[7] Cleveland, “What Is Cardiac Arrest?,” Cleveland Clinic. Accessed: Mar. 03, 2024. [Online]. Available: https://my.clevelandclinic.org/health/diseases/21736-cardiac-arrest

[8] M. O. Elhussain *et al.*, “The Role of Automated External Defibrillator Use in the Out-of-Hospital Cardiac Arrest Survival Rate and Outcome: A Systematic Review,” *Cureus*, vol. 15, no. 10, p. e47721, doi: 10.7759/cureus.47721.

[9] R. A. Pollack *et al.*, “Impact of Bystander Automated External Defibrillator Use on Survival and Functional Outcomes in Shockable Observed Public Cardiac Arrests,” *Circulation*, vol. 137, no. 20, pp. 2104–2113, May 2018, doi: 10.1161/CIRCULATIONAHA.117.030700.

[10] P. Wendling, “Bystander Use of AEDs Could Double the Number of Survivors,” Sudden Cardiac Arrest Foundation. Accessed: Apr. 13, 2024. [Online]. Available: https://www.sca-aware.org/sca-news/bystander-use-of-aeds-could-double-the-number-of-survivors

[11] F. Sellers, “CPR training equipment a game changer on West Side,” The Enquirer. Accessed: Mar. 19, 2024. [Online]. Available: https://www.cincinnati.com/story/news/2017/08/24/cpr-training-equipment-game-changer-west-side/599233001/

[12] A. Fan, P. Han, and B. Liu, “Shockable Rhythm Detection Algorithms for Electrocardiograph Rhythm in Automated Defibrillators,” *AASRI Procedia*, vol. 1, pp. 21–26, Jan. 2012, doi: 10.1016/j.aasri.2012.06.005.

[13] G. Rodriguez, “Shockable vs. Non Shockable Heart Rhythms - Avive AED.” Accessed: Apr. 15, 2024. [Online]. Available: https://avive.life/blog/shockable-vs-non-shockable-heart-rhythms/

[14] C. Foth, M. K. Gangwani, I. Ahmed, and H. Alvey, “Ventricular Tachycardia,” in *StatPearls*, Treasure Island (FL): StatPearls Publishing, 2024. Accessed: Apr. 15, 2024. [Online]. Available: http://www.ncbi.nlm.nih.gov/books/NBK532954/

[15] D. Ludhwani, A. Goyal, and M. Jagtap, “Ventricular Fibrillation,” in *StatPearls*, Treasure Island (FL): StatPearls Publishing, 2024. Accessed: Apr. 15, 2024. [Online]. Available: http://www.ncbi.nlm.nih.gov/books/NBK537120/

[16] Perry, “Monophasic vs. Biphasic Shocks - What’s the Difference.” Accessed: Mar. 03, 2024. [Online]. Available: https://avive.life/blog/monophasic-vs-biphasic/

[17] F. M. Charbonnier, “External defibrillators and emergency external pacemakers,” *Proc. IEEE*, vol. 84, no. 3, pp. 487–499, Mar. 1996, doi: 10.1109/5.486750.

[18] Y. Kim and P. H. Schimpf, “Electrical behavior of defibrillation and pacing electrodes,” *Proc. IEEE*, vol. 84, no. 3, pp. 446–456, Mar. 1996, doi: 10.1109/5.486746.

[19]P. Romanowski, “How external defibrillator is made - material, production process, making, history, used, parts, components, procedure,” How Products are Made. Accessed: Feb. 25, 2024. [Online]. Available: https://www.madehow.com/Volume-7/External-Defibrillator.html
[20]R. E. Kerber *et al.*, “Automatic external defibrillators for public access defibrillation: recommendations for specifying and reporting arrhythmia analysis algorithm performance, incorporating new waveforms, and enhancing safety. A statement for health professionals from the American Heart Association Task Force on Automatic External Defibrillation, Subcommittee on AED Safety and Efficacy,” *Circulation*, vol. 95, no. 6, pp. 1677–1682, Mar. 1997, doi: 10.1161/01.cir.95.6.1677.
[21]AEDUSA, “Defibrillator Joules Volts | aedusa.com.” Accessed: Mar. 04, 2024. [Online]. Available: https://www.aedusa.com/knowledge/defibrillator-joules-volts/
[22]G. W. McNaughton, J. P. Wyatt, and J. C. Byrne, “Defibrillation--a burning issue in coronary care units!,” *Scott. Med. J.*, vol. 41, no. 2, pp. 47–48, Apr. 1996, doi: 10.1177/003693309604100205.
[23]S. J. Sirna, D. W. Ferguson, F. Charbonnier, and R. E. Kerber, “Factors affecting transthoracic impedance during electrical cardioversion,” *Am. J. Cardiol.*, vol. 62, no. 16, pp. 1048–1052, Nov. 1988, doi: 10.1016/0002-9149(88)90546-2.
[24]C.-M. Yu *et al.*, “Intrathoracic Impedance Monitoring in Patients With Heart Failure,” *Circulation*, vol. 112, no. 6, pp. 841–848, Aug. 2005, doi: 10.1161/CIRCULATIONAHA.104.492207.
[25]C. D. Deakin, D. M. Sado, G. W. Petley, and F. Clewlow, “Differential contribution of skin impedance and thoracic volume to transthoracic impedance during external defibrillation,” *Resuscitation*, vol. 60, no. 2, pp. 171–174, Feb. 2004, doi: 10.1016/j.resuscitation.2003.10.001.
[26]Nagarkar, “Skincare science: Skin anatomy,” Nagarkar Plastic Surgery. Accessed: Mar. 03, 2024. [Online]. Available: https://drnagarkar.com/skin-anatomy/
[27]F. Lu *et al.*, “Review of Stratum Corneum Impedance Measurement in Non-Invasive Penetration Application,” *Biosensors*, vol. 8, no. 2, p. 31, Mar. 2018, doi: 10.3390/bios8020031.
[28]H. Yousef, M. Alhajj, and S. Sharma, “Anatomy, Skin (Integument), Epidermis,” in *StatPearls*, Treasure Island (FL): StatPearls Publishing, 2024. Accessed: Mar. 03, 2024. [Online]. Available: http://www.ncbi.nlm.nih.gov/books/NBK470464/
[29]A. Olejnik, J. A. Semba, A. Kulpa, A. Dańczak-Pazdrowska, J. D. Rybka, and J. Gornowicz-Porowska, “3D Bioprinting in Skin Related Research: Recent Achievements and Application Perspectives,” *ACS Synth. Biol.*, vol. 11, no. 1, pp. 26–38, Jan. 2022, doi: 10.1021/acssynbio.1c00547.
[30]S.-Y. Roh *et al.*, “The Impact of Personal Thoracic Impedance on Electrical Cardioversion in Patients with Atrial Arrhythmias,” *Medicina (Mex.)*, vol. 57, no. 6, p. 618, Jun. 2021, doi: 10.3390/medicina57060618.
[31]B. Grunau *et al.*, “Public access defibrillators: Gender-based inequities in access and application,” *Resuscitation*, vol. 150, pp. 17–22, May 2020, doi: 10.1016/j.resuscitation.2020.02.024.
[32]J. Sandby-Møller, T. Poulsen, and H. C. Wulf, “Epidermal thickness at different body sites: relationship to age, gender, pigmentation, blood content, skin type and smoking habits,” *Acta Derm. Venereol.*, vol. 83, no. 6, pp. 410–413, 2003, doi: 10.1080/00015550310015419.
[33]C. Czekalla, K. H. Schönborn, J. Lademann, and M. C. Meinke, “Noninvasive Determination of Epidermal and Stratum Corneum Thickness in vivo Using Two-Photon Microscopy and Optical Coherence Tomography: Impact of Body Area, Age, and Gender,” *Skin Pharmacol. Physiol.*, vol. 32, no. 3, pp. 142–150, Mar. 2019, doi: 10.1159/000497475.
[34]T. Poonawalla, “Anatomy of the Skin.” Accessed: Mar. 03, 2024. [Online]. Available: https://www.utmb.edu/pedi_ed/CoreV2/Dermatology/page_03.htm

[35]A. I. Ianov, H. Kawamoto, and Y. Sankai, “Development of a capacitive coupling electrode for bioelectrical signal measurements and assistive device use,” in *2012 ICME International Conference on Complex Medical Engineering (CME)*, Jul. 2012, pp. 593–598. doi: 10.1109/ICCME.2012.6275720.
[36]X. Xu, H. Zhang, Y. Yan, J. Wang, and L. Guo, “Effects of electrical stimulation on skin surface,” *Acta Mech. Sin. Li Xue Xue Bao*, vol. 37, no. 12, pp. 1843–1871, 2021, doi: 10.1007/s10409-020-01026-2.
[37]HeartSine, “Product manuals for Canada - HeartSine.” Accessed: Mar. 05, 2024. [Online]. Available: https://heartsine.com/product-manuals-for-canada/
[38]SisneoBioscience, “What is the conductive gel used for? | Sisneo Bioscience.” Accessed: Mar. 04, 2024. [Online]. Available: https://sisneo.com/en/blog/what-is-the-conductive-gel-used-for/
[39]H. Carim, “Cohesive nonsticky electrically conductive gel composition,” WO1981000785A1, Mar. 19, 1981 Accessed: Mar. 04, 2024. [Online]. Available: https://patents.google.com/patent/WO1981000785A1/en
[40]F. K. Aldawood, A. Andar, and S. Desai, “A Comprehensive Review of Microneedles: Types, Materials, Processes, Characterizations and Applications,” *Polymers*, vol. 13, no. 16, p. 2815, Aug. 2021, doi: 10.3390/polym13162815.
[41]L. Ren, B. Liu, W. Zhou, and L. Jiang, “A Mini Review of Microneedle Array Electrode for Bio-Signal Recording: A Review,” *IEEE Sens. J.*, vol. 20, no. 2, pp. 577–590, Jan. 2020, doi: 10.1109/JSEN.2019.2944847.
[42]X. Luo, L. Yang, and Y. Cui, “Microneedles: materials, fabrication, and biomedical applications,” *Biomed. Microdevices*, vol. 25, no. 3, p. 20, 2023, doi: 10.1007/s10544-023-00658-y.
[43]V. P. Chavda, “Chapter 4 - Nanobased Nano Drug Delivery: A Comprehensive Review,” in *Applications of Targeted Nano Drugs and Delivery Systems*, S. S. Mohapatra, S. Ranjan, N. Dasgupta, R. K. Mishra, and S. Thomas, Eds., in Micro and Nano Technologies. , Elsevier, 2019, pp. 69–92. doi: 10.1016/B978-0-12-814029-1.00004-1.
[44]Mayo Clinic, “Electrocardiogram (ECG or EKG) - Mayo Clinic.” Accessed: Mar. 04, 2024. [Online]. Available: https://www.mayoclinic.org/tests-procedures/ekg/about/pac-20384983
[45]John Hopkins, “Electromyography (EMG).” Accessed: Mar. 04, 2024. [Online]. Available: https://www.hopkinsmedicine.org/health/treatment-tests-and-therapies/electromyography-emg
[46]Mayo Clinic, “EEG (electroencephalogram) - Mayo Clinic.” Accessed: Mar. 04, 2024. [Online]. Available: https://www.mayoclinic.org/tests-procedures/eeg/about/pac-20393875
[47]E. Volna, M. Kotyrba, and H. Habiballa, “ECG Prediction Based on Classification via Neural Networks and Linguistic Fuzzy Logic Forecaster,” *ScientificWorldJournal*, vol. 2015, p. 205749, Jun. 2015, doi: 10.1155/2015/205749.
[48]P. Salvo, R. Raedt, E. Carrette, D. Schaubroeck, J. Vanfleteren, and L. Cardon, “A 3D printed dry electrode for ECG/EEG recording,” *Sens. Actuators Phys.*, vol. 174, pp. 96–102, Feb. 2012, doi: 10.1016/j.sna.2011.12.017.
[49]E. Forvi *et al.*, “Preliminary technological assessment of microneedles-based dry electrodes for biopotential monitoring in clinical examinations,” *Sens. Actuators Phys.*, vol. 180, pp. 177–186, Jun. 2012, doi: 10.1016/j.sna.2012.04.019.
[50]L. M. Yu, F. E. H. Tay, D. G. Guo, L. Xu, and K. L. Yap, “A microfabricated electrode with hollow microneedles for ECG measurement,” *Sens. Actuators Phys.*, vol. 151, no. 1, pp. 17–22, Apr. 2009, doi: 10.1016/j.sna.2009.01.020.
[51]C. O’Mahony, F. Pini, A. Blake, C. Webster, J. O’Brien, and K. G. McCarthy, “Microneedle-based electrodes with integrated through-silicon via for biopotential recording,” *Sens. Actuators Phys.*, vol. 186, pp. 130–136, Oct. 2012, doi: 10.1016/j.sna.2012.04.037.

[52]L.-S. Hsu, S.-W. Tung, C.-H. Kuo, and Y.-J. Yang, “Developing Barbed Microtip-Based Electrode Arrays for Biopotential Measurement.,” Jul. 2014, Accessed: Mar. 05, 2024. [Online]. Available: http://archive.org/details/pubmed-PMC4168478
[53]M. Matteucci *et al.*, “Micropatterned dry electrodes for brain–computer interface,” *Microelectron. Eng.*, vol. 84, no. 5, pp. 1737–1740, May 2007, doi: 10.1016/j.mee.2007.01.243.
[54]Y. Sun, L. Ren, L. Jiang, Y. Tang, and B. Liu, “Fabrication of Composite Microneedle Array Electrode for Temperature and Bio-Signal Monitoring,” *Sensors*, vol. 18, no. 4, Art. no. 4, Apr. 2018, doi: 10.3390/s18041193.
[55]K. Chen, L. Ren, Z. Chen, C. Pan, W. Zhou, and L. Jiang, “Fabrication of Micro-Needle Electrodes for Bio-Signal Recording by a Magnetization-Induced Self-Assembly Method,” *Sensors*, vol. 16, no. 9, p. 1533, Sep. 2016, doi: 10.3390/s16091533.
[56]C.-W. Dong, C.-J. Lee, D.-H. Lee, S.-H. Moon, and W.-T. Park, “Fabrication of barbed-microneedle array for bio-signal measurement,” *Sens. Actuators Phys.*, vol. 367, p. 115040, Mar. 2024, doi: 10.1016/j.sna.2024.115040.
[57]L. Ren *et al.*, “Fabrication of Flexible Microneedle Array Electrodes for Wearable Bio-Signal Recording,” *Sensors*, vol. 18, p. 1191, Apr. 2018, doi: 10.3390/s18041191.
[58]L. Ren *et al.*, “Flexible microneedle array electrode using magnetorheological drawing lithography for bio-signal monitoring,” *Sens. Actuators Phys.*, vol. 268, pp. 38–45, Dec. 2017, doi: 10.1016/j.sna.2017.10.042.
[59]A. K. Srivastava, B. Bhartia, K. Mukhopadhyay, and A. Sharma, “Long term biopotential recording by body conformable photolithography fabricated low cost polymeric microneedle arrays,” *Sens. Actuators Phys.*, vol. 236, pp. 164–172, Dec. 2015, doi: 10.1016/j.sna.2015.10.041.
[60]L.-W. Lo *et al.*, “Stretchable Sponge Electrodes for Long-Term and Motion-Artifact-Tolerant Recording of High-Quality Electrophysiologic Signals,” *ACS Nano*, vol. 16, no. 8, pp. 11792–11801, Aug. 2022, doi: 10.1021/acsnano.2c04962.
[61]S. Yao *et al.*, “Ultrasoft Porous 3D Conductive Dry Electrodes for Electrophysiological Sensing and Myoelectric Control,” *Adv. Mater. Technol.*, vol. 7, no. 10, p. 2101637, Oct. 2022, doi: 10.1002/admt.202101637.
[62]N. Kitamura, J. Chim, and N. Miki, “Electrotactile display using microfabricated micro-needle array,” *J. Micromechanics Microengineering*, vol. 25, no. 2, p. 025016, Jan. 2015, doi: 10.1088/0960-1317/25/2/025016.
[63]M. Tezuka, N. Kitamura, and N. Miki, “Information transfer using wearable thin electrotactile displays with microneedle electrodes,” *Jpn. J. Appl. Phys.*, vol. 55, no. 6S1, p. 06GP15, May 2016, doi: 10.7567/JJAP.55.06GP15.
[64]X. Tang *et al.*, “Using microneedle array electrodes for non-invasive electrophysiological signal acquisition and sensory feedback evoking,” *Front. Bioeng. Biotechnol.*, vol. 11, 2023, Accessed: Mar. 05, 2024. [Online]. Available: https://www.frontiersin.org/articles/10.3389/fbioe.2023.1238210
[65]M. Williams, “A lot of needles may help restart a heart,” Rice University. Accessed: Feb. 25, 2024. [Online]. Available: https://news2.rice.edu/2018/04/12/a-lot-of-needles-may-help-restart-a-heart/
[66]RiceUniversity, “OEDK - Rice University - Team Zfib Member public profile.” Accessed: Mar. 05, 2024. [Online]. Available: https://oedk.wildapricot.org/Sys/PublicProfile/41415896/4330110
[67]J. Kugelberg, “The Interelectrode Electrical Resistance at Defibrillation,” *Scand. J. Thorac. Cardiovasc. Surg.*, Jan. 1972, doi: 10.3109/14017437209134810.
[68]J. E. Kugelberg, “Ventricular defibrillation with double square pulse,” *Med. Biol. Eng.*, vol. 6, no. 2, pp. 167–169, Mar. 1968, doi: 10.1007/BF02474270.

[69]L. Shi, S. Vedantham, A. Karellas, and A. M. O'Connell, "Technical Note: Skin thickness measurements using high-resolution flat-panel cone-beam dedicated breast CT," *Med. Phys.*, vol. 40, no. 3, p. 031913, Mar. 2013, doi: 10.1118/1.4793257.
[70]J. Lachner *et al.*, "An In Vitro Model of Avian Skin Reveals Evolutionarily Conserved Transcriptional Regulation of Epidermal Barrier Formation," *J. Invest. Dermatol.*, vol. 141, no. 12, pp. 2829–2837, Dec. 2021, doi: 10.1016/j.jid.2021.04.029.
[71]A. Summerfield, F. Meurens, and M. Ricklin, "The immunology of the porcine skin and its value as a model for human skin," *Mol. Immunol.*, vol. 66, Nov. 2014, doi: 10.1016/j.molimm.2014.10.023.
[72]A. Helmenstine, "Table of Electrical Resistivity and Conductivity," Science Notes and Projects. Accessed: Feb. 25, 2024. [Online]. Available: https://sciencenotes.org/table-of-electrical-resistivity-and-conductivity/
[73]A. Bouazizi, G. Zaibi, M. Samet, and A. Kachouri, "Parametric study on the dielectric properties of biological tissues," in *2015 16th International Conference on Sciences and Techniques of Automatic Control and Computer Engineering (STA)*, Dec. 2015, pp. 54–57. doi: 10.1109/STA.2015.7505138.
[74]R. M. Fish and L. A. Geddes, "Conduction of Electrical Current to and Through the Human Body: A Review," *Eplasty*, vol. 9, p. e44, Oct. 2009.
[75]S. Sarang, S. K. Sastry, and L. Knipe, "Electrical conductivity of fruits and meats during ohmic heating," *J. Food Eng.*, vol. 87, no. 3, pp. 351–356, Aug. 2008, doi: 10.1016/j.jfoodeng.2007.12.012.
[76]P. Tonog and A. D. Lakhkar, "Normal Saline," in *StatPearls*, Treasure Island (FL): StatPearls Publishing, 2024. Accessed: Feb. 26, 2024. [Online]. Available: http://www.ncbi.nlm.nih.gov/books/NBK545210/
[77]C. O'Mahony *et al.*, "Characterisation of Microneedle-Based ECG Electrodes Fabricated Using an Industrial Injection-Moulding Process," in *2019 IEEE 32nd International Conference on Micro Electro Mechanical Systems (MEMS)*, Jan. 2019, pp. 557–560. doi: 10.1109/MEMSYS.2019.8870721.
[78]M. Tilli, "Silicon Wafer - an overview | ScienceDirect Topics." Accessed: Feb. 28, 2024. [Online]. Available: https://www.sciencedirect.com/topics/materials-science/silicon-wafer
[79]V. E. Del Bene, "Temperature," in *Clinical Methods: The History, Physical, and Laboratory Examinations*, 3rd ed., H. K. Walker, W. D. Hall, and J. W. Hurst, Eds., Boston: Butterworths, 1990. Accessed: Mar. 01, 2024. [Online]. Available: http://www.ncbi.nlm.nih.gov/books/NBK331/
[80]Heartsmart, "AED Pad Placement | Heartsmart," Blogs. Accessed: Mar. 01, 2024. [Online]. Available: https://www.heartsmart.com/blogs/aed-pad-placement/
[81]W. Storr, "Capacitive Reactance - The Reactance of Capacitors," Basic Electronics Tutorials. Accessed: Mar. 20, 2024. [Online]. Available: https://www.electronics-tutorials.ws/filter/filter_1.html
[82]Murata, "Fundamental Knowledge of High-Frequency Characteristics in Inductors and Capacitors – Impedance and Resonance (1) | Murata Manufacturing Articles." Accessed: Mar. 20, 2024. [Online]. Available: https://article.murata.com/en-us/article/basics-of-l-and-c-hf-characteristics-imp-and-res-1
[83]A. Taylor-Jackson, "The 5 Different Trend Lines Explained," The Data School Down Under. Accessed: Mar. 09, 2024. [Online]. Available: https://www.thedataschool.com.au/alex-taylor-jackson/the-5-different-trend-lines-explained/
[84]Y. Onuki, U. Bhardwaj, F. Papadimitrakopoulos, and D. J. Burgess, "A Review of the Biocompatibility of Implantable Devices: Current Challenges to Overcome Foreign Body Response," *J. Diabetes Sci. Technol. Online*, vol. 2, no. 6, pp. 1003–1015, Nov. 2008.
[85]C. N. Elias, J. H. C. Lima, R. Valiev, and M. A. Meyers, "Biomedical applications of titanium and its alloys," *JOM*, vol. 60, no. 3, pp. 46–49, Mar. 2008, doi: 10.1007/s11837-008-0031-1.

[86]E. T. K. Demann, P. S. Stein, and J. E. Haubenreich, “Gold as an implant in medicine and dentistry,” *J. Long. Term Eff. Med. Implants*, vol. 15, no. 6, pp. 687–698, 2005, doi: 10.1615/jlongtermeffmedimplants.v15.i6.100.
[87]K. Mozafari, S. Santos, S. Ohri, M. Prajwal Mane Manohar, and F. Tiesenga, “Rare Metallic Allergy Reaction Presentation to Cholecystectomy Surgical Clip,” *Cureus*, vol. 14, no. 12, p. e32934, doi: 10.7759/cureus.32934.